

DISS. ETH Nr. 17743

**Microbial NADPH balancing mechanisms in seven diverse
species and its regulation in *Escherichia coli***

A dissertation submitted to the
Swiss Federal Institute of Technology Zurich
for the degree of
Dr. sc. ETH Zurich

Presented by
Tobias Fuhrer
Dipl. Natw. ETH
born January 12th, 1979
citizen of Trubschachen BE, Switzerland

Accepted on the recommendation of
Prof. Dr. U. Sauer, examiner
Prof. Dr. H. Hennecke, co-examiner
Dr. M. Heinemann, co-examiner

2008

Acknowledgements

This PhD thesis would not have been possible without the contribution of a number of persons. Here, I wish to acknowledge their contributions to the success of this work:

I thank Uwe Sauer for the excellent supervision during the past four years. I appreciated his constant availability, constructive support and direct way of communication. I esteemed his efforts to “educate” me to scientific thinking and writing.

I thank the co-examiners Prof. Dr. H. Hennecke and Dr. M. Heinemann and the chair Prof. Dr. R. Glockshuber for being on the committee for the examination and for their contribution to the final reviewing of this thesis.

For the nice working environment and support on many details I thank the entire Sauer group. In particular, I am very grateful to Eliane Fischer and Nicola Zamboni who answered my never ending flow of questions concerning all subtleties of labeling experiments, use of instruments and MATLAB[®]. Many thanks go to Simon Tännler, my companion throughout almost 5 years, for many fruitful discussions and support in genetics. Furthermore I would like to mention the support of Lars Küpfer and Robert Schütz using FBA and MATLAB[®]. In addition I would like to thank Stefan Christen and Reto Wijker, which, as part of their undergraduate studies, worked with me on sections of this thesis.

I wish to thank the former IBT and present IMSB members for the nice atmosphere and specially Johannes Michel and Christian Wolfrum for support and expertise in use of FPLC.

Finally I owe a big “thank you” to Karina, my parents and friends outside IMSB for their non-scientific support in many different ways.

Table of contents

Table of contents	5
Summary	6
Zusammenfassung	8
Chapter 1 - General Introduction	11
Chapter 2 - Experimental identification and quantification of glucose metabolism in seven bacterial species	33
Chapter 3 - Different biochemical mechanisms ensure network-wide balancing of reducing equivalents in microbial metabolism	57
Chapter 4 - Transhydrogenase expression in <i>Escherichia coli</i> is substrate dependent	79
Chapter 5 - Pentose phosphate pathway flux in <i>Escherichia coli</i> is limited by the levels of glucose-6P- and 6P-gluconate dehydrogenase	101
Conclusions and Outlook	128
References	131
Appendix	143
Curriculum Vitae	164

Summary

Microbes evolved a broad metabolic diversity with a complex interplay of pathways. ^{13}C labeling experiments enable insight into these diverse metabolisms by determining the contributions of the different metabolic pathways to glucose degradation. So far, ^{13}C labeling experiments have been performed mainly for species common in laboratories e.g. *Escherichia coli*, *Bacillus subtilis*, *Corynebacterium glutamicum* and *Saccharomyces cerevisiae*. They all use mainly the Embden-Meyerhof-Parnas and the pentose phosphate pathway for glucose degradation. In **Chapter 2**, we asked how representative the accumulated knowledge on these model species is by comparing relative pathway usage in seven diverse species of different genera with model species *E. coli* and *B. subtilis*. Unlike these two model species, all other species investigated rely on the Entner-Doudoroff pathway as the main catabolic pathway for glucose degradation. This contrasts to some extent with the generally held view on Embden-Meyerhof-Parnas pathway as the main glucose degradation pathway. The results revealed also that the range of catabolic flux rates varies widely, in some cases organism exhibited two to four times higher catabolic rates than the model species, yet grew entirely respiratory without any overflow metabolism.

In **Chapter 3**, we were interested in how species with such distinct patterns of glucose degradation manage their catabolic NADPH production to match the requirements for anabolic reactions. Therefore, we quantified NADPH metabolism by combining the net fluxes with experimentally determined cofactor specificities and NADPH requirements for biomass. *E. coli* was the only species with an insufficient NADPH production and compensated the lack of NADPH by the membrane-bound transhydrogenase. In *Pseudomonas fluorescens*, the NADPH production matched the requirements while all other species exhibited significant overproduction of NADPH, with *Paracoccus versutus* as the most extreme case. For the NADPH overproducing species it was observed that all of them had dual cofactor specificity in the two dehydrogenases of the PP pathway. Since all of them used the Entner-Doudoroff pathway as the almost exclusive pathway for glucose degradation,

the unspecificity of the glucose-6P dehydrogenase allowed reducing NADPH production to match the requirements and thus reach a balanced NADPH pool. For *Paracoccus versutus*, however, even assuming NAD⁺-specific glucose-6P dehydrogenase did not allow for a balanced NADPH pool. Thus, this species mostly likely uses the experimentally detected membrane-bound transhydrogenase to counter-balance the NADPH overproduction.

Based on **Chapters 2 and 3**, *E. coli* was exceptional in several ways: it has three alternative ways of glucose catabolism but uses mainly EMP pathway; unlike the other species, it has cofactor specific dehydrogenases throughout the relevant reaction for NADPH production and it has been shown to use the membrane-bound transhydrogenase to compensate for insufficient NADPH production during batch growth on glucose. However, how and why it uses PP pathway usage for NADPH generation and transhydrogenases for NADPH balancing remained unclear.

The most straightforward expectation would be transcriptional regulation of transhydrogenases, which we tested in **Chapter 4**. We monitored the expression of the two transhydrogenases of *E. coli* in 23 metabolic mutants on 7 different substrates, which resembled extreme cases of NADPH over- or underproduction. We could not observe a correlation between predicted fluxes through transhydrogenases and expression levels of both membrane-bound and soluble transhydrogenases and concluded that another mechanism might be relevant, which does not involve the NADPH balance of the cell. A possible mechanism was observed where expression of both transhydrogenases correlated with the nature of substrates, i.e. gluconeogenic substrates such as acetate and succinate could be clearly distinguished from other substrates such glucose or glycerol.

In **Chapter 5**, the role of the PP pathway in NADPH generation was investigated in more detail. Specifically, we wanted to know how the flux through PP pathway and concomitant NADPH production is regulated in *E. coli*. For this purpose, we characterized the kinetic parameters of the two dehydrogenases of the oxidative PP pathway and tested for different types of inhibition. Based on intracellular metabolite concentrations in wild-type and Pgi mutant, NADPH turnover was not limiting PP pathway flux and 6P-gluconate dehydrogenase was determined to be the rate limiting step of the PP pathway in both wild-type and Pgi mutant.

Zusammenfassung

In Mikroorganismen hat sich eine breite metabolische Diversität entwickelt, welche auf einem komplexen Zusammenspiel von Stoffwechselwegen basiert. Deren relative Beiträge zum Glukosestoffwechsel werden mit ^{13}C Markierungsexperimenten analysiert. Bis heute wurden diese Markierungsexperimente meist in Mikroorganismen durchgeführt, welche in Laboratorien weit verbreitet sind, wie zum Beispiel *Escherichia coli*, *Bacillus subtilis*, *Corynebacterium glutamicum* und *Saccharomyces cerevisiae*. Die wichtigsten Glukoseabbauwege in diesen Mikroorganismen sind der Embden-Meyerhof-Parnasweg und der Pentosephosphatweg. In **Kapitel 2** beschäftigten wir uns mit der Frage, wie repräsentativ diese Modellorganismen eigentlich wirklich sind, indem wir deren Glukosestoffwechsel mit dem von sieben unterschiedlichen Mikroorganismen aus verschiedenen Gattungen verglichen. Im Unterschied zu *E. coli* und *B. subtilis* benützten diese sieben Mikroorganismen hauptsächlich den Entner-Doudoroffweg für den Glukoseabbau, was der allgemein angenommen Dominanz des Embden-Meyerhof-Parnasweges widerspricht. Des weiteren wuchsen die sieben Mikroorganismen mit einer Ausnahme respirativ, produzierten keine Fermentationsprodukte und hatten sehr unterschiedliche Flussraten im Vergleich zu *E. coli* und *B. subtilis*.

Das Reduktionsäquivalent NADPH wird beim Glukoseabbau gebildet und für die Biomasseproduktion gebraucht. In **Kapitel 3** untersuchten wir, wie die Zelle dessen Produktion den Bedürfnissen anpasst. Dazu quantifizierten wir die NADPH-Produktion mit Hilfe der Flüsse aus **Kapitel 2** und gemessenen Kofaktorspezifitäten. Einzig in *E. coli* war die Produktion von NADPH ungenügend und das Defizit wurde durch die membran-gebundene Transhydrogenase kompensiert. Während in *Pseudomonas fluorescens* die Bilanz ausgeglichen war, produzierten alle anderen Mikroorganismen zuviel NADPH, zeigten jedoch Dehydrogenaseaktivitäten, welche überraschend kofaktor-unspezifisch waren. Dadurch konnte die NADPH-Überproduktion praktisch vollständig abgewendet werden, mit Ausnahme von *Paracoccus versutus*, dessen ausgeprägter NADPH-Überschuss auch dadurch

nicht verhindert wurde. Daraus lässt sich schliessen, dass in diesem Fall der NADPH-Überschuss durch die gemessene Transhydrogenaseaktivität ausgeglichen wurde.

In **Kapitel 2 und 3** haben wir gesehen, dass *E. coli* in verschiedener Hinsicht ein Spezialfall darstellt: Erstens hat es die Möglichkeit drei verschiedene Glukoseabbauwege zu benützen, wobei der Embden-Meyerhof-Parnasweg der wichtigste ist. Zweitens sind seine Dehydrogenasen im zentralen Kohlenstoffwechsel allesamt spezifisch für NADPH oder NADH. Drittens wird das NADPH-Defizit während des Wachstums auf Glukose durch die membran-gebundene Transhydrogenase ausgeglichen. Die Gründe, warum ein Teil des NADPH durch Pentosephosphatweg gebildet wird und das übrigbleibende NADPH-Defizit durch die genannte Transhydrogenase kompensiert wird, sind ebenso unklar wie die zugrunde liegenden regulatorischen und kinetischen Mechanismen. Transkriptionelle Regulation der Transhydrogenasen wurde in **Kapitel 4** mittels Analyse der Transhydrogenasenexpression in 23 metabolischen Mutanten auf 7 verschiedenen Kohlenstoffquellen untersucht. Obwohl dabei extreme Situationen für die NADPH Produktion analysiert wurden, konnten wir keine Korrelation zwischen den daraus resultierenden unterschiedlichen Transhydrogenaseflüssen und der Transhydrogenasesexpression beobachten. Hingegen korrelierten die Expressionlevel mit der Art der Kohlenstoffquelle. Glykolytische und glukoneogenetische Substrate führten zu unterschiedlicher Expression welche über alle Mutanten für dasselbe Substrat ähnlich waren. Dies lässt auf einen noch unbekannten Regulationsmechanismus schliessen.

Die Regulation des Flusses durch den Pentosephosphatweg wurde in **Kapitel 5** eingehender untersucht. Es stellte sich die zentrale Frage, warum nicht mehr NADPH mittels höherem Fluss durch diesen Weg gebildet wird. Dazu wurden die Glukose-6P- und die 6P-Glukonatdehydrogenase aufgereinigt und kinetisch charakterisiert, sowie die intrazellulären Konzentrationen der entsprechenden Substrate und Produkte (einschliesslich Kofaktoren) bestimmt. Dabei zeigte sich, dass beide Dehydrogenasen erheblich durch deren Produkte und Kofaktoren inhibiert werden, wodurch das V_{max} zu mindestens 50% reduziert wurde. Des weiteren waren in einer Phosphoglukoseisomerase-Mutante die Substratkonzentrationen zehnfach erhöht, was zur völligen Sättigung beider Enzyme in dieser Mutante führte und somit den Fluss durch den Pentosephosphatweg entscheidend limitierte.

Chapter 1

General Introduction

Microbial Glucose Degradation

Carbon metabolism in general

Carbon metabolism of bacteria is one of the best studied biological systems. Our current knowledge is based on large collection of biochemical, physiological and genomic evidence that are available through databases and textbooks, which refer to original literature (84, 114, 131). Over more than half a century, pathways of carbon metabolism were examined and assembled step by step into an interconnected network. Biochemical and kinetic properties of the enzymes within the network are properties that are obtained from in vitro experiments. The interaction between the enzyme components is usually described as pathways with distinct metabolic functions. Within the entire network of around 1000 metabolic reactions, central carbon metabolism constitutes a core network that supplies essentially all biosynthetic building blocks, cofactors and energy to enable growth and survival under varying conditions.

In microbiology, we often deal with species that use organic compounds as energy and carbon source, which are therefore called chemoorganotrophs. These species can grow on various substrates that may enter the metabolic network at different points. Rhizobia for example, consume organic acids (usually succinate, malate and fumarate) from plants as carbon substrates (51). Other species degrade very niche-specific carbon substrates such as fatty acids by beta oxidation and glyoxylate shunt or hydrocarbons by the mono/dioxygenase or hydroxylase reaction (88, 127, 211).

Glucose degradation pathways

One of the best studied carbon substrates are hexoses, in particular glucose, due to their abundance as building block in many different biomaterials such as starch or cellulose. In the following, the glucose metabolism will be introduced in detail as it is the main carbon substrate throughout this thesis. In microbes, glucose can generally be catabolized through three main degradation pathways (Fig. 1). Besides the well known Embden-Meyerhof-Parnas

(EMP) and pentose phosphate (PP) pathways, many species also use the Entner-Doudoroff (ED) pathway for glucose degradation (35, 151). All three pathways make hexoses available for central carbon metabolism and yield common metabolites such as triose-phosphates, phosphoenolpyruvate (PEP) and pyruvate.

The classical glycolysis or EMP pathway is the best studied and main glucose degradation pathway in many species (72). The upper part of glycolysis consists of the enzymes glucokinase/phosphotransferase system, glucose-6P isomerase, 6P-fructokinase, fructose-1,6-bisphosphatase and triosephosphate isomerase, which phosphorylate the glucose twice and split it into two triosephosphates. The two trioses are subsequently converted into pyruvate by the lower part of glycolysis, which involves glyceraldehyde-3P dehydrogenase, phosphoglycerate kinase, phosphoglycerate mutase, enolase and pyruvate kinase. Thus, catabolized through glycolysis, 1 molecule of glucose yields 2 molecules each of pyruvate, NADH and ATP. In *Escherichia coli* and *Bacillus subtilis* 70-80 % of the carbon are catabolized through the EMP pathway during batch growth on glucose, as determined by ^{13}C tracer experiments (40, 65).

An alternative route to the EMP pathway is the PP pathway, which can be divided into the upper oxidative and the lower non-oxidative part. The oxidative part includes the enzymes glucose-6P dehydrogenase, 6P-gluconolactonase, 6P-gluconate dehydrogenase to convert glucose-6P into ribulose-5P. The non-oxidative part involves ribulose-5P epimerase, ribose-5P isomerase, transketolase and transaldolase to convert ribulose-5P to glyceraldehyde-3P. The main role of the PP pathway is to provide precursors (erythrose-4P and ribose-5P) and reducing equivalents for biomass synthesis (NAD(P)H) (97, 228). In *E. coli* and *B. subtilis*, 20-30 % of the glucose is usually degraded by the PP pathway. Interestingly, this exceeds by far the precursor and NADPH demand for biomass production (40, 65).

The ED pathway is less investigated because it is either absent or not the main glucose degradation pathway in most of the well investigated species such as *B. subtilis*, *E. coli* and *Saccharomyces cerevisiae* (65). However, the ED pathway is relevant for degradation of gluconate and the two involved enzymes are present in other well studied species such as pseudomonads or in some archaea and prokaryotes (96, 107, 155).

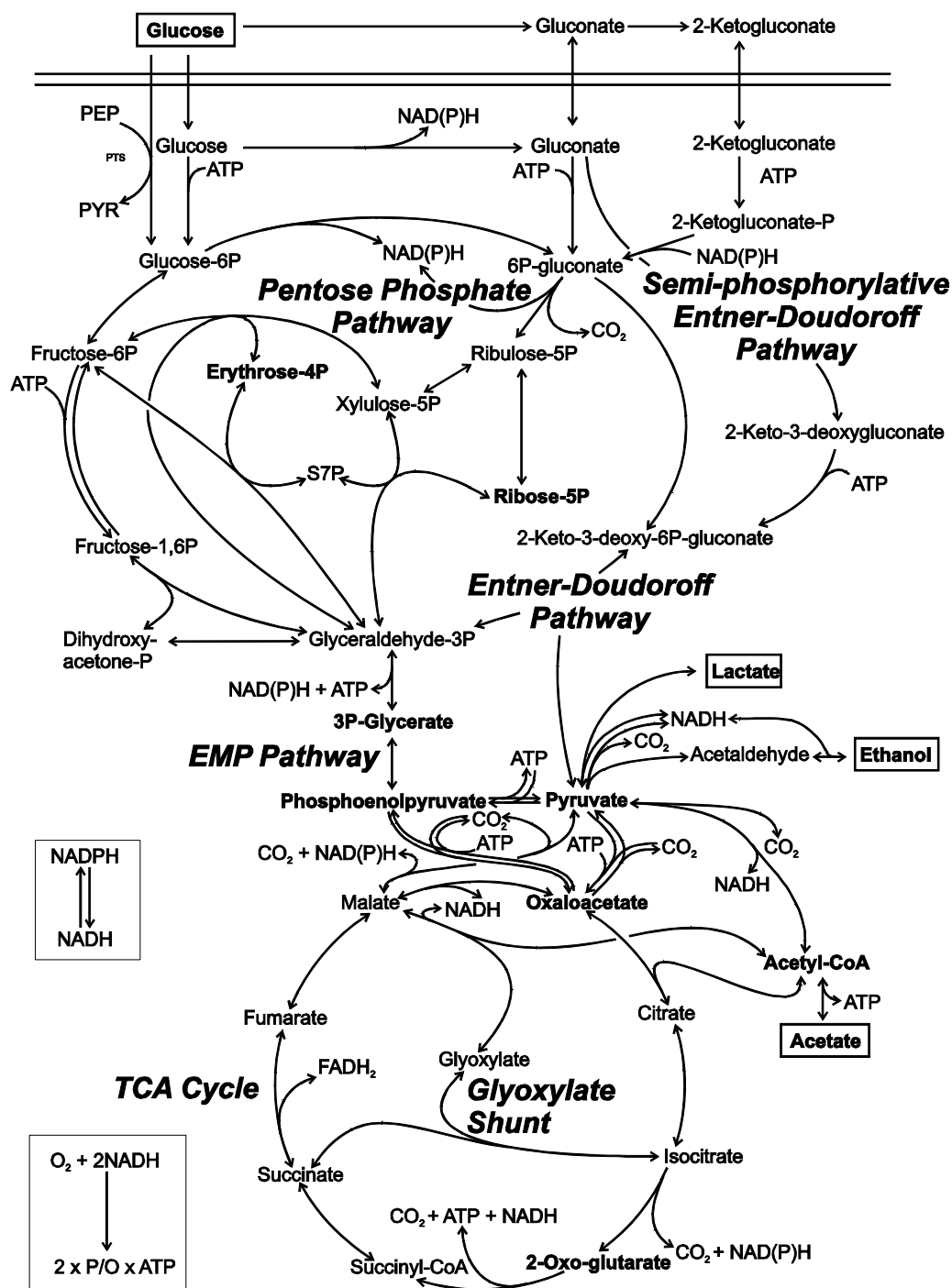


Figure 1 - Generic network of central carbon metabolism during growth on glucose. Abbreviations: S7P, sedoheptulose-7P; PTS, phosphotransferase system; PYR, pyruvate; PEP, phosphoenolpyruvate; EMP pathway, Embden-Meyerhof-Parnas pathway; TCA cycle, tricarboxylic acid cycle.

Currently, three different variations of the ED pathway are known. In the classical phosphorylative ED pathway, glucose-6P is oxidized to 6P-gluconate by glucose-6P dehydrogenase and subsequently dehydrated by 6P-gluconate dehydratase into 2-keto-3-deoxy-6P-gluconate (KDPG), the characteristic intermediate of the pathway. KDPG cleavage by KDPG aldolase forms pyruvate and glyceraldehyde-3P (GAP), which is converted to pyruvate by the enzymes also used in the EMP pathway (192). A variation to the classical ED pathway is the semi-phosphorylative ED pathway, also known as the modified ED pathway (1). It differs from the classical pathway by the direct conversion of glucose into 2-keto-3-deoxy-gluconate, which is then phosphorylated and split into pyruvate and GAP. As another variation, the non-phosphorylative ED pathway does not yield GAP but directly 2P-glycerate without any phosphorylative step (108). The classical and the semi-phosphorylative ED pathway yield 1 mol ATP per mol glucose, while the net yield is zero for the non-phosphorylative variant (192). Interestingly, from an evolutionary point of view, it seems that the ED pathway is actually the oldest hexose degrading mechanism, while the EMP pathway was originally a gluconeogenic pathway (168, 169).

Taken these three pathways together, they cover the upper part of glucose catabolism throughout different species to produce phosphoenolpyruvate (PEP) and pyruvate which both connect upper part of glucose metabolism and tricarboxylic acid (TCA) cycle (Fig. 1). The question arises how these catabolic pathways are distributed among diverse species. The presence of these catabolic pathways has been investigated mainly by enzymatic assays as for example for the ED pathway (1, 107, 108, 192). Alternatively, one can derive the information from genome information as there are more and more annotated fully sequenced genomes available. At the moment, based on information available from NCBI (<http://www.ncbi.nlm.nih.gov/>), 599 microbial genomes are completely sequenced and 879 are in progress. In total 730 genomes are available at the KEGG database (<http://www.genome.jp/kegg/>) including 125 eukaryotic, 557 bacterial and 48 archaea entries. The KEGG database genomes sequences are mainly derived from NCBI RefSeq and annotated by Sequence Similarity DataBase (SSDB) and manual knockout assignments (143).

The abundances of the genes encoding for EMP, PP and ED pathway throughout the so far completed genomes were derived from KEGG and are illustrated in Figure 2. In addition, the abundances of the genes for the lower part of EMP pathway are shown separately because they are necessary for the PP and ED pathway too. The exceptional high fraction of absent genes for the eukaryotes is based on the scarce annotation up to date (except for few yeast and plants). The genes of the phosphorylative ED pathway (*edd* and *eda*) are well annotated and mainly present in bacteria but for the archaea the annotation is poor. However, the presence of the genes of lower glycolysis points to the presence of the ED pathway in archaea.

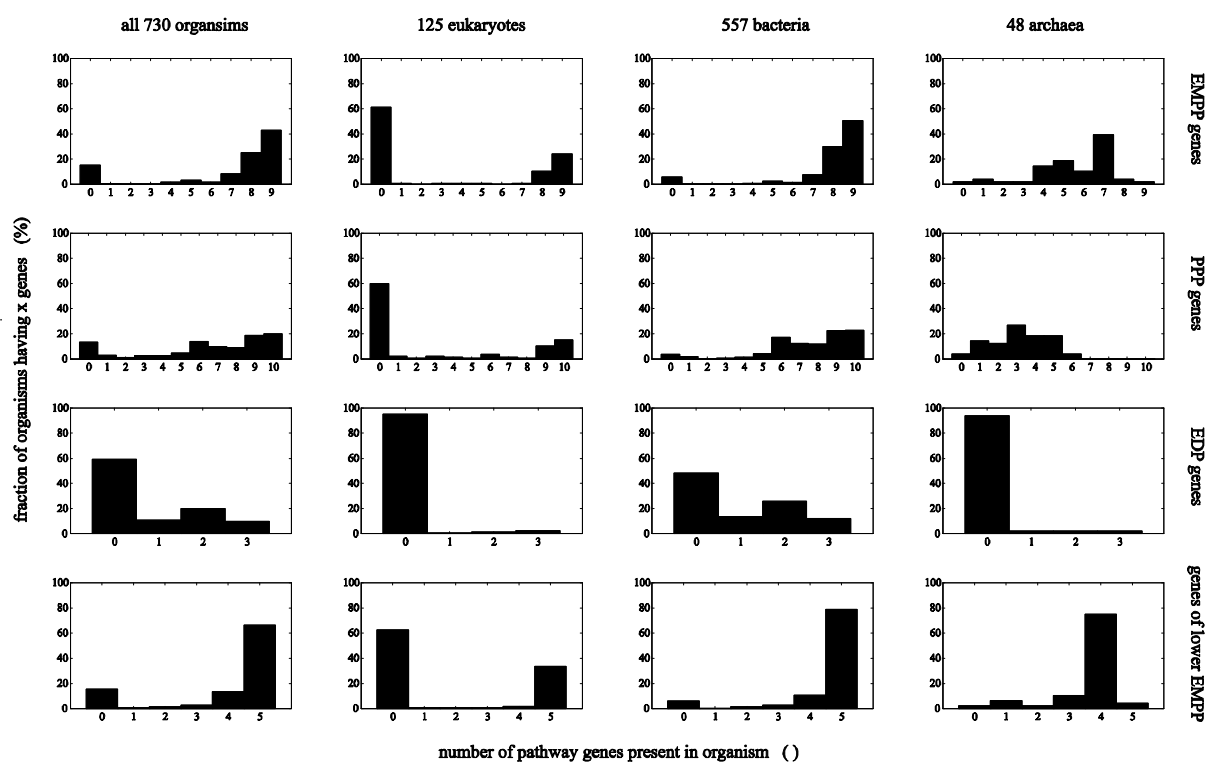


Figure 2 - Relative abundances of genes for EMP pathway (EMPP, maximally 9 genes), ED pathway (EDP, maximally 3 genes), PP pathway (PPP, maximally 10 genes) and lower EMP pathway (maximally 5 genes). The PP pathway included also 6P-fructokinase, fructose-1,6-bisphosphatase and triosephosphate isomerase from the EMP pathway to be a fully catabolic pathway. ED pathway included phosphogluconate dehydratase and 2-dehydro-3-deoxyphosphogluconate aldolase for the phosphorylative and 2-dehydro-3-deoxygluconokinase for the semi-phosphorylative variant.

Energy generation and conservation

ATP is the most important energy storage compound in living organisms because it contains high-energy phosphate bonds. ATP is primarily used as energy source for biomass synthesis and is provided by substrate-level and/or oxidative phosphorylation. During oxidative phosphorylation, electrons are transferred from the carbon substrate to the terminal electron acceptor O_2 , driving ATP synthesis by ATPase at the expense of the proton motive force (84). Under anaerobic conditions, electron acceptors other than O_2 are used, which is referred to as anaerobic respiration. Electron acceptors used under these conditions include nitrate, ferric ions, sulfate and carbonate (125).

Besides the respiratory chain, ATP is also formed by substrate-level phosphorylation in the catabolic pathways and/or from formation of secreted acids such as acetate (Fig 1). Fermentation takes place in the absence of oxygen or any inorganic terminal electron acceptor. In this case, e.g. lactate or ethanol serve as the final electron acceptors and are excreted by the cell. ATP is then generated exclusively by substrate-level phosphorylation.

During batch growth on glucose, ATP usually is produced in excess estimated from net flux distributions and known ATP demands for biomass. It is assumed that the excess ATP is used for maintaining different kinds of gradients (salt ions, protons) across the microbial membrane (172).

Biomass formation

For biomass production, precursor metabolites are constantly withdrawn from central carbon metabolism during exponential growth. In the catabolic pathways, these demands are usually easily fulfilled due to the high turnover of the precursor pools. For the TCA cycle, the situation is different because the ratio between anaplerotic and respirative TCA cycle flux has to be such that sufficient precursors for biomass are provided. The anaplerotic reactions - from pyruvate or phosphoenolpyruvate to oxaloacetate - refill the TCA cycle to balance the precursor metabolites withdrawn for biomass. Produced from pyruvate, acetyl-CoA is usually burned into CO_2 if not consumed by the anaplerotic glyoxylate shunt, which happens e.g. during growth on acetate (66). As an alternative to the mentioned anaplerotic reactions above,

a novel anaplerotic pathway was described recently in hungry *E. coli* involving the glyoxylate shunt and PEP carboxykinase (66, 126).

Cofactors

The generalized, not species specific reaction network shown in Figure 1 covers most reactions of central carbon metabolism of a typical microbial cell degrading glucose. Many reactions of the catabolic pathways involve cofactors such as ATP, NADPH or NADH. These metabolites - among others - resemble thus the most important interconnections between pathways and need therefore to be well balanced to maintain metabolic homeostasis, a prerequisite for exponential growth at steady state (68).

NADH mainly serves as electron donor for the respiratory chain and is therefore considered to be rapidly reoxidized under aerobic conditions. It is regenerated mainly by glyceraldehyde-3P dehydrogenase in the EMP pathway, 2-oxoglutarate and malate dehydrogenases in the TCA cycle, pyruvate dehydrogenase complex and to a minor extent in the malic enzyme reaction (Fig. 1). Thus, both ATP and NADH are primarily involved in energy generation and catabolism where an accumulation can be rapidly counterbalanced.

NADPH, in contrast, cannot be used by the respiratory chain but delivers reducing equivalents for biomass production reactions. As a result, its metabolic function differs significantly from NADH and ATP. In the next section we will take a closer look at the role of NADPH.

The NADPH balance

NADPH is distinct from other cofactors such as NADH or ATP: First, the reduced form is produced by only few dehydrogenase reactions, most prominently in the PP pathway and by isocitrate dehydrogenase in the TCA cycle. There are some additional potential contributors such as malic enzyme or NADPH-dependent glyceraldehyde-3P dehydrogenase in e.g. *B. subtilis*. However, their role is less clear but probably minor. Second, the requirements for NADPH as reducing equivalent during steady state growth are well defined by the biomass

production. Other NADPH demands such as for stress response or fast reoxidizing mechanism as for NADH can be neglected under steady state growth conditions. Third, as consequence of the first two characteristics, the production and consumption of NADPH as reducing equivalent is tightly connected.

Transhydrogenases and the NADPH balance

The tight connection between NADPH regeneration and NADPH demand for biomass production couples anabolism and catabolism. This coupling is an indirect but strong constraint for carbon flux distribution, because the summed NADPH regeneration of the involved dehydrogenases has to meet the requirements for biomass. This holds true for microbial growth in all conditions and thus on any carbon substrate. For example, a substrate catabolized exclusively by the PP pathway will yield drastically more NADPH than a substrate entering i.e. TCA cycle. Such potential differences in NADPH metabolism can be counterbalanced by the action of transhydrogenases which interconvert NADH and NADPH. Two different reaction mechanisms are known for transhydrogenases (Fig. 3).

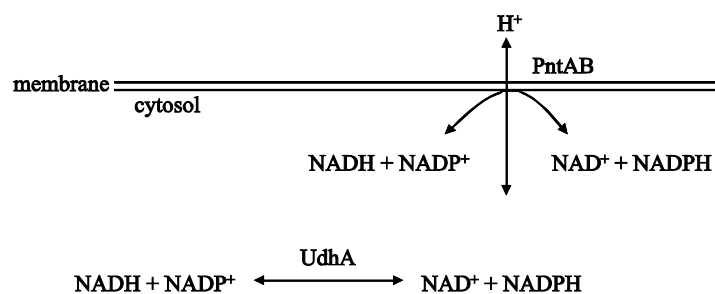


Figure 3 - The two known forms of transhydrogenase. Soluble transhydrogenase present in the cytosol (UdhA) and membrane-bound, proton-translocating transhydrogenase (PntAB).

The first mechanism involves a membrane-bound enzyme that translocates protons. The membrane-bound transhydrogenase has been investigated in some species such as *Rhodobacter sphaeroides*, and in detail for *E. coli* (7, 8, 20, 93). Since the genes *pntA* and *pntB* encoding its two domains were characterized for *E. coli* in 1986 by the work of Clarke

et al. (32), a lot of work has been published on its structure and reaction mechanism but its physiological function and/or regulation are still unclear (3, 4, 21, 145, 231). Physiological functions were first hypothesized for a membrane-bound transhydrogenase in animal mitochondria, suggesting a role in both energy depletion and high NADPH demand conditions (8, 94).

The second, energy-independent transhydrogenase reaction is catalyzed by a soluble enzyme, which has been identified so far in *Pseudomonas fluorescens* (73) and *E. coli* (24). Although the *udhA* gene is known and overexpression with subsequent basic characterization was performed for the transhydrogenase of *P. fluorescens* (73), only little is known about its regulation or physiological function (179). Based on the KEGG database, about 42% of the sequenced bacteria have a *udhA* gene while only about 20% have a *pntA* or *pntB* or both genes (143). Only a single archaea contains the *udhA* gene and none a *pntA* or *pntB* gene.

Now, what is the exact role of the two transhydrogenases and why are sometimes even both forms present in one organism such as in *E. coli*? As a defined condition to investigate the physiological function of both transhydrogenases, glucose batch growth of *E. coli* was used (179). Under this condition, about 37 and 21% of the NADPH required for biomass production are regenerated by the PP pathway and by the isocitrate dehydrogenase respectively based on ^{13}C determined fluxes. The remaining 42% are not provided directly by the glucose catabolizing pathways but by the enzymatically determined activity of a membrane bound transhydrogenase (PntAB) (179).

The soluble and energy-independent transhydrogenase (UdhA) was shown to be essential in a phosphoglucosomerase (blocked EMP pathway) mutant where glucose catabolism is catabolized mainly through the PP pathway and thus causes a significant NADPH overproduction (179). During growth on acetate a high NADPH overproduction can be expected in the TCA cycle and indeed, UdhA is essential also in this situation (unpublished). These two examples strongly indicate that UdhA could counterbalance overproduction of NADPH. The transhydrogenases, at least in *E. coli*, thus constitute crucial mechanisms in redox metabolism that uncouple catabolism from anabolism. These findings agree well with the current understanding of both NADH and NADPH metabolism linked by transhydrogenase reaction, which is depicted in Figure 4 based on pioneering work of

Voordouw *et al.* for *Azotobacter vinelandii* (218). In this work it was proposed that the NADP(H) pool is more reduced than the NAD(H) pool, which is supported by intracellular cofactor concentrations in *E. coli* from own data and previous publications (6, 31). Despite the important roles of transhydrogenases in linking the fundamental processes of anabolism and catabolism, quantitative NADPH metabolism has only been just recently addressed for *E. coli* during growth on glucose (179). However, even for *E. coli* there still remains a general lack of knowledge about the exact physiological function of transhydrogenase and the involved regulation.

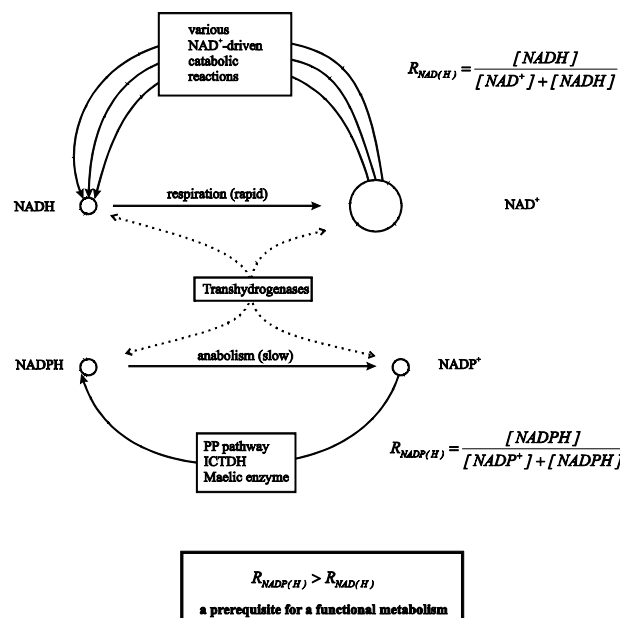


Figure 4 – Schematic representation of redox metabolism. The circle size resembles the intracellular cofactor concentrations, the arrows enzymatic reactions altering these pools. Adapted from Voordouw *et al.* (218).

NADPH requirements and regenerating mechanisms

Beyond the fundamental relevance of NADPH metabolism in linking catabolism and anabolism, it is also important for metabolic engineering. For biocatalytic processes, glucose degradation fluxes are often rerouted by genetic manipulations to obtain beneficial overproduction of the desired product. However, most manipulations of fluxes lead to an

alteration of the redox state of the cell. A quantification of the redox balance is a necessity for successful metabolic engineering and has not been extensively addressed despite its importance. This is mostly due to the fact that it is not possible to quantify NADPH metabolism directly by e.g. a single measurement. NADPH metabolism relies on several contributors throughout central carbon metabolism, which all need to be determined.

For systematic quantification of NADPH metabolism, one needs to know the NADPH requirements of the cell, the carbon flux through the involved dehydrogenases and their cofactor specificities. The exact requirements of NADPH for biomass production during steady state growth are necessary to quantify the NADPH balance. With known standard *E. coli* biomass composition and biochemical knowledge, one can quantify the biosynthetic requirements of NADPH (138). For each component like amino acids or cell wall constituents, the stoichiometric NADPH requirements are derived and summed up. The exact biomass composition of a cell depends on the growth conditions. On a defined medium, dependency on the maximal growth rate was determined reflecting mainly the variation in RNA and protein content of the cell (60). For slow growing cells the protein content is higher than for fast growing cells while for the RNA content the opposite could be observed. A typical value of NADPH demand for *E. coli* is 16 mmol NADPH per gram cell dry weight at a growth rate of 0.67 h^{-1} , which gives a net NADPH flux into biomass of about $11\text{ mmol g}^{-1}\text{ h}^{-1}$ (60). For the gram-positive *Bacillus subtilis* and for the anaerobic *Zymomonas mobilis* corresponding values are about 18 and 15 mmol NADPH per gram cell dry weight at a growth rate of 0.67 h^{-1} and 0.30 h^{-1} respectively, which corresponds to a net NADPH flux into biomass of about 12 and $4.5\text{ mmol g}^{-1}\text{ h}^{-1}$ respectively (42, 44).

There are other situations such as oxidative stress conditions where additional NADPH is required. Besides respiration, many reactions in a living cell use O_2 as terminal electron acceptor such as desoxyribonucleotide synthesis, protein repair or H_2O_2 reduction (9, 209). To be countered, such O_2 -dependent redox reactions are reversed by electrons supplied by the reducing equivalents NADPH or NADH. Reducing power is mainly transferred from NADPH by thioredoxin which involves the redox properties of the thiol group of cysteine, which is either present in the reduced thiol (SH) or oxidized disulfide bond (-S-S-) form (9, 209).

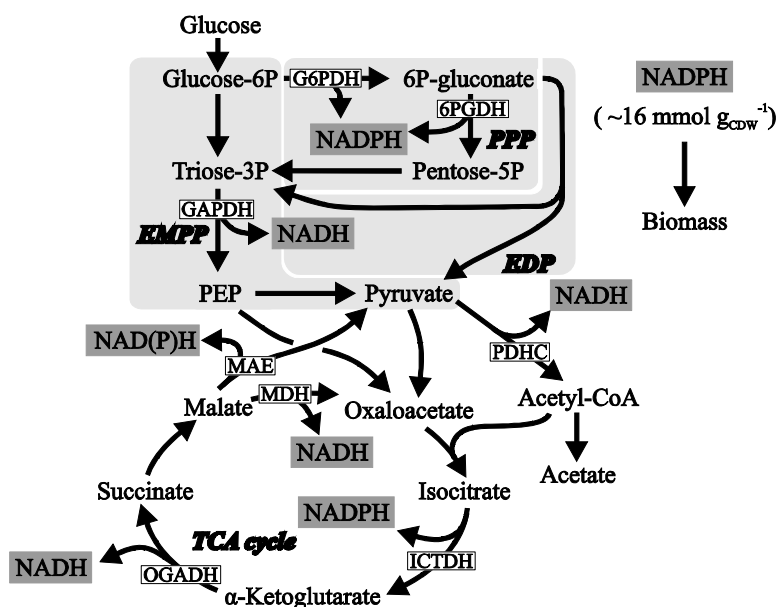


Figure 5 - Schematic representation of central carbon metabolism with all sources of NADPH indicated. Abbreviations: PEP, phosphoenolpyruvate; G6PDH, glucose-6P dehydrogenase; 6PGDH, 6P-gluconate dehydrogenase; GAPDH, glyceraldehyde-3P dehydrogenase; PDHC, pyruvate dehydrogenase complex; ICTDH, isocitrate dehydrogenase; OGADH, 2-oxoglutarate dehydrogenase system; MDH, non decarboxylating malate dehydrogenase; MAE, malic enzyme. Typical NADPH demand in *E. coli* was calculated based on growth rate and biomass composition.

production flux includes all dehydrogenases in the central carbon metabolism which are basically redox reactions regenerating NADPH from NADP^+ . Each single contributing reaction has to be normalized with the relative cofactor specificity for NADPH. The quantitative basis of the NADPH balancing, the in vivo net fluxes, are outlined in the next section.

Currently, the NADPH balance was quantitatively addressed at least in *E. coli* for growth on glucose where NADPH over- and underproduction was analyzed in different metabolic mutants. It was found that UdhA indeed is necessary during NADPH overproduction conditions and PntAB compensated underproduction, which could partly be replaced by an elevated PP pathway flux (179). The exact role of the PP pathway itself remains unclear. Generally, it is assumed that the PP pathway operates primarily to fulfill requirements for the biosynthetic building blocks ribose-5P and erythrose-4P and/or NADPH (72, 84). But it is not clear why and how the relative contributions of both PP pathway and PntAB are regulated in wild-type *E. coli*. During batch growth on glucose, UdhA is not required and the question remains to be answered if UdhA is just kinetically inactive or if there is an active genetic regulation, which responds to NADPH overproduction. To summarize, *E. coli* comes along with flexibility in NADPH metabolism having different catabolic pathways and both known forms of transhydrogenases. However, this flexibility also requires regulatory mechanism to ensure growth under different conditions.

Quantifying in vivo Carbon Fluxes

Understanding metabolism is crucial for metabolic engineering and many different methods for it have been developed over the past decades (13, 195). In its simplest form, understanding of carbon metabolism relies on knock-out studies and determination of the corresponding growth phenotypes, which typically involve all the descriptive parameters of microbial growth behavior such as biomass yield, maximal growth rate and substrate

consumption and product formation rates. More detailed information about microbial metabolism can be retrieved from mRNA transcripts, proteins or metabolite levels. With the availability of genome sequences, genome-scale reaction network models were reconstructed for various organisms describing the interconversion of hundreds of metabolites (71, 92, 144, 164, 184).

These interconversions can be quantified by intracellular carbon fluxes, which are fundamental determinants of cell physiology because they identify the engagement of various pathways in cellular function and metabolic processes (198). The accurate quantification of pathway fluxes in vivo (i.e. net fluxes) is thus an important goal in metabolic engineering, especially for the interconversion of a metabolite into a product of interest. The net fluxes also determine the interconversion rates of oxidized NAD(P)H into the reduced forms or vice versa throughout the metabolic network and thus are a necessity for quantifying the NADPH balance.

Despite the availability of lots of omics data and genome-scale models, quantification of intracellular fluxes is not possible with this kind of data. However, the single reactions of a pathway can be described by enzyme kinetics and local flux predictions are possible on the basis of reactants and enzyme concentrations. The determination of quantitative carbon flux through an entire pathway and/or the relative distributions within metabolism is in theory possible using kinetic models but has limitations, which will be further discussed below. Modern flux analysis techniques became available during the 1990s, which not only allowed for confirmation of known pathways or identification of new pathways but also enabled in vivo quantification of carbon metabolism (95, 176, 197).

Predicting fluxes by kinetic models

Individual enzymatic reactions can be described by mechanistic and non-mechanistic models, which approximate the true underlying enzyme kinetics. The formulation of mechanistic functions requires detailed knowledge of the mechanism of enzyme catalysis. The best-known one is the Michaelis-Menten kinetics for a unidirectional single-substrate reaction. However, most of the enzymatic reactions in the central carbon metabolism are reversible and include possible allosteric and non-allosteric inhibition and activation (37).

Mechanistic models have good extrapolation capacity in terms of metabolite concentrations, but are highly non-linear and contain a large number of parameters. Thus, the development of a complete mechanistic kinetic model of central carbon metabolism would involve a vast amount of kinetic parameters, protein and metabolite concentrations to be experimentally determined. Since this would be extremely laborious, mechanistic kinetic models up to date do not cover all reactions of central carbon metabolism and involve often parameter estimation (31, 207). Alternatively to mechanistic models, non-mechanistic models aim to approximate enzyme kinetics within a limited range of metabolite concentrations, often chosen around a reference state (91). Presently, there are no kinetic models available which fulfill both predictive power and metabolism-wide coverage. In addition, kinetic *in silico* models will always lack the proof that they indeed resemble the *in vivo* conditions and thus cannot reliably predict fluxes. Therefore, alternative methodologies to quantify central carbon metabolism not only *in silico* but *in vivo* are of great interest, which will be introduced below.

Tracer experiments

As early as in the fifties, the first steps into quantifying *in vivo* fluxes included CO₂ radiorespirometry to follow the fate of ¹⁴C labeled substrates. The method is based on off gas analysis using CO₂ traps and radioactivity measurements (220). This method has limited resolution capacity because CO₂ is released in many different reactions in the network. The method was mainly used to differentiate relatively between EMP, PP and ED pathway flux.

More elaborate methods were developed in the nineties, which trace ¹³C throughout central carbon metabolism by the use of NMR or MS techniques (180, 204, 222). There are two main approaches, which make use of labeling information. In one, a comprehensive isotope isomer (isotopomer) model of metabolism is used to map metabolic fluxes in an iterative fitting procedure on the isotopomer pattern of network metabolites that are obtained from nuclear magnetic resonance (NMR) or mass spectrometry (MS) analysis (40, 113, 150, 154). Since the predicted flux solution represents the best fit to physiological and labeling data, its outcome strongly depends on the quality of the network and on measurements accuracy.

In the other approach, metabolic flux ratio (METAFor) analysis gives analytical solutions for local flux nodes within the metabolic network and no physiological data is required (60, 65, 203). METAFor analysis quantifies the relative contribution of two or more converging pathways to a given metabolite by probabilistic equations that relate mass distributions in proteinogenic amino acid to pathway activity (135). The labeling content of proteinogenic amino acids resembles the steady state labeling pattern of the precursor metabolites and is easily accessible since the amino acids accumulate in the protein throughout the exponential growth phase. The labeling data of proteinogenic amino acids are usually determined by GC-MS and corrected for both natural abundance of naturally occurring isotopes and unlabeled biomass from the inoculum. Based on the well conserved biosynthesis pathways for the amino acids, the labeling of the carbon backbones of the precursor metabolites such as pyruvate, ribose-5P or oxaloacetate can be derived (203). The principle of such flux ratio analysis is outlined below for the example of the flux ratios serine derived through EMP and pyruvate derived through ED pathway (135).

Metabolic flux ratio analysis (METAFor)

The ratio serine through EMP pathway quantifies the fraction of serine (triose-3P) derived through EMP pathway versus the fraction of serine (triose-3P) derived through the PP or ED pathways (Fig. 1). This ratio can be quantified from positional labeling using cells grown exclusively on [1-¹³C]glucose. Indeed, if triose-3P and thus serine molecules originate from EMP pathway, half of the serine molecules will be labeled at position 3 while the other half will be unlabeled (Fig. 6). If the serine molecules originate from the oxidative PP pathway, none of the molecules will be labeled because the ¹³C-labeled carbon at position one is lost as CO₂ in the oxidative part of the PP pathway (Fig. 6). The serine molecules derived through the ED pathway yield unlabeled triose-3P molecules (Fig. 6) but also directly pyruvate, which can be differentiated from pyruvate through EMP pathway because the label ends up in position 1 instead of position 3 (Fig. 6) (135). There are more nodes in central carbon metabolism where such local ratios can be determined depending on the chosen substrate labeling (65). The most frequent used substrate labeling is either [1-¹³C]glucose or [U-¹³C₆]glucose (65).

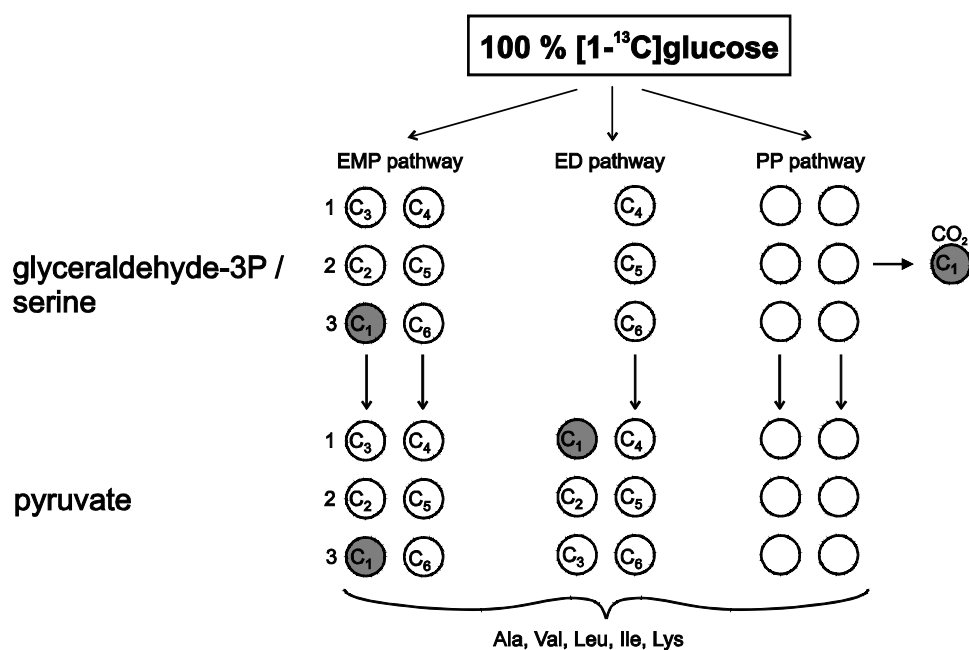


Figure 6 - Positional labeling in serine and pyruvate using 100% [1-¹³C]glucose. The circles represent C atoms. Numbering in the circles represents the original numbering in the glucose molecule, while numbering next to the circles represents serine and pyruvate C atoms. The gray circles represent the ¹³C-labeled C atoms. Abbreviations: ED pathway, Entner-Doudoroff pathway; PP pathway, pentose phosphate pathway.

To finally obtain quantitative carbon fluxes (i.e. mmol g⁻¹ h⁻¹), these ratios are used as constraints in flux balancing to obtain net flux distributions, which resemble the best fit to physiological parameters such as growth, glucose uptake and acetate production rate and the flux ratios (67). Basically, the method involves the known flux balance analysis approach using a defined reaction network, which also includes a biomass formation reaction (62, 233). The flux ratios and physiological parameters are needed as constraints to get a determined system, which yields feasible net flux solutions. With the previously published implementation into the programming platform MATLAB[®], it is possible to interactively modify reaction reversibilities, upper- and lower bounds, the physiological parameters and flux ratios (233).

Outline of this Thesis

In this thesis, central carbon and NADPH metabolism was quantitatively investigated for seven diverse species in **Chapter 2 and 3** followed by in depth analysis of the regulation of NADPH metabolism in *E. coli* in **Chapter 4 and 5**.

In **Chapter 2**, the metabolic network topology was analyzed and central carbon fluxes were quantified for *Agrobacterium tumefaciens*, *Pseudomonas fluorescens*, *Pseudomonas putida*, *Sinorhizobium meliloti*, *Rhodobacter sphaeroides*, *Zymomonas mobilis*, *Paracoccus versutus* and the two model species *Escherichia coli* and *Bacillus subtilis* during growth on glucose as the sole carbon source. These species represent fundamentally different metabolic lifestyles (aerobic, anaerobic, photoheterotrophic, and chemoheterotrophic), and are phylogenetically distinct (firmicutes, γ -proteobacteria, and α -proteobacteria).

In **Chapter 3**, the ^{13}C -quantified carbon fluxes of **Chapter 2** were used, together with experimentally determined cofactor specificities of key NADPH producing enzymes, to quantify the NADPH balances. The coupling between catabolism and anabolism via NADPH was elucidated in the different species and potential mechanisms involved in NADPH balancing are discussed. A main conclusion from **Chapter 2 and 3** is that *E. coli* features a rather exceptional metabolism, both with respect to flux distribution and cofactor specificities. Transhydrogenases were shown to play an important role in *E. coli*.

Their regulation was therefore investigated in more detail in **Chapter 4**. Potential regulation at the genetic level was analyzed by measuring the expression levels of *E. coli* transhydrogenase. Using GFP reporter plasmids, expression levels and dynamics of both transhydrogenases PntAB and UdhA were systematically recorded for different growth conditions. Different metabolic mutants and growth substrates were used to perturb NADPH metabolism.

In **Chapter 5**, we investigated how and why *E. coli* metabolism chooses between the membrane-bound transhydrogenase PntAB and the PP pathway to generate NADPH in *E. coli*. Both are two alternative mechanisms for NADPH generation and could compensate for each other. We reevaluated the kinetic properties of two dehydrogenases of the oxidative PP pathway, glucose-6P- and 6P-gluconate dehydrogenase (Fig. 1). Together with intracellular

concentrations of the involved metabolites, the kinetic properties of the PP pathway were investigated in *E. coli* wild-type and mutants with perturbed NADPH metabolism. In addition, the energetic and thermodynamic properties of PP pathway and membrane-bound transhydrogenase are compared.

Additional projects

In addition to the chapters presented here, following collaboration projects covered other specific questions, which are not part of this PhD thesis:

Revelles, O., M. Espinosa-Urgel, T. Fuhrer, U. Sauer, and J. L. Ramos. 2005.

“Multiple and interconnected pathways for L-lysine catabolism in *Pseudomonas putida* KT2440.” *J. Bacteriol.* **187**:7500-7510.

P. putida KT2440 has different parallel pathways for L-lysine degradation. To shed more light on this matter, labeled L-lysine was used as additional carbon source and its fate was traced by the same approach as for the GC-MS analysis in **Chapter 2** together with qualitative detection of intracellular degradation products (166). **Own contribution:** Assistance in experimental work, adaptation of MATLAB[®] based software, data analysis and writing part of the manuscript.

Nanchen, A., T. Fuhrer, and U. Sauer. 2006.

“Determination of metabolic flux ratios from ¹³C-experiments and gas chromatography-mass spectrometry data: protocol and principles.” *Methods. Mol. Biol.* **358**:177-198.

This book chapter is a tutorial on metabolic flux ratio analysis in detail covering all aspects of experimental sample treatment, GC-MS analysis and data interpretation using MATLAB[®] as used for **Chapter 2** (135). **Own contribution:** Writing part of the manuscript and generating part of the figures.

del Castillo, T., J. L. Ramos, J. J. Rodriguez-Herva, T. Fuhrer, U. Sauer, and E. Duque. 2007.

“Convergent peripheral pathways catalyze initial glucose catabolism in *Pseudomonas putida*: genomic and flux analysis.” J. Bacteriol. **189**:5142-5152.

Upper part of glucose degradation and its uptake routes in *P. putida* KT2440 were investigated in more details using knock-outs in these routes. Besides precise physiological characterization, METAFoR analysis was used to track changes in the relative flux distribution due to the mutations (46). **Own contribution:** Assistance in experimental work, adaptation of MATLAB® based software, data analysis and writing part of the manuscript.

Fuhrer, T., L. Chen, U. Sauer, and D. Vitkup. 2007.

Computational prediction and experimental verification of the gene encoding the NAD⁺/NADP⁺-dependent succinate semialdehyde dehydrogenase in *Escherichia coli*. J. Bacteriol. **189**:8073-8078.

Cofactor specificity not only plays an important role in central carbon metabolism but also under very specific growth conditions. Here we investigated degradation of alternative nitrogen sources such as γ -amino butyric acid or hydroxyphenyl-acetic acid. In this degradation pathway, *yneI* was predicted by computation to encode the succinate semialdehyde dehydrogenase using a gap-filling algorithm. The prediction was confirmed by extensive experimental data, which also revealed that *yneI* accepts both NADPH and NADH as cofactor (74). **Own contribution:** Experimental verification of the gene prediction done by Lifeng Chen, which included detailed physiological characterization of knock-out mutant as well as enzyme overexpression, purification and characterization. Writing the main part of the manuscript.

Reher, M., T. Fuhrer, U. Sauer, and P. Schoenheit. 2008.

manuscript in preparation.

As mentioned in the introduction, different variations of the ED pathway for glucose degradation are known to be present in archaea. This was investigated in detail for *Picrophilus torridus* by the use of both enzymatic analyses and labeling experiments (manuscript in preparation). **Own contribution:** GC-MS measurements, subsequent data analysis and writing part of the manuscript.

Chapter 2

Experimental identification and quantification of glucose metabolism in seven bacterial species

Tobias Fuhrer, Eliane Fischer and Uwe Sauer

Institute of Molecular Systems Biology, ETH Zürich, Zürich, Switzerland

Journal of Bacteriology, 2005, Vol. 187, No. 5, p. 1581–1590

Eliane Fischer designed the project, supervised the work and contributed to the writing.
Prof. Dr. Uwe Sauer designed the project, supervised the work and contributed to the writing.

Abstract

The structurally conserved and ubiquitous pathways of central carbon metabolism provide building blocks and cofactors for the biosynthesis of cellular macromolecules. The relative use of pathways and reactions, however, varies widely between species and conditions and some are not used at all. Here, we identify the network topology of glucose metabolism and its in vivo operation by quantification of intracellular carbon fluxes from ^{13}C -tracer experiments. Specifically, we investigated *Agrobacterium tumefaciens*, two pseudomonads, *Sinorhizobium meliloti*, *Rhodobacter sphaeroides*, *Zymomonas mobilis* and *Paracoccus versutus*, which grow on glucose as the sole carbon source, represent fundamentally different metabolic life styles (aerobic, anaerobic, photoheterotrophs and chemoheterotrophs), and are phylogenetically distinct (firmicutes, γ -proteobacteria and α -proteobacteria). When compared to the model bacteria *Escherichia coli* and *Bacillus subtilis*, metabolism in the investigated species differed significantly in several respects: i) the Entner-Doudoroff pathway was the almost exclusive catabolic route, ii) the pentose phosphate pathway exhibited exclusively biosynthetic functions, in many cases requiring also flux through the non-oxidative branch, iii) all aerobes exhibited fully respiratory metabolism without significant overflow metabolism, and iv) all aerobes used the pyruvate bypass of the malate dehydrogenase reaction to a significant extent. Exclusively, *Pseudomonas fluorescens* converted most glucose extracellularly to gluconate and 2-keto-gluconate. Overall, the results suggest that metabolic data from model species with extensive industrial and laboratory history are not representative for microbial metabolism, at least not quantitatively.

Introduction

Based on ^{13}C tracer experiments, metabolic flux analysis emerged as a key methodology to identify the network topology of active reactions and to quantify the in vivo distribution of molecular fluxes throughout metabolism (178, 222). In contrast to global protein, mRNA, or metabolite concentration analyses that assess network composition, flux methods directly assess the operation of metabolic networks by quantifying in vivo reaction velocities. The general principle is based on MS or NMR detection of ^{13}C -pattern in products of metabolism. Often protein-bound amino acids are used that preserve the carbon backbone of the eight metabolic key intermediates. The ^{13}C -isotope patterns reflect the activity of intracellular pathways and reactions, whose fluxes can be quantified from the isotope data by using mathematical models of varying complexity. In the simplest approach, algebraic equations are used to determine strictly local ratios of converging fluxes analytically by so-called metabolic flux ratio (METAFor) analysis (23, 65, 181, 203). Absolute intracellular fluxes in mmol per g biomass and h may be estimated indirectly by combining such ^{13}C -data with quantitative physiological data on fluxes in and out of cells (222). In this case, the estimated fluxes are the best fit to the available data within the specified metabolic model. Beyond the quantification of flux through the well-known biochemical pathways, flux methods have recently demonstrated their value for the identification of novel (66) or unexpected metabolic pathways (86, 154, 179, 180).

For obvious reasons, such flux methods were primarily applied to model microbes with industrial relevance such as *Escherichia coli* (60, 98, 181), *Bacillus subtilis* (43, 180), *Corynebacterium glutamicum* (129, 223), or *Saccharomyces cerevisiae* (23, 80). While the accumulated biochemical and metabolic data on these species are also the basis of much of our textbook knowledge, it is clear that these model species are not representative for all, perhaps not even most microbes. One example is the widely distributed Entner-Doudoroff (ED) pathway (35, 107) whose genes are absent from *B. subtilis*, *S. cerevisiae* and *C. glutamicum*, and which is used by *E. coli* mainly during growth on gluconate (58). For glucose metabolism, all four model species rely primarily on the Emden-Meyerhof-Parnas (EMP) pathway and, in some cases, to a substantial extent also on the pentose phosphate (PP)

pathway (43, 65, 80, 223, 235). This raises the general question on how representative the accumulated metabolic knowledge on these model species is. Here we attempt a quantitative comparison of intracellular metabolism in the two model microbes *E. coli* and *B. subtilis* with seven metabolically and phylogenetically distinct species that can grow on glucose as the sole carbon source.

In particular, we identify the network topology of active reactions by METAFoR analysis based on GC-MS analysis of proteinogenic amino acids from [U-¹³C] and [1-¹³C]glucose batch experiments (65). Quantification of in vivo molecular fluxes is then achieved by ¹³C-constrained flux analysis (67, 180). In particular, we chose the anaerobic *Zymomonas mobilis*, the rhizobiaceae *Agrobacterium tumefaciens* and *Sinorhizobium meliloti*, the metabolically versatile facultative phototroph *Rhodobacter sphaeroides*, the facultative autotroph *Paracoccus versutus*, and versatile pseudomonads *Pseudomonas fluorescens* and *Pseudomonas putida*.

Materials and Methods

Strains, media and growth conditions

The following 9 bacterial species were analyzed: *A. tumefaciens* C58 (F. Narberhaus), *P. fluorescens* 52-1C (B. Witholt), *P. putida* KT2440 (B. Witholt), *R. sphaeroides* ATH 2.4.1 (German Collection of Microorganisms and Cell Cultures, DSMZ 158), *P. versutus* A2 (DSMZ 582), *S. meliloti* (DSMZ 1981) and *Z. mobilis* NRRL B-806 (DSMZ 424), as well as *E. coli* MG1655 (*E. coli* Genetic Stock Center 6300) and *B. subtilis* 168 *trpC2* (*Bacillus* Genetic Stock Center). Aerobic batch cultures were grown at 30°C in 500 mL baffled flasks with 50 mL of M9 minimal medium (*P. versutus* and *Z. mobilis* were grown in special minimal media) on a gyratory shaker at 225 rpm (250 rpm for *P. fluorescens*). Anaerobic cultures of *Z. mobilis* were grown at 30°C in 125 mL sealed glass flasks with 50 mL minimal medium on magnetic stirrers at 225 rpm. The sterile medium was gassed with sterile filtered N₂ for 15 min.

The M9 minimal medium contained per liter of deionized water: 7.52 g Na₂HPO₄•2H₂O, 3.0 g KH₂PO₄, 0.5 g NaCl and 2.5 g (NH₄)₂SO₄. The following components were sterilized separately and then added (per liter of final medium): 1 mL 0.1 M CaCl₂, 1 mL 1 M MgSO₄, 0.6 mL 100 mM FeCl₃, 2 mL of vitamin solution (filter sterilized) and 10 mL M9 trace salts solution. The vitamin solution contained (per 50 mL): 25 mg of each biotin, cyanocobalamin, niacin, calcium pantothenate, pyridoxine HCl and thiamine HCl. The M9 trace salts solution contained (per liter): 0.18 g ZnSO₄•7H₂O, 0.12 g CuCl₂•2H₂O, 0.12 g MnSO₄•H₂O and 0.18 g CoCl₂•6H₂O. For *R. sphaeroides* a special trace salts solution was used that contained (per liter): 1.5 g nitrilotriacetic acid, 3.0 g MgSO₄•7H₂O, 0.5 g MnSO₄•H₂O, 1.0 g NaCl, 0.1 g FeSO₄•7H₂O, 0.1 g CoCl₂•6H₂O, 0.135 g CaCl₂•2H₂O, 0.1 g ZnSO₄•7H₂O, 0.01 g CuSO₄•5H₂O, 0.01 g H₃BO₃, 0.01 g Na₂MoO₄•2H₂O, 0.015 g NiCl₂, 0.02 g Na₂SeO₃, and the pH was adjusted to 6.5 with KOH.

The *Z. mobilis* minimal medium contained (per liter): 0.18 g KH₂PO₄, 0.082 g MgSO₄•7H₂O, 0.002 g FeSO₄•7H₂O, 0.87 g NH₄Cl, 0.142 g trisodium citrate dihydrate, 10 g potassium hydrogen phthalate and 2 mL of the above vitamin solution (filter sterilized). The pH was adjusted to 5.8 with KOH. The *P. versutus* minimal medium was composed of two

solutions that were mixed at a ratio of 1:10 after heat sterilization. Solution A contained (per 100 mL): 4.2 g $\text{Na}_2\text{HPO}_4 \cdot 2 \text{H}_2\text{O}$, 1.5 g KH_2PO_4 and 1.0 g NH_4Cl , and pH was adjusted to 9.0. Solution B contained (per liter): 0.1 g $\text{MgSO}_4 \cdot 7 \text{H}_2\text{O}$ and 5.0 ml trace salts solution, and the pH was adjusted to 6.0 with KOH. The trace salts solution contained (per liter): 50.0 g EDTA, 22.0 g $\text{ZnSO}_4 \cdot 7 \text{H}_2\text{O}$, 5.54 g $\text{CaCl}_2 \cdot 2 \text{H}_2\text{O}$, 5.06 g $\text{MnCl}_2 \cdot 4 \text{H}_2\text{O}$, 4.99 g $\text{FeSO}_4 \cdot 7 \text{H}_2\text{O}$, 1.10 g $\text{MoNH}_4 \cdot 4 \text{H}_2\text{O}$, 1.57 g $\text{CuSO}_4 \cdot 5 \text{H}_2\text{O}$ and 1.61 g $\text{CoCl}_2 \cdot 6 \text{H}_2\text{O}$.

In all experiments, sterile glucose was supplemented at a final concentration of 3 g/L glucose (4 g/L for *P. fluorescens* and 10 g/L for *Z. mobilis*). For ^{13}C -labeling experiments, glucose was added either entirely as the $[1-^{13}\text{C}]$ labeled isotope isomer (99%; Omicron Biochemical's Inc., South Bend, IN) or as a mixture of 20% (w/w) $[\text{U}-^{13}\text{C}]$ (> 99%; Martek Biosciences Corporation, Columbia, MD) and 80% (w/w) natural glucose. To elucidate the influence of unlabeled CO_2 on the ^{13}C -labeling patterns of *Z. mobilis*, cultures were continuously flushed with filter-sterilized technical CO_2 through an inlet and outlet needle.

Analytical procedures and physiological parameters

Cell growth was monitored by measuring the optical density at 600 nm. Glucose and acetate concentrations were determined enzymatically with commercially available kits (Beckman, Enzytec, and Boehringer Mannheim). Ethanol concentrations were quantified by gas chromatography (GC) in a Hewlett Packard 5890 Series II Plus using a Macherey-Nagel fused silica capillary column (Permaabond-CW20M-0.25, 25 m \times 0.25 mm ID) with butyrate as the internal standard. Organic acids in culture supernatants were detected by high-pressure liquid chromatography (HPLC) analysis (Perkin Elmer) at a wavelength of 210 nm, using a Supelcogel C8 column (4.6 by 250 mm) and 0.2% (vol/vol) sulfuric acid as the mobile phase at a flow rate of 0.3 ml/min and at 30°C. The following physiological parameters were determined by regression analysis during the exponential growth phase in batch culture as described previously (181): maximum specific growth rate, biomass yield on glucose, specific glucose consumption and byproduct formation rates. Cellular dry weight (CDW) was inferred from OD_{600} measurements using a predetermined correlation factor k . To determine k , CDW was determined from at least 4 parallel 2 ml cell suspensions that were harvested by centrifugation at $15,800 \times g$ in an Eppendorf table top centrifuge using pre-dried and weighed

2 ml Eppendorf cups. The pellets were washed with 0.9% NaCl and dried at 105° C for 24 h to constant weight.

For *P. fluorescens*, the theoretical extracellular pool concentration of gluconate/2-keto-gluconate d was calculated from the integrated product of the specific growth rate μ_{max} and the gluconate/2-keto-gluconate accumulation rate c :

$$d = \int_0^t c \times k \times (m \times e^{\mu_{max} \times t}) dt \quad (1)$$

where m was a coefficient, c the glucose decrease rate minus the total carbon uptake rate and t the time in hours for growth on glucose.

Sample preparation and GC-MS analysis

Cell aliquots were harvested during mid-exponential growth by centrifuging 35-40 ml culture broth at $1200 \times g$ and 4°C for 20 min. The pellet was washed twice with 1 ml 0.9% NaCl, hydrolyzed in 1.5 ml 6 M HCl for 24 h at 110°C in sealed 2 ml Eppendorf tubes and desiccated overnight in a heating block at 85°C under a constant air stream. The hydrolyzate was dissolved in 50 μ l 99.8% dimethyl formamide and transferred into a new Eppendorf cup within a few seconds. For derivatization, 30 μ l N-methyl-N-(tert-butyldimethylsilyl)-trifluoroacetamide were added, which readily silylates hydroxyl groups, thiols, primary amines, amides and carboxyl groups (41), and the mixture was incubated at 550 rpm and 85°C for 60 min. 1 μ l of the derivatized sample was injected into a Series 8000 GC, combined with a MD 800 mass spectrometer (MS) (Fisons Instruments) and analyzed as described earlier (41, 65).

Metabolic flux ratio analysis

For METAFoR analysis, mass spectra of the derivatized amino acids alanine, glycine, valine, leucine, isoleucine, proline, serine, threonine, phenylalanine, aspartate, glutamate, histidine and tyrosine were corrected for the natural abundance of all stable isotopes and unlabeled biomass from inoculum. Lysine and methionine are not required for METAFoR analysis used in this study whereas arginine, asparagine, cysteine, glutamine and tryptophane

are not detectable. The amino acids are synthesized from one or more metabolic intermediates and the mass isotopomer distribution vectors (MDV) of these metabolites could easily be derived from the MDVs of the amino acids (65). The metabolite MDVs were then used to calculate the fractional contribution of a given pathway or reaction to a target metabolite pool (metabolic flux ratios) by using sets of algebraic equations implemented in MATLAB-based program Fiat Flux Version 1.04 as described previously (65). The end result is direct and quantitative evidence for strictly local ratios of two or more reactions / pathways to a metabolic intermediate.

Net flux analysis and master reaction network

The metabolic models used for net flux analysis were based on the master reaction network shown in Fig. 1, which included 45 reactions and 33 metabolites. Respiration, biomass formation and a transhydrogenase reaction were included as additional reactions, and ATP and the cofactors NADH and NADPH as additional metabolites. Net fluxes were then calculated using (i) the stoichiometric reaction matrix, (ii) the METAFoR-derived flux ratios, (iii) physiological data and (iv) precursor requirements for biomass synthesis, as was described before (67). Specifically, the following flux ratios were used: serine derived through the EMP pathway, pyruvate derived through the ED pathway, oxaloacetate (OAA) originating from phosphoenolpyruvate (PEP) or pyruvate, PEP originating from OAA, the lower and upper bounds of pyruvate originating from malate, and the upper bound of PEP derived through the PP pathway. For the particular stoichiometric matrix of each organism, several reactions were omitted from the master network based on information from the ^{13}C -labeling experiments and literature knowledge (see below). The stoichiometric matrix was then solved with the MATLAB-based program Netto Version 1.04 (67) by minimizing the sum of the weighted square residuals of the constraints from both metabolite balances and flux ratios to obtain estimated net fluxes.

Biomass requirements and organism-specific networks

E. coli and *B. subtilis* were routinely analyzed as control experiments using the previously established growth rate-dependent biomass requirements and network models (42, 60). For

the gram-negative *P. fluorescens*, *P. putida*, *S. meliloti*, *A. tumefaciens* and *R. sphaeroides*, the biomass requirements were assumed to be similar to *E. coli* (60), and for the gram-positive *P. versutus* the requirements were taken from the *B. subtilis* model (42). For *Z. mobilis* the precursor requirements were based on the published biomass composition (44).

The metabolic network used for *Z. mobilis* lacks a functional EMP pathway due to the absence of the key enzyme phosphofructokinase. Furthermore, the TCA cycle is incomplete and it does not contain a transaldolase, thus pentoses are synthesized from fructose-6P and glyceraldehyde-3P via the reversible transketolase (44, 140, 147). The resulting network of *Z. mobilis* included the following reactions (compare with Fig. 1): 1-3, 6-14, 16-18, 21-23, 30 and 31. The network model for *P. fluorescens* and *P. putida* was adapted from previous literature (118, 215). Besides the direct uptake, glucose may also be converted extracellularly to gluconate and 2-keto-gluconate, both of which can be taken up by the cell. Additionally the EMP pathway is absent due to the lack of phosphofructokinase. Thus, the network of both pseudomonads included the following reactions: 1-3, 5-22, 24, 25, 37 and 39-42. Reaction 5 principally enables a cyclic flux through the ED pathway that could not be resolved by the present ^{13}C -labeling experiments, nevertheless a weak flux was obtained through reaction 5 in *P. putida* (see Appendix). The network models for *A. tumefaciens* and *S. meliloti* were basically the same as that of *P. fluorescens* (11, 55, 83, 100, 157). Since we did not detect gluconate or 2-keto-gluconate accumulation, however, glucose uptake was assumed to be direct in both organisms. Thus, the networks consisted of the reactions 1-3, 5-22, 24 and 25. The network models for the metabolically versatile *R. sphaeroides* (34, 35, 93, 229) and *P. versutus* (227) included the reactions 1-4, 6-22, 24 and 25.

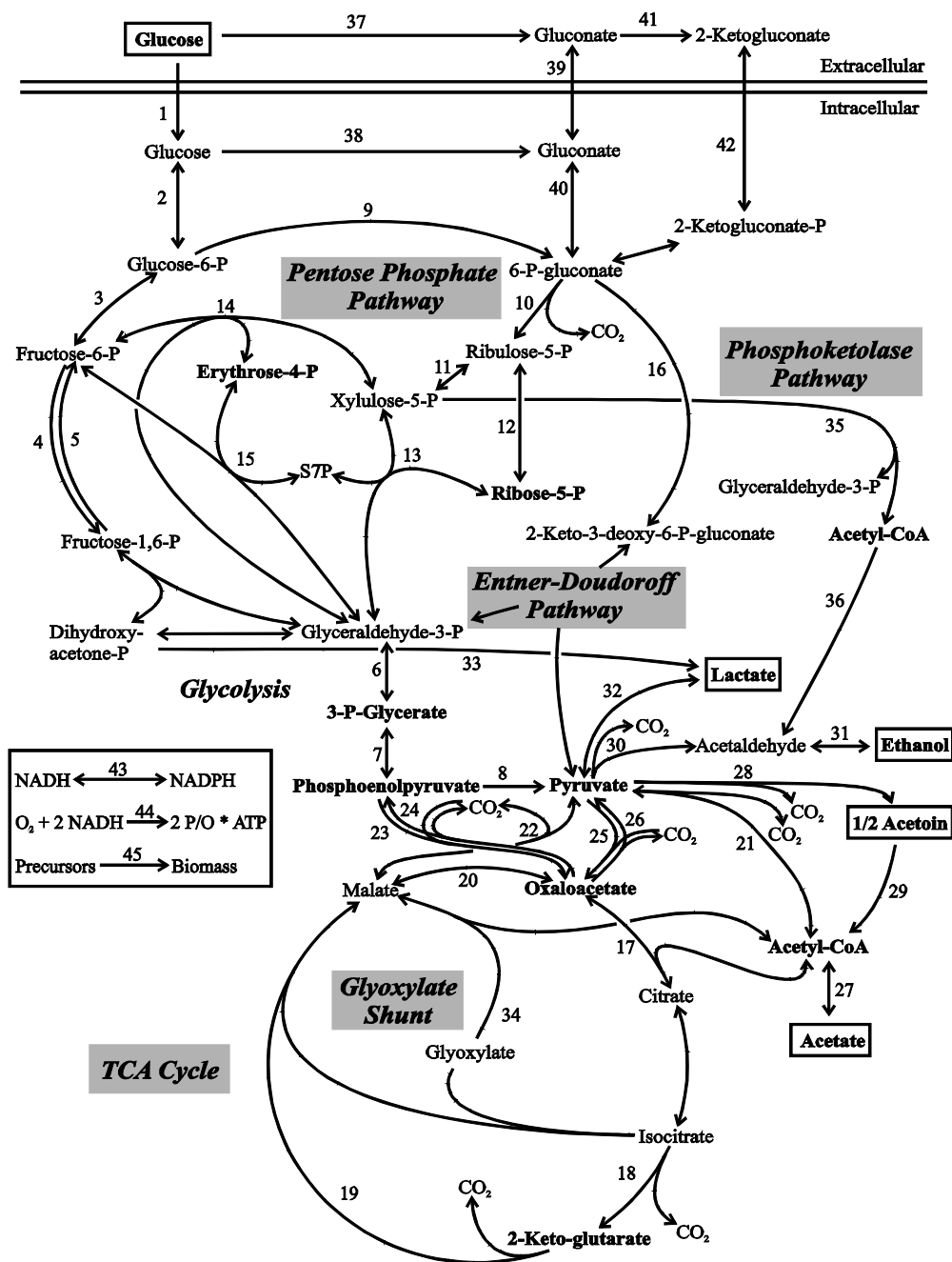


Figure 1 - Master reaction network that was used as the basis for net flux analysis. Metabolites in bold were precursors for amino acid biosynthesis and metabolites in boxes were extracellular substrates or products. Doubled-headed arrows indicate the assumed reaction reversibility. Abbreviation: sedoheptulose-7P, S7P.

Results

Network identification and flux analysis

To experimentally identify metabolic networks of active reactions, we used ^{13}C -constrained metabolic flux analysis that relies on the detection of mass isotopomer pattern in proteinogenic amino acids (65, 67). Since amino acid biosynthesis may differ between species, we first verified the biosynthetic routes. For each amino acid, the labeling pattern depended on that of the precursor it was synthesized from, e.g. the alanine carbon skeleton is derived from pyruvate. Since valine and leucine are typically synthesized also from pyruvate, the redundant information in all three amino acids must be identical if indeed synthesized from pyruvate. Generally, all detected labeling patterns were consistent with the amino acid biosynthesis pathways of *E. coli* (203) and no discrepancies were detected within the labeling patterns of the redundant amino acids.

Based on the established amino acid biosynthesis schemes, we then calculated intracellular flux ratios from the labeling patterns of the amino acids by using the algebraic equations of METAFoR analysis (65). These flux ratios represent direct, local evidence for the in vivo activity of particular pathways and reactions. From the thus elucidated network topology of active reactions and literature data, organism-specific metabolic reaction models were deduced from the master network model (Fig. 1). Absolute net fluxes were then calculated with these network models from the physiological data (Table 1) and the flux ratios (Table 2) (67, 180). Since the analytically determined flux ratios constrain the flux within their experimental error, this approach is referred to as ^{13}C -constrained flux analysis.

Table 1 - Growth physiology

Organism	Max. specific growth rate (h ⁻¹)	Biomass yield (g _{CDW} /g _{glucose})	Glucose uptake (mmol g ⁻¹ h ⁻¹)	By-product accumulation (mmol g ⁻¹ h ⁻¹) ^a
<i>Z. mobilis</i>	0.34 ± 0.03	0.03 ± 0.01	61.5 ± 2.1	102.1 ± 5.0
<i>P. fluorescens</i>	0.49 ± 0.03	0.44 ± 0.01	4.5 ± 0.1 ^b	-
<i>S. meliloti</i>	0.17 ± 0.01	0.41 ± 0.02	2.3 ± 0.1	-
<i>A. tumefaciens</i>	0.3 ± 0.01	0.41 ± 0.04	4.1 ± 0.2	-
<i>P. versutus</i>	0.70 ± 0.01 ^c	0.21 ± 0.03	18.9 ± 2.1	-
<i>R. sphaeroides</i>	0.15 ± 0.02	0.41 ± 0.06	1.8 ± 0.1	-
<i>E. coli</i>	0.39 ± 0.01	0.30 ± 0.03	7.8 ± 0.4	3.5 ± 0.1
<i>B. subtilis</i>	0.30 ± 0.03	0.35 ± 0.01	4.8 ± 0.3	2.1 ± 0.1

^a The detected by-products were: ethanol for *Z. mobilis* and acetate for *E. coli* and *B. subtilis*. The following metabolites were determined by HPLC to be present only in trace amounts: citrate, formate, fumarate, malonate, pyruvate and succinate.

^b Total substrate uptake rate.

^c Values were determined from the culture that was fully adapted to growth on glucose (after 2 subcultivations).

Z. mobilis

Without a respiratory chain, *Z. mobilis* is an obligate fermenter and produces a single ATP molecule per molecule of metabolized glucose. This energetically ineffective metabolism leads to very high fermentative fluxes with a very low biomass yield of 20 mg cells per g glucose (50). Among the species investigated here, the glucose uptake rate of *Z. mobilis* was at least an order of magnitude higher than that of most others (Fig. 2A, Table 1). This flux was exclusively catalyzed by the ED pathway (Fig. 2A, Table 2), the enzymes of which constitute up to 50% of the cell's total protein (194). Absence of the EMP pathway was confirmed in [1-¹³C]glucose experiments, where no ¹³C-label was detected at the C3 position of pyruvate due to the missing phosphofructokinase (data not shown). The absence of transaldolase (44) was also verified from the pentose labeling patterns in the 20% [U-

^{13}C]glucose experiment that were consistent with that expected when only transketolase B is active (Table 3).

Table 2 - Metabolic flux ratios obtained by METAFoR analysis of 100% [$1\text{-}^{13}\text{C}$]glucose and 20% [$\text{U-}^{13}\text{C}$] / 80% naturally labeled glucose experiments^a

Organism	Relative split ratios (%)						
	Ser through glycolysis ^b	Pyr through EDP ^b	PEP through PPP (ub)	OAA from PEP (or Pyr)	PEP from OAA	Pyr from Mal (lb)	Pyr from Mal (ub)
<i>Z. mobilis</i>	- ^c	100 ± 1	-	99 ± 4	1 ± 1	-	-
<i>P. fluorescens</i>	-	91 ± 1	2 ± 5	85 ± 4	17 ± 1	17 ± 2	55 ± 11
<i>S. meliloti</i>	-	95 ± 1	0 ± 5	34 ± 2	6 ± 7	13 ± 2	19 ± 3
<i>A. tumefaciens</i>	-	86 ± 1	0 ± 5	39 ± 2	10 ± 1	11 ± 1	18 ± 2
<i>P. versutus</i>	0 ± 1	100 ± 1	26 ± 5	44 ± 2	6 ± 1	11 ± 2	19 ± 3
<i>R. sphaeroides</i>	0 ± 1	100 ± 1	0 ± 5	46 ± 2	4 ± 1	13 ± 1	22 ± 3
<i>E. coli</i>	79 ± 1	7 ± 3	1 ± 5	63 ± 4	3 ± 1	0 ± 2	0 ± 4
<i>B. subtilis</i>	62 ± 1	-	27 ± 5	62 ± 3	5 ± 1	2 ± 2	5 ± 5

^a Abbreviations: serine (Ser), pyruvate (Pyr), ED pathway (EDP), phosphoenolpyruvate (PEP), PP pathway (PPP), oxaloacetate (OAA), malate (Mal) and upper and lower bound (ub, lb respectively).

^b Split ratios obtained from 100% [$1\text{-}^{13}\text{C}$]glucose experiments.

^c Pathway was considered to be absent based on literature data.

Although the EMP pathway was inactive, ^{13}C -label was detected at the C3 position of serine from 100% [$1\text{-}^{13}\text{C}$]glucose experiments (Table 4). Thus, labeled carbon must have been introduced through C1-metabolism (Fig. 3). The tetrahydrofolyl (THF) cycle is replenished with C1 that originates from formate, which in turn is generated from pyruvate via pyruvate formate lyase or from CO_2 via formate dehydrogenase. To differentiate between the two routes, we (i) added formate to strongly reduce the fraction of labeled formate in the medium, and (ii) continuously gassed the culture with unlabelled CO_2 , which should dilute the serine label if the formate dehydrogenase was active. Although noticeable, the influence of unlabeled CO_2 on the m_1 signal of serine was far less significant than adding formate

(Table 4). This indicates that pyruvate formate-lyase rather than formate dehydrogenase generates the formate in *Z. mobilis* that leads to C3-labeled serine.

Table 3 - Mass isotopomer distribution in pentose-5-P in *Z. mobilis*^a. The data are from a 20% [U-¹³C]glucose experiment and the theoretical patterns were calculated assuming only transketolase B or transaldolase and transketolase A to be active

Fractional labeling	m_0^b	m_1	m_2	m_3	m_4	m_5
Pentose-5-P 1-5	0.67	0.00	0.15	0.14	0.00	0.04
Transketolase B ^c	0.64	0.00	0.16	0.16	0.00	0.04
Transketolase A + Transaldolase ^d	0.66	0.13	0.02	0.06	0.03	0.10

^a Mass isotopomer distribution in pentose-5-P was deduced from the mass isotopomer distribution in histidine.

^b m_0 is the fractional abundance of the fragments with the lowest mass and $m_{i>0}$ the abundances of molecules with higher masses.

^c Theoretical pattern expected from exclusive operation of transketolase B, which cleaves fructose-6-P into a C₂ and a C₄ fragment. The C₂ and the C₃ fragment originating from glyceraldehyde-3-P combine to give the theoretical labeling pattern.

^d Theoretical pattern expected from the concerted operation of transaldolase (combines a C₁ from erythrose-4P with fructose-6P to give sedoheptulose-7P) and transketolase A (transfers a C₂ from sedoheptulose-7-P to glyceraldehyde-3-P to give two pentoses).

Pseudomonads

In *P. fluorescens*, but not in *P. putida*, extracellular glucose was converted to gluconate and 2-ketogluconate that were subsequently consumed during the later growth phase (Fig. 4), as was described before (57, 118, 206). Considering the simplified glucose uptake scheme shown in Fig. 5, the total gluconate/2-keto-gluconate accumulation rate c during growth on glucose was calculated as $15.21 \text{ mmol g}^{-1} \text{ h}^{-1}$ from the experimentally determined extracellular glucose decrease rate ($a = 19.75 \text{ mmol g}^{-1} \text{ h}^{-1}$) minus the total carbon uptake rate ($b = 4.54 \text{ mmol g}^{-1} \text{ h}^{-1}$). The experimentally determined extracellular concentration of gluconate and 2-keto-gluconate was consistent with that calculated from equation 1, which strongly suggests that there was no co-catabolism of gluconate/2-keto-gluconate during growth on glucose. Upon glucose depletion, the carbon uptake rate from both gluconate and 2-keto-gluconate almost doubled to $9.42 \text{ mmol g}^{-1} \text{ h}^{-1}$. Based on the above conclusions, the

total carbon uptake rate for net flux analysis was assumed to be exclusively from glucose in the first phase and from gluconate/2-keto-gluconate (e) in the second phase. The relative proportion of gluconate and 2-keto-gluconate uptake could not be resolved because the carbon skeleton remained unchanged, thus leading to identical labeling patterns.

Table 4 - Mass isotopomer distributions of serine in *Z. mobilis* at different formate concentrations

serine 1-3	m_0	m_1^a	m_2	m_3
control	0.601	0.394	0.004	0.000
1 mM formate	0.807	0.190	0.003	0.000
5 mM formate	0.835	0.164	0.000	0.001
CO ₂ aerated	0.665	0.334	0.001	0.001

^a m_1 mass fraction reveals the C1 position of pyruvate, assuming the pyruvate-formate lyase to be the predominant supply reaction for the C1-metabolism.

During growth on glucose, *P. fluorescens* secreted very little metabolic by-products (Table 1) and ED pathway and TCA cycle were the almost exclusive catabolic pathways prior to (Fig. 2B, Table 2) and after glucose depletion (data not shown). Unlike most other bacteria, however, the TCA cycle did not operate via malate dehydrogenase, but mostly via the so-called pyruvate shunt that is catalyzed by malic enzyme and pyruvate carboxylase (from malate to pyruvate to OAA). Moreover, a relatively high gluconeogenic flux of 17% through the PEP carboxykinase was detected. The higher carbon uptake rate of 9.42 mmol g⁻¹ h⁻¹ during the second growth phase resulted in a higher TCA cycle flux and a decreased biomass yield of 0.29, compared to 0.44 (g_{CDW}/g_{glucose}) during growth on glucose. In *P. putida*, very little gluconate or 2-keto-gluconate accumulated (below 2 mM), hence carbon uptake was most likely via the direct glucose uptake route. Net flux analysis with a lumped total carbon uptake resulted in a distribution that was very similar to that of *P. fluorescens* (data not shown).

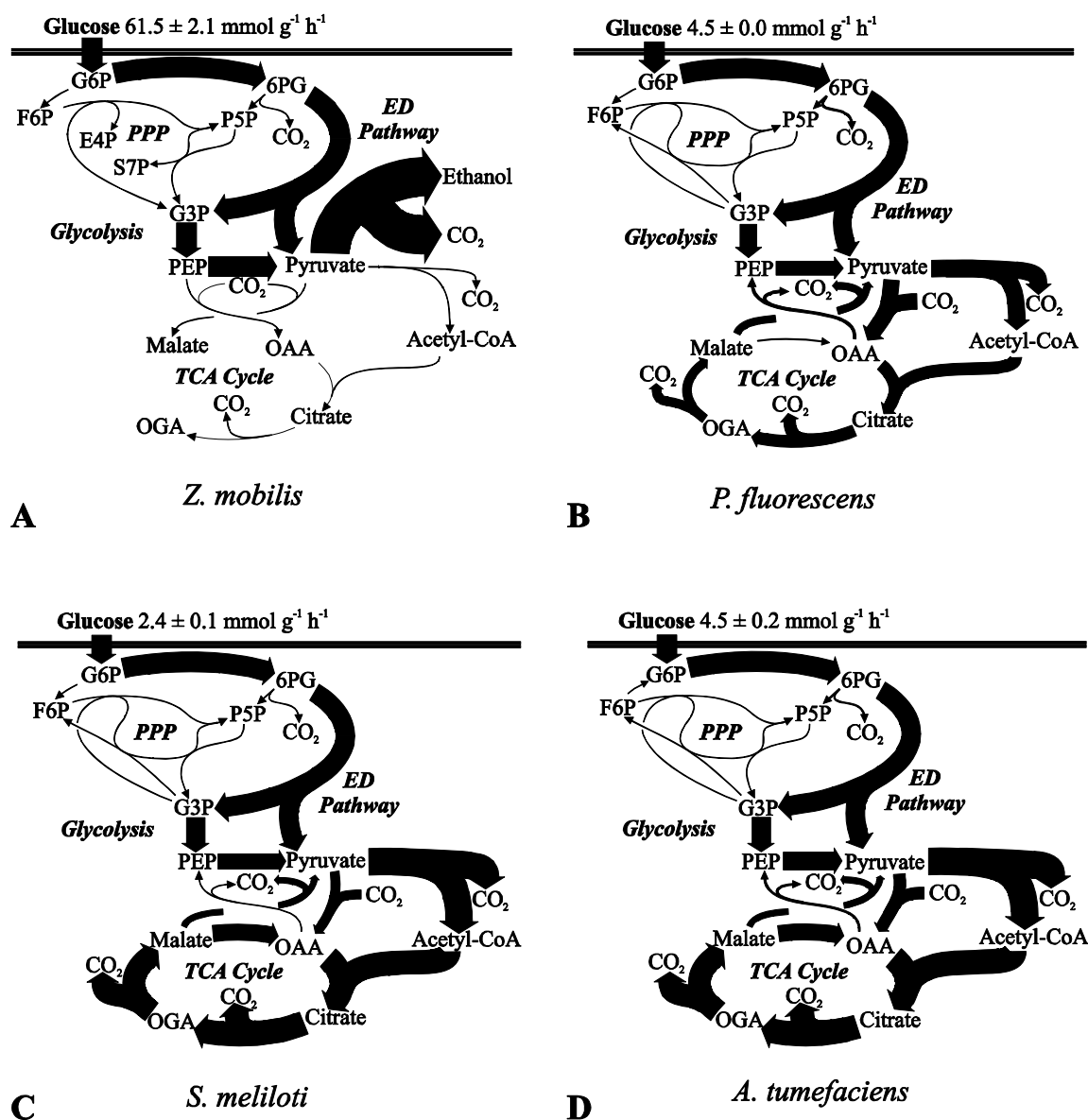


Figure 2 - In vivo carbon flux distribution in *Z. mobilis* (A), *P. fluorescens* (B), *S. meliloti* (C) and *A. tumefaciens* (D). All fluxes were normalized to the glucose uptake rate that is given at the top and the arrows are scaled to the relative flux in %. Fluxes below 2.6% of the glucose uptake rate are represented by non-scaled hairlines. Possible cyclic fluxes through the ED pathway in *P. fluorescens* and *S. meliloti* are not resolved by the data and are not shown. Generally, the 95% confidence intervals were between 5 to 10% for the major fluxes. Larger confidence intervals were estimated for reactions with low flux. Abbreviations: glucose-6P, G6P; 6P-gluconate, 6PG; fructose-6P, F6P; pentose-5P, P5P; erythrose-4P, E4P; sedoheptulose-7P, S7P; glyceraldehyde-3P, G3P; 2-keto-glutarate, OGA.

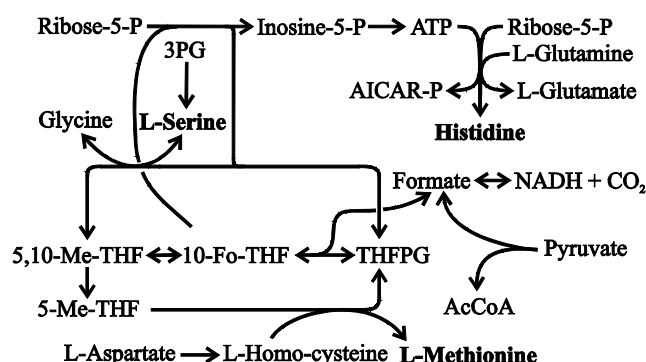


Figure 3 - Possible reactions that introduce C1 fragments into serine, methionine and histidine (131). Abbreviations: 5-aminoimidazole-4-carboxamide-1-ribotide, AICAR-P; tetrahydrofolylpolyglutamate, THFPG; 10-formyl-tetrahydrofolyl, 10-Fo-THF; 5,10-methyl-tetrahydrofolyl, 5,10-Me-THF; and 3P-glycerate, 3PG.

Rhizobiaceae

As a “fast”-growing rhizobium with a generation time of less than six hours on complex medium, *S. meliloti* was reported to be able to convert glucose to gluconate, which then enters metabolism (157, 200). Since less than 1 mM gluconate accumulated and the labeling data did not allow to resolve the different uptake routes, both were lumped for net flux analysis. In *S. meliloti*, pyruvate carboxylase was assumed as the anaplerotic reaction by analogy to *A. tumefaciens* (55). Both the PP and ED pathways were reported to be present and glycolysis absent in both rhizobia (11, 200), which was confirmed by METAFoR analysis (Table 2). In both rhizobia, the ED pathway was basically the exclusive pathway of glucose degradation, while the pentose-5-P precursors for biomass were generated through the oxidative and the non-oxidative branch of the PP pathway (Fig. 2C, D). With a flux well above 100% relative to the glucose uptake rate, both species exhibited higher TCA cycle fluxes than most species investigated here (Fig. 2C, D).

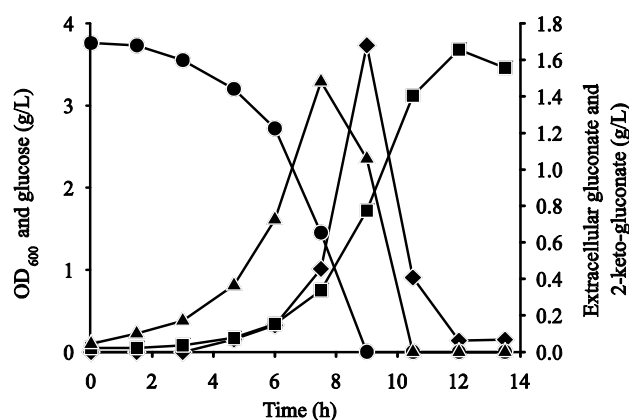


Figure 4 - Time course of OD₆₀₀ (squares), extracellular glucose (circles), gluconate (triangles) and 2-keto-gluconate (diamonds) in *P. fluorescens*.

P. versutus

As a member of the genus *Paracoccus*, *P. versutus* (synonyms: *Thiobacillus versutus* and *Paracoccus* A2) belongs to the group of α -proteobacteria and is closely related to the *Rhodobacteraceae* and distantly to pseudomonads (15). As a facultative autotroph, *P. versutus* is capable of heterotrophic growth on a wide range of organic substrates that include mono-, di- and trisaccharides (225). Extensive radiorespirometric and enzymatic analyses of the main carbon-degrading pathways indicated the presence of the EMP, ED and PP pathways (225-227). Consistent with the reported adaptation to growth on sole glucose, the specific rate of growth increased from 0.29 h^{-1} to 0.70 h^{-1} (Table 1). In the rapidly growing culture, METAFoR analysis revealed an inactive EMP pathway, some PP pathway activity and predominant catabolic flux through the ED pathway (Table 2). Since *P. versutus* exhibited the highest aerobic glucose uptake rate of all species investigated, it was surprising that its metabolism was fully respirative with very high TCA cycle flux (Fig. 6A).

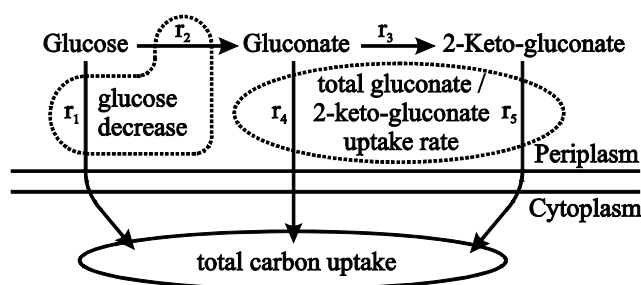


Figure 5 - Glucose uptake in *P. fluorescens*. The following fluxes are involved in glucose uptake: direct glucose uptake (r_1), membrane-bound glucose dehydrogenase (r_2) and gluconate dehydrogenase (r_3), uptake of gluconate (r_4) and 2-keto-gluconate (r_5). The experimentally determined extracellular glucose decrease rate a is split into $r_1 + r_2$, the total carbon uptake rate by the cell b is defined by $r_1 + r_4 + r_5$, and the total gluconate/2-keto-gluconate uptake rate e is given by $r_4 + r_5$.

R. sphaeroides

The purple, facultative photosynthetic bacterium *R. sphaeroides* has an unusually versatile metabolism, capable of aerobic chemoheterotrophic and anaerobic photoheterotrophic growth (112). Aerobic growth on glucose, however, was rather slow (Table 1). While the EMP and ED pathways were reported to be present (33, 34), only the ED pathway was active during aerobic growth on glucose (Table 1, Fig. 6B). The m_1 mass fractions of pyruvate 1-3 and 2-3 fragments (52% and 2% respectively; detected in alanine, isoleucine, leucine, lysine and valine) directly demonstrated exclusive use of the ED pathway, whereas the almost completely unlabelled PEP (detected in phenylalanine, tryptophane and tyrosine) verified the absence of EMP pathway flux (data not shown). Akin to most previously analyzed bacteria, glucose was catabolized almost exclusively via ED pathway and TCA cycle, with little by-product formation but some contribution of the pyruvate shunt via malic enzyme and pyruvate carboxylase (Fig. 6B). The PP pathway operated exclusively to provide precursors for biosynthesis and the EMP pathway catalyzed even small gluconeogenic fluxes from glyceraldehyde-3-P to fructose-6-P.

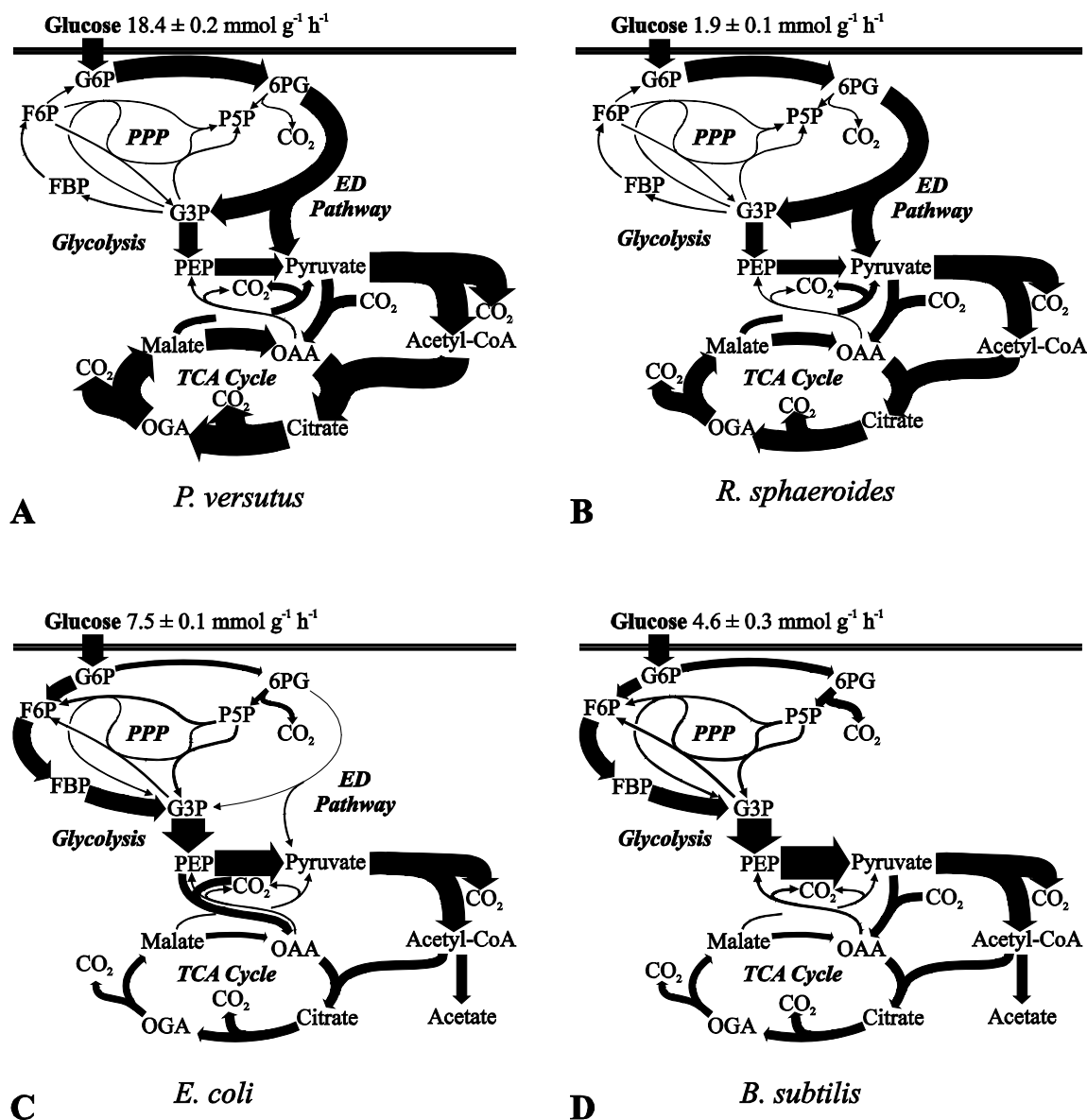


Figure 6 - In vivo carbon flux distribution in *P. versutus* (A), *R. sphaeroides* (B), *E. coli* (C) and *B. subtilis* (D). All fluxes were normalized to the glucose uptake rate that is given at the top and the arrows are scaled to the relative flux in %. Fluxes below 2.6% of the glucose uptake rate are represented by non-scaled hairlines. Generally, the 95% confidence intervals were between 5 to 10% for the major fluxes. Larger confidence intervals were estimated for reactions with low flux. Abbreviations: glucose-6P, G6P; 6P-gluconate, 6PG; fructose-6P, F6P; fructose-1,6-bisphosphate, FBP; pentose-5P, P5P; glyceraldehyde-3P, G3P; 2-keto-glutarate, OGA.

Table 5 - Relative molecular carbon flow into PP pathway and catabolic PP pathway flux

Organism	Flux into PP pathway (%) ^a	Catabolic PP pathway flux (%) ^b
<i>Z. mobilis</i>	0 ± 0	0 ± 0
<i>P. fluorescens</i>	10 ± 1	-2 ± 1 ^c
<i>S. meliloti</i>	4 ± 1	-2 ± 1
<i>A. tumefaciens</i>	6 ± 2	-1 ± 2
<i>P. versutus</i>	0 ± 2	-4 ± 2
<i>R. sphaeroides</i>	0 ± 5	-7 ± 5
<i>E. coli</i>	21 ± 4	12 ± 4
<i>B. subtilis</i>	38 ± 1	27 ± 1

^a Carbon flux into the PP pathway was calculated as the flux through 6-P-gluconate dehydrogenase divided by total carbon uptake rate.

^b For the catabolic PP pathway flux, CO₂ production and precursors flux of erythrose-4P and ribulose-5P into biomass were subtracted from 6P-gluconate dehydrogenase.

^c Negative values indicate backward flux into PP pathway from fructose-6P and/or glyceraldehyde-3P.

E. coli* and *B. subtilis

In sharp contrast to all other bacteria analyzed here, the gram-positive and gram-negative model bacteria *E. coli* and *B. subtilis* rely primarily on the EMP pathway for glucose catabolism (Fig. 6C, D). Moreover, the relative TCA cycle flux was much lower than in the other species because secretion of the incompletely oxidized overflow product acetate was extensive. With 38%, the PP pathway flux in *B. subtilis* was the highest observed in all species (Table 5). Generally, the overall estimated flux distribution in both species was similar to that obtained previously in 37°C batch cultures except the elevated TCA cycle activity in *E. coli* at 30°C and elevated anaplerosis (OAA from pyruvate) in *B. subtilis* at 30°C, which was due to lower relative acetate formation (179, 235). Apart from the about 30-50% lower growth rates, there were only minor changes that are related to the lower overall rate of metabolism at the 30°C used here.

Discussion

In all seven newly investigated species, the ED pathway was the almost exclusive route of glucose catabolism, while the EMP pathway was mostly absent and the PP pathway served exclusively biosynthetic functions. Although widely distributed (35, 107) and probably the oldest catabolic pathway (168), the predominance of the ED pathway was unexpected in species capable of all three routes of glucose catabolism such as *P. versutus* (225) or in *R. sphaeroides* (34). The generally held view of the EMP pathway as the major route of glucose catabolism may thus be a misconception because most quantitative metabolic studies were done with the model microbes *E. coli*, *B. subtilis*, *C. glutamicum*, and *S. cerevisiae* that exhibit unusually high glycolytic fluxes.

Beyond the ED pathway, the presented flux data reveal a number of additional “abnormalities” in glucose catabolism of the more frequently investigated model bacteria. Firstly, all non-model species used the PP pathway exclusively for biosynthesis of biomass precursors, and in many case the flux to the building blocks was through both the oxidative and the non-oxidative branches of the pathway (Table 5). In sharp contrast, the *E. coli* and *B. subtilis* PP pathway flux contributed substantially to catabolism (12 and 27%, respectively), which is consistent with previous analyses (179, 235) and also true for *C. glutamicum* (223). Secondly, the *E. coli* and *B. subtilis* TCA cycle flux was relatively low and metabolism not fully respiratory with extensive overflow metabolism that is also referred to as aerobic fermentation. None of the aerobic species investigated here exhibited this phenomenon to a significant extent, which is particularly surprising for species like *P. versutus* that exhibit much higher catabolic rates than the model microbes. Thus, it is not unreasonable to speculate that overflow metabolism is not a typical microbial trait but rather an adaptation to industrial or laboratory conditions. The most prominent example is *S. cerevisiae* that has been cultivated and selected over millennia by mankind and strongly increases its rate of aerobic fermentation at high growth rates (23). Thirdly, all aerobic, non-model species routed between 29 and 35% of their carbon flux through the so-called pyruvate shunt that bypasses malate dehydrogenase. In the case of *P. fluorescens*, the pyruvate shunt was the predominant

route of malate to OAA conversion. Although *B. subtilis* was reported to use the pyruvate bypass under glucose limitation (180), its activity is very low in glucose batch cultures (Fig. 6D) (235).

In addition to the linear ED pathway, which may be inducible as in *E. coli* during growth on gluconate or constitutive as in *Z. mobilis*, cyclic operation of the ED pathway was reported in organisms that lack phosphofructokinase, e.g. pseudomonads (118) or *S. meliloti* (100). In the absence of both phosphofructokinase and fructose-1,6-P aldolase, *A. tumefaciens* cannot operate a cyclic ED pathway but may alternatively use a cyclic PP pathway (11). Cyclic operation of either pathway is known from proteobacteria such as *Acetobacter*, *Agrobacterium*, *Azotobacter*, *Pseudomonas*, *Rhizobium*, *Paracoccus* and *Xanthomonas*, which preferentially utilize organic acids rather than sugars and secrete exopolysaccharides (156). The cyclic pathway operation may facilitate the formation of the polysaccharide precursor fructose-6P in cases where the EMP pathway is absent (83). The extent to which glyceraldehyde-3P is recycled into the ED pathway is unclear from the present data and may vary between species. However, an increased demand for fructose-6-P and also glucose-6-P due to (exo)polysaccharide synthesis was assumed to be negligible under non-nitrogen-limited batch culture conditions (81, 156, 238).

Ideally, identification of reaction networks and quantification of metabolic fluxes is based on annotated genome data, a large body of biochemical data, and comprehensive tracer experiments. Here we demonstrate that important quantitative information can also be inferred from a much smaller data basis than is typically available for model microbes by using well-designed ^{13}C -experiments. Besides the above quantification of the different catabolic routes in each species, several new findings were made. Although the overall glucose flux was, of course, from hexoses to trioses, low but significant gluconeogenic flux occurs in *R. sphaeroides* and *P. versutus* from glyceraldehyde-3P to glucose-6P. Both were also the only species where pentose phosphates were mostly synthesized via the non-oxidative branch of the PP pathway, despite high catabolic fluxes passing through the other possible precursor, 6P-gluconate. During the first growth phase, *P. fluorescens* converts a major fraction of glucose extracellularly to gluconate and 2-ketogluconate, which are metabolized during the later growth phases, which is in contrast to physiological data that

suggested direct utilization of glucose (124). In *Z. mobilis*, C1 metabolism introduces a significant fraction of (^{13}C -labeled) pyruvate formate lyase-derived formate into serine. Such experimental identification of metabolic networks and quantification of in vivo molecular fluxes by ^{13}C -tracer experiments has great potential for application in novel or not yet characterized species.

Chapter 3

Different biochemical mechanisms ensure network-wide balancing of reducing equivalents in microbial metabolism

Tobias Fuhrer and Uwe Sauer

Institute of Molecular Systems Biology, ETH Zürich, Zürich, Switzerland

submitted

Prof. Dr. Uwe Sauer designed the project, supervised the work and contributed to the writing.

Abstract

To sustain growth, catabolic formation of the redox equivalent NADPH must be balanced with the anabolic demand, but the mechanisms that ensure this balance are not understood quantitatively. Based on ^{13}C -detected intracellular fluxes and cofactor specificities in all relevant central metabolic enzymes, we quantified NADPH production in *Agrobacterium tumefaciens*, *Paracoccus versutus*, *Pseudomonas fluorescens*, *Rhodobacter sphaeroides*, *Sinorhizobium meliloti*, *Zymomonas mobilis* and *Escherichia coli*. Five species produced more NADPH from glucose catabolism than was required for biomass synthesis. Exceptions were *P. fluorescens* with balanced rates and *E. coli* with insufficient catabolic production, where the remainder is reduced via the membrane-bound transhydrogenase. *P. versutus* was the only species that might rely on transhydrogenases for redox balancing during growth on glucose. For the other four species, the main redox balancing mechanism appears to be dual cofactor specificity in several catabolic enzymes, in particular in the glucose-6-phosphate dehydrogenase. An unexpected key finding for all species except *E. coli* was the lack of cofactor specificity in the oxidative pentose phosphate pathway, which contrasts with the textbook view on NADPH formation as one main function of this pathway.

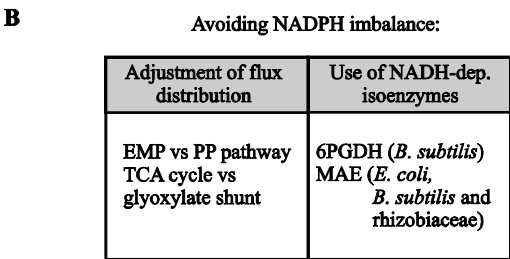
Introduction

For all combinations of substrates, the about 60 reactions of central carbon metabolism (131) provide the building blocks and energy at appropriate rates and stoichiometries to fuel about 300 anabolic reactions. Additionally, redox equivalents must be appropriately balanced between large numbers of producing and consuming reactions. Aerobically, the primary role of the redox cofactor NADH is respiratory ATP generation via oxidative phosphorylation. Anaerobically, it is primarily a catabolic byproduct that must be recycled through formation of reduced end-products such as ethanol or lactate. The chemically very similar redox cofactor NADPH, in contrast, serves the different function of driving anabolic reductions. To fulfill these rather distinct functions, the two redox couples are generally maintained far away from their thermodynamical equilibriums, with the NADPH-to-NADP⁺ ratio in a more reduced state than the NADH-to-NAD⁺ ratio (89).

During growth on glucose, the major NADPH-generating reactions are considered to be the oxidative pentose phosphate (PP) pathway, the Entner-Doudoroff (ED) pathway and isocitrate dehydrogenase in the tricarboxylic acid (TCA) cycle (Fig. 1A). The precise formation rate of NADPH depends on the actual carbon fluxes through those catabolic pathways, which can vary significantly with the environmental conditions. The anabolic demand for NADPH, in contrast, is coupled to the rate of biomass formation (138) and, to a varying extent, to the reduction of thioredoxin for maintaining an appropriate redox state (9). Thus, in the absence of reactions that reoxidize NADPH at the expense of NAD⁺, the catabolic fluxes through the NADPH-generating reactions must be perfectly balanced with the requirements for NADPH in about 100 anabolic reactions. This situation is indeed found in *Saccharomyces cerevisiae* (16, 22). However, bacteria with often extensive catabolic fluxes through NADPH-producing reactions (75) find themselves inevitably in situations where the stoichiometric coupling of NADPH formation to catabolic fluxes will exceed the anabolic demand, or, at high biomass yields, will be insufficient (179). Hence, a key question of metabolic network operation is: how do bacteria balance catabolic NADPH formation with anabolic consumption?

Potential biochemical mechanisms that could provide such NADPH balancing can be divided into those that avoid imbalances in the first place and those that decouple NADPH formation from catabolism (Fig. 1B). Imbalance avoiding mechanisms include the appropriate choice of catabolic pathways as in *S. cerevisiae* (22), differential expression of isoenzymes with different cofactor specificities (49, 52), and possibly a broader cofactor specificity of catabolic enzymes, although the latter was not yet shown to be metabolically relevant.

Decoupling of catabolic NADPH formation from anabolism can potentially be achieved through three distinct mechanisms. First, through either a membrane-bound, proton-translocating or a soluble, energy-independent transhydrogenase reaction (19, 94). As the currently best studied microbe, *Escherichia coli* (24, 32) contains both isoforms, thus is capable to counterbalance situations of catabolic under- and overproduction of NADPH. While the membrane-bound transhydrogenase PntAB provides about 40% of the entire NADPH during growth on glucose in batch culture (179), glucose-limited chemostat growth with extensive TCA cycle fluxes results in a significant overproduction of NADPH (60, 232), which is presumably balanced through the soluble transhydrogenase UdhA that was shown to carry out this function during growth on acetate and in mutants with high PP pathway fluxes (179). This counterbalancing of NADPH overproduction can be readily transferred to other microbes through heterologous expression of the soluble transhydrogenase, as was demonstrated by restoring growth of an NADPH-overproducing, phosphoglucisomerase-deficient *S. cerevisiae* mutant, which catabolized glucose exclusively through the NADPH generating PP pathway (63). Second, some organisms such as *E. coli* (105, 237), *S. cerevisiae* (148) and archaea (104, 173) contain NAD(H) kinases that can directly convert NAD(H) into NAD(P)H at the expense of ATP. This mechanism has not yet been implicated with NADPH balancing because it does not affect the redox state but rather the ratio between phosphorylated and non-phosphorylated form. Third, biochemical redox cycles - combinations of reactions or isoenzymes with different cofactor specificities - can catalyze an effective transhydrogenation without affecting the net catabolic flux. Examples of such redox cycles include simultaneous isoform operation of isocitrate dehydrogenase in animal



61

mitochondria (182) and glyceraldehyde-3P and alcohol dehydrogenases in *Kluyveromyces lactis* (149, 213). In the first case, a glyceraldehyde-3P dehydrogenase accepting both NAD^+ and NADP^+ from *K. lactis* could restore the capability of a phosphoglucosomerase knockout in *S. cerevisiae* to grow on glucose which was confirmed by phenotype and enzymatic analysis. Similarly, in the second case, increased enzyme activities of cytosolic and mitochondrial alcohol dehydrogenases with distinct cofactor specificities demonstrated the operation of such redox cycles equilibrating NADPH overproduction in a *K. lactis* phosphoglucosomerase mutant.

Here we address the question how seven metabolically diverse bacterial species balance their NADPH metabolism. The analysis relies on inferring catabolic in vivo NAD(P)H formation rates from previously published ^{13}C -detected intracellular fluxes (75), comprehensive in vitro determination of redox cofactor specificities in all major NAD(P)H producing reactions, in vitro transhydrogenase activities and network-wide cofactor balancing.

Materials and Methods

Strains, media and growth conditions

The following bacterial species were analyzed: *Agrobacterium tumefaciens* C58 (F. Narberhaus), *Pseudomonas fluorescens* 52-1C (B. Witholt), *Rhodobacter sphaeroides* ATH 2.4.1 (German Collection of Microorganisms and Cell Cultures, DSMZ 158), *R. sphaeroides* GA wild-type and *pntAB* knockout strain (T. Donohue), *Paracoccus versutus* A2 (DSMZ 582), *Sinorhizobium meliloti* (DSMZ 1981), *Zymomonas mobilis* NRRL B-806 (DSMZ 424) and *E. coli* MG1655 (*E. coli* Genetic Stock Center 6300). All physiological experiments were conducted in minimal medium supplemented with 3 g/liter glucose as the sole carbon source. For most species, M9 medium was used that contained per liter of deionized water: 7.52 g $\text{Na}_2\text{HPO}_4 \cdot 2\text{H}_2\text{O}$, 3.0 g KH_2PO_4 , 0.5 g NaCl and 2.5 g $(\text{NH}_4)_2\text{SO}_4$. The following components were sterilized separately and then added (per liter of final medium): 1 ml 0.1 M CaCl_2 , 1 ml 1 M MgSO_4 , 0.6 ml 100 mM FeCl_3 , 2 mL of vitamin solution (filter sterilized) and 10 ml M9 trace salts solution. The vitamins solution contained (per 50 mL): 25 mg of each biotin, cyanocobalamin, niacin, calcium pantothenate, pyridoxine HCl and thiamine HCl. The M9 trace salts solution contained (per liter): 0.18 g $\text{ZnSO}_4 \cdot 7\text{H}_2\text{O}$, 0.12 g $\text{CuCl}_2 \cdot 2\text{H}_2\text{O}$, 0.12 g $\text{MnSO}_4 \cdot \text{H}_2\text{O}$ and 0.18 g $\text{CoCl}_2 \cdot 6\text{H}_2\text{O}$. For *R. sphaeroides* a special trace salts solutions was used that contained (per liter): 1.5 g nitrilotriacetic acid, 3.0 g $\text{MgSO}_4 \cdot 7\text{H}_2\text{O}$, 0.5 g $\text{MnSO}_4 \cdot \text{H}_2\text{O}$, 1.0 g NaCl , 0.1 g $\text{FeSO}_4 \cdot 7\text{H}_2\text{O}$, 0.1 g $\text{CoCl}_2 \cdot 6\text{H}_2\text{O}$, 0.135 g $\text{CaCl}_2 \cdot 2\text{H}_2\text{O}$, 0.1 g $\text{ZnSO}_4 \cdot 7\text{H}_2\text{O}$, 0.01 g $\text{CuSO}_4 \cdot 5\text{H}_2\text{O}$, 0.01 g H_3BO_3 , 0.01 g $\text{Na}_2\text{MoO}_4 \cdot 2\text{H}_2\text{O}$, 0.015 g NiCl_2 , 0.02 g Na_2SeO_3 , and the pH was adjusted to 6.5 with KOH. Aerobic batch cultures were grown at 30°C in 500 mL baffled flasks with 50 mL of M9 medium (*P. versutus* and *Z. mobilis* were grown in special minimal media (75)) on a gyratory shaker at 225 rpm (250 rpm for *P. fluorescens*). Anaerobic cultures of *Z. mobilis* were grown at 30°C in 125 mL sealed glass flasks with 50 ml minimal medium on magnetic stirrers at 225 rpm. The sterile medium was gassed with sterile filtered N_2 for 15 min.

Construction of mutants

A. tumefaciens soluble transhydrogenase (*sTH*), membrane-bound transhydrogenase (*pntAB*) and the double knockout were constructed using pK18mobsacB suicide vector (139, 183). The two homologous flanking regions of the *sTH* and *pntAB* genes were amplified by the polymerase chain reaction (PCR) using following oligonucleotide primer pairs: 5'-gcacttagaccgcatgggtgagttgaagaagga-3' and 5'-gcaggatccaaggcggggcaggtggtggatacg-3'; 5'-gcagtcgacatgaaaagatcgatgtgaaggtg-3' and 5'-gcacttagaatttgacgatggggagtg-3' for *sTH* and 5'-gcaggatccgactgcggctccgggcgactg-3' and 5'-gcacttagatccttaggcgttccgattetcaaa-3'; 5'-gcagtcgacatggcgatgcgaagaagt-3' and 5'-gcaaagcttcgcgctagggctggatac-3' for *pntAB*, digested with the restriction enzymes BamHI / XbaI and XbaI / SalI respectively for *sTH* and BamHI / XbaI and SalI / HindIII respectively for *pntAB* and ligated into pK18mobsacB vector. The resulting plasmid was transferred into *A. tumefaciens* by electroporation and kanamycin-resistant clones were selected, which had the plasmid inserted into the chromosome. Those clones were grown on LB without kanamycin and then streaked out on plates containing 10% sucrose to select for a second homologous recombination event as described previously (139). Positive knockouts were analyzed by PCR using a primer inside the *sTH* or *pntAB* sequence and one outside the flanking sequences used for the recombinations: 5'-caccgcgccttcgatccctaccc-3' and 5'-gcttgccgtgccgcgaatgtgct-3' for *sTH* and 5'-gccgccgccgccgaagatt-3' and 5'-agccgccaaaggatgaccgagatga-3' for *pntAB*.

In vitro enzyme activities

Cells were harvested by centrifugation at 4°C and washed twice in 0.9% NaCl and 10 mM MgSO₄. Upon 10-fold concentration in cell lysis buffer (100 mM Tris-HCl, pH 7.5, 5 mM MgCl₂, 1 mM dithiothreitol and Complete™ EDTA-free protease inhibitor cocktail (Roche)), cells were disrupted by passage through a French press at 4°C. Cell-free extracts were obtained by centrifugation at 23,100 x g and 30 min at 4°C. The supernatant was used for the enzymatic assays in 1 ml reaction buffer at 25°C. Reduction of NAD(P)⁺ or oxidation of NAD(P)H was monitored spectrophotometrically at 340 nm. Protein concentrations of the extracts were determined by the Biuret assay (82).

In vitro enzyme activities of glucose-6P-, 6P-gluconate- and isocitrate dehydrogenase were determined under the following assay conditions: 100 mM Tris-HCl, pH 7.5, 2.5 mM MnCl_2 , 50 μl extract, 1 mM NAD(P)^+ and 2 mM of glucose-6P, 6P-gluconate or isocitrate (2). Glyceraldehyde-3P dehydrogenase: 125 mM triethanolamine, 5 mM L-cysteine, 20 mM potassium arsenate, 50 mM K_2HPO_4 , pH 9.2, 50 μl extract, 1 mM NAD(P)^+ and 3 mM glyceraldehyde-3P (64). The reverse reaction of malate dehydrogenase: 100 mM Tris-HCl, pH 8.8, 20 μl extract, 0.2 mM NAD(P)H and 1 mM oxaloacetate (2). NADP^+ -dependent malic enzyme: 100 mM Tris-HCl, pH 7.8, 5 mM MgCl_2 , 50 mM KCl, 100 μl extract, 1 mM NADP^+ and 30 mM L-malate pH 7.8 (2, 52). Malic enzyme was only assayed for NADP^+ -dependent activity since interference of the NAD^+ -dependent activity with malate dehydrogenase could not be excluded. Alcohol dehydrogenase in *Z. mobilis*: 100 mM Tris-HCl, pH 7.5, 2.5 mM MnCl_2 , 10 μl extract, 0.2 mM NAD(P)H and 1 mM acetaldehyde. All reactions were started by adding the substrate and the specific activities were obtained by dividing the measured slope of NAD(P)H formation or consumption by the total cell protein concentration.

Membrane fraction and membrane-free cell extract were separated by centrifuging the previously obtained supernatant at $159,000 \times g$ at 4°C for 3 h. Reverse transhydrogenase activity in the membrane fraction was then assayed in 50 mM NaP, pH 7.0, 100 μl membranes (resuspended in the same amount of NaP buffer as the total volume during centrifugation), 0.2 mM NADPH and 1 mM 3-acetylpyridine adenine dinucleotide (APAD^+) (230). Forward soluble transhydrogenase activity in the membrane-free cell extract was assayed in 50 mM Tris-HCl, pH 7.6, 2 mM MgCl_2 , 100 μl membrane-free cell extract, 0.2 mM NADPH and 1 mM APAD^+ (179). Both reduction of APAD^+ and oxidation of NADPH were monitored spectrophotometrically at 400 nm and 310 nm simultaneously to exclude interferences in the adsorption of both NADPH and APADH. The extinction coefficients were experimentally determined by standard curves to be $1.75 \text{ mM}^{-1} \text{ cm}^{-1}$ at 310 nm and $3.51 \text{ mM}^{-1} \text{ cm}^{-1}$ at 400 nm for APADH and $3.24 \text{ mM}^{-1} \text{ cm}^{-1}$ at 310 nm and $0.16 \text{ mM}^{-1} \text{ cm}^{-1}$ at 400 nm for NADPH.

NADPH balancing

Previously published net carbon fluxes (75) were used as basis for all the calculations except for *E. coli*, where a newer unpublished data set was used. For *E. coli*, the overall flux distribution at 30°C was experimentally revised in comparison to 37°C and the altered redox balance was considered for the current manuscript. NADPH formation was determined from the carbon fluxes through the cofactor-dependent reactions and multiplied with the experimentally determined relative cofactor specificity for NADP⁺. NADPH consumption was calculated from the NADPH requirements for biomass production (42, 138). To estimate maximal and minimal possible NADPH production rates, 20% variation in cofactor specificity for NAD⁺ or NADP⁺ were assumed for all reactions where activity with both cofactors was experimentally determined (Table 2); i.e. for glucose-6P- and 6P-gluconate dehydrogenase. For malic enzyme, only the detection of NADP⁺-dependent activity was possible and the cofactor specificities were therefore assumed on the basis of literature data for each organism (Table 1). For *P. versutus*, which was assumed to be similar to *Bacillus subtilis*, and *E. coli* the malic enzyme was chosen to be NAD⁺-dependent under these conditions on the basis of previously published network models (40, 60).

Variances in biomass composition

For the standard biomass composition of *E. coli* (60, 138), about 63, 22 and 8% of NADPH are required for protein, lipids and RNA biosynthesis respectively, which cover together more than 90% of total NADPH demand. The remainder includes NADPH requirements for macromolecules such as DNA, peptidoglycans, glycogen and polyamine and was not considered to be growth dependent. The dependency of NADPH requirements for protein and RNA on the growth rate was already included in the previously published biomass composition model (42, 60). However, the third major anabolic sink of NADPH, lipids, was not considered to be growth rate dependent, hence its contribution to cellular biomass was varied between 5 and 15% to account for variations in biomass compositions among species. The differences in the relative lipid content were equally balanced by altering both RNA and protein content and the consecutive changes in NADPH requirements for biomass production were calculated as described previously (42, 60).

Reversibility analysis for membrane-bound transhydrogenase

For the reaction catalyzed by the membrane-bound form of transhydrogenase, which involves the translocation of protons over the membrane, the Gibbs energy of reaction was determined as follows:

$$\Delta_r G' = \sum_i v_i \Delta_f G_i'^0 + RT \ln \left(\frac{[NAD^+][NADPH]}{[NADH][NADP^+]} \right) - z(2.3RT\Delta pH + F\Delta\phi)$$

where v_i is the stoichiometric coefficient of the reactants, $\Delta_f G_i'^0$ the transformed standard Gibbs energy of formation for each reactant, ΔpH the pH difference between periplasm and cytoplasm, z the number of the translocated protons per reaction and $\Delta\phi$ the membrane potential. Intracellular concentrations ratios of cofactors and transformed standard Gibbs energies of reaction were taken from **Chapter 5** and Kümmel *et al.*, respectively (117). Different membrane potentials were considered to account for variations among species (79, 103, 106, 122, 167).

Results

Cofactor specificity of main NADPH producing enzymes

For a broader elucidation of how microbes manage their NADPH metabolism, we chose seven metabolically diverse bacterial species for which intracellular flux data were already available (75). These are the anaerobic *Z. mobilis*, the rhizobiaceae *A. tumefaciens* and *S. meliloti*, the metabolically versatile facultative phototroph *R. sphaeroides*, the facultative autotroph *P. versutus*, the versatile *P. fluorescens* and the model bacterium *E. coli*. For some of these species, significant NADPH overproduction is expected from the flux distribution during growth on glucose; i.e. *P. fluorescens* and *Z. mobilis* with exclusive catabolism through the Entner-Doudoroff (ED) pathway and *P. versutus* with high TCA cycle flux (75). Based on textbook knowledge, typically exclusive cofactor specificities are assumed in stoichiometric models for experimental determination of metabolic fluxes (60, 98, 129, 180) or genome-scale computational analyses (158). Since any conclusion on NADPH metabolism critically depends on the validity of this assumption, we first searched the literature for enzymatic evidence and public data bases for genetic evidence of redox cofactor specificities in all reactions that could principally generate or consume NADPH in central metabolism of the seven species (Table 1). Direct biochemical evidence for cofactor specificity was available for only few enzyme-organism combinations where K_M values were determined separately for both NAD^+ and NADP^+ . In few cases, distinct binding sites for NADH and NADPH in the deduced protein sequences suggested that these enzymes might indeed exhibit dual cofactor specificities (137). Such cofactor specificity typically depends on conserved domains where distinct amino acids stabilize or interfere with the additional phosphate group of NADPH (27, 99, 137). Hence, available protein sequences were analyzed to obtain indications of cofactor specificities (Table 1). Overall, this survey indicated that cofactor specificity was at least questionable in many cases.

For more direct biochemical evidence, we then determined in vitro redox cofactor specificities of all reactions that could principally provide or consume NADPH in central metabolism of all seven species (Appendix). In contrast to the common believe, both

dehydrogenases in the oxidative PP pathway of most species exhibited significant activity also with NADH, ranging from 20 to 50% of the total activity (Table 2). The exclusive exception with complete specificity for NADPH was *E. coli* as was also shown earlier (38). Species like *Z. mobilis* and *P. fluorescens*, in contrast, contain glucose-6P- and 6P-gluconate dehydrogenases without any apparent preference for either cofactor or two isoenzymes with different cofactor specificities.

While glyceraldehyde-3P dehydrogenases were mostly specific for NAD^+ , the *P. fluorescens* enzyme exhibited a small but significant activity also with NADP^+ . Unlike *B. subtilis*, which contains a second, NADP^+ -dependent isoform that catalyzes the gluconeogenic direction and is repressed during growth on glucose (64), *P. fluorescens* contains only a single glyceraldehyde-3P dehydrogenase-encoding gene. Hence, the NADP^+ -dependent activity is a property of the same enzyme as was described for *K. lactis* (213). Throughout all species investigated, the two TCA cycle enzymes isocitrate and malate dehydrogenase were highly specific for the cofactors NADP^+ and NAD^+ , respectively (Table 1,2). Although malic enzyme activity is not required during growth on glucose, significant malic enzyme fluxes through the so-called pyruvate shunt were described previously for *P. fluorescens* (75). Operation of the pyruvate shunt in this organism was confirmed here by basically absent and exceptionally high in vitro activities of malate dehydrogenase and malic enzyme, respectively (Appendix).

Potential further sources of NAD(P)H are the pyruvate dehydrogenase complex and the 2-oxo-glutarate dehydrogenase. Since both contain the NAD^+ -specific dihydrolipoamid dehydrogenase, they are highly specific for NAD^+ (47, 188). Succinate dehydrogenase delivers electrons directly to the respiratory chain via FADH_2 , hence does not react with NADP^+ . The cofactor dehydrogenases in the bacterial respiratory chains were assumed to be specific for NADH, since specificity for NADPH has been described so far only for mitochondria (90, 205). The active alcohol dehydrogenase in *Z. mobilis* was determined to be exclusively specific for NADH ($896 \pm 52 \mu\text{mol min}^{-1} \text{ g}_{\text{cell protein}}^{-1}$ for NADH and $1 \pm 6 \mu\text{mol min}^{-1} \text{ g}_{\text{cell protein}}^{-1}$ for NADPH), which is in agreement with reported values (109, 165).

Table 2 - Relative cofactor specificities of enzymes^a

Enzyme	Cofactor	<i>A. tumefaciens</i>	<i>S. meliloti</i>	<i>P. fluorescens</i>	<i>R. sphaeroides</i>	<i>P. versutus</i>	<i>Z. mobilis</i>	<i>E. coli</i>
G6PDH ^b	NADP ⁺	66 ± 6 ^c	63 ± 3	56 ± 11	70 ± 2	78 ± 4	51 ± 3	100 ± 0
	NAD ⁺	34 ± 6	37 ± 3	44 ± 11	30 ± 2	22 ± 4	49 ± 3	0 ± 0
6PGDH	NADP ⁺	87 ± 0	93 ± 0	47 ± 10	- ^d	94 ± 8	-	100 ± 0
	NAD ⁺	13 ± 0	7 ± 0	53 ± 10	-	6 ± 8	-	0 ± 0
GAPDH	NADP ⁺	0 ± 0	0 ± 0	13 ± 6	2 ± 0	1 ± 1	1 ± 0	2 ± 2
	NAD ⁺	100 ± 0	100 ± 0	87 ± 6	98 ± 0	99 ± 1	99 ± 0	98 ± 2
ICTDH	NADP ⁺	98 ± 1	98 ± 0	99 ± 1	96 ± 3	99 ± 0	-	100 ± 0
	NAD ⁺	2 ± 1	2 ± 0	1 ± 1	4 ± 3	1 ± 0	-	0 ± 0
MDH	NADP ⁺	0 ± 0	0 ± 0	-	1 ± 1	0 ± 0	-	1 ± 2
	NAD ⁺	100 ± 0	100 ± 0	-	99 ± 1	100 ± 0	-	99 ± 2

^a Relative cofactor specificities in % were derived from absolute specific units separately determined for both NAD⁺ and NADP⁺ (μmol min⁻¹ Ecdf protein⁻¹, supplemental data).

^b Enzyme purified from *E. coli* strain *W* (ATCC 8739) grown in minimal medium with glucose as the sole carbon source. ^c Data from [1]. ^d Data from [2].

NADPH balancing

^{13}C -determined intracellular carbon fluxes specify the total amount of redox cofactors that are produced in each dehydrogenase reactions. For cofactor-specific enzymes, carbon flux data thus quantify the concomitant formation/consumption rate of this cofactor. For all non-specific enzymes, we estimated cofactor conversion rates by multiplying the absolute carbon flux values (75) with the experimentally determined in vitro specificities for either cofactor (Table 2). Since the in vivo conditions might vary considerably from those used to determine the in vitro activities, we assumed a 20% error in all determined cofactor ratios, thus yielding a confidence region for the NADPH balance (Fig. 2).

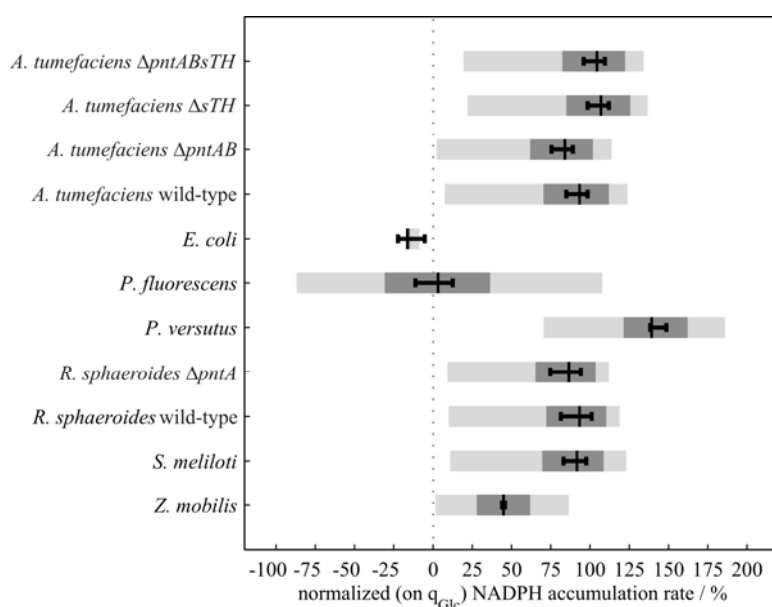


Figure 2 - NADPH accumulation based on measured cofactor specificities and net flux distributions (black bars). The error bars indicate variances of NADPH requirements for biomass. Dark gray bars represent the confidence region based on dual cofactor specificities with a tolerance of 20% for glucose-6P-, 6P-gluconate- and glyceraldehyde-3P dehydrogenase and for malic enzyme. Light gray bars indicate the NADPH balance when 0 or 100% specificity is assumed in all cases where isoenzymes are supposed to be present or activity with both NADPH and NADH was measured.

E. coli was the only species with a negative NADPH balance, which is fully consistent with the previously reported NADPH-formation through the membrane-bound transhydrogenase PntAB under this condition (179). While no clear trend was discernible for

P. fluorescens, the other five species exhibited positive NADPH balances, with *P. versutus* as the most extreme case (Fig. 2). This conclusion of catabolic NADPH overproduction was qualitatively independent of the assumed uncertainties in the cofactor specificity of 20%. Even assuming extreme NADPH specificities of 0 or 100% for all reactions where literature, genetic or experimental data indicated the presence of unspecific isoenzymes resulted in a significant overproduction of NADPH for *P. versutus* (Fig. 2). Potential variances in the biomass composition, in particular the lipid content that would affect the anabolic NADPH requirement were comparatively small (Fig. 2). Thus, independent of the above uncertainties, all five species with catabolic NADPH overproduction must operate mechanisms that regenerate NADP^+ or avoid an overproduction of NADPH. For *A. tumefaciens*, *Z. mobilis*, *S. meliloti* and *R. sphaeroides*, the dual cofactor specificity would potentially suffice to avoid NADPH overproduction, while some regeneration mechanism appears to be mandatory for *P. versutus*.

Transhydrogenase activity

An obvious mechanism to close the NADPH balance could be catalyzed by transhydrogenases. Therefore, we determined in vitro activities of both the soluble and membrane-bound transhydrogenases in all species (Fig. 3). Significant activities above $1 \text{ U g}_{\text{cell protein}}^{-1}$ for the membrane-bound enzyme were only detected in *A. tumefaciens*, *R. sphaeroides*, *P. versutus* and *E. coli*. The soluble isoform, in contrast, could not be detected in any of the seven species under the glucose batch conditions used, with the possible exception of very low activities in *E. coli* and *P. versutus*. The background activity was determined to be $2.8 \pm 0.2 \text{ U g}_{\text{cell protein}}^{-1}$ in an *E. coli pntAB-udhA* double mutant (179) and $1.2 \pm 0.3 \text{ U g}_{\text{cell protein}}^{-1}$ in an *A. tumefaciens pntAB-sTH* mutant (Fig. 3). In both mutants, both known forms of transhydrogenases were deleted and the remaining background activity arises from unspecific reduction of APAD^+ in the soluble fraction that contains also other dehydrogenases. Functionality of the assay was verified by transhydrogenase activities in the soluble fraction of $84.1 \pm 7.3 \text{ U g}_{\text{cell protein}}^{-1}$ when analyzing diluted crude cell extracts from plasmid-based over-expression of *E. coli* UdhA in the *E. coli pntAB-udhA* double mutant.

With the possible exception of *P. versutus*, the above results reveal that the soluble transhydrogenase cannot constitute the balancing mechanism. Could a reversible membrane-bound transhydrogenase be responsible? Depending on the assumed proton motive force (ΔpH of 0.2 and $\Delta\Psi$ of -0.1 to -0.18 V) and typical intracellular concentration ratios of reduced and oxidized cofactors ($[\text{NADH}]/[\text{NAD}^+]$ of 1/200 and $[\text{NADPH}]/[\text{NADP}^+]$ of 2 (103, 117, 122, 167)), the Gibbs energy would be in the range of -3.6 to 4.0 kJ mol⁻¹. Thus the reaction is potentially reversible under physiological conditions and could possibly balance the NADPH overproduction in *A. tumefaciens*, *R. sphaeroides* and *P. versutus*. To test this hypothesis, we generated *pntAB*, *sTH* and *pntAB-sTH* mutants of *A. tumefaciens* and also used an available *R. sphaeroides pntA* mutant (93). The *R. sphaeroides pntA* mutant exhibited a small but significant growth defect of about 11% compared to its parent at unaltered biomass yield. In *A. tumefaciens pntAB* mutant the growth rate and biomass yield did not differ significantly from the parent. The *sTH* and the *pntAB-sTH* mutants, however,

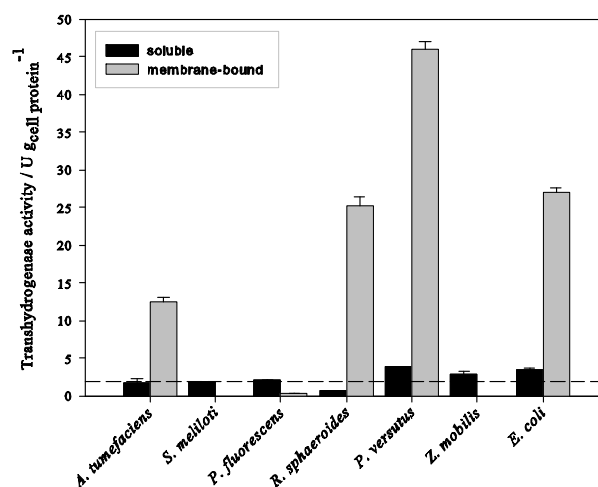


Figure 3 - Transhydrogenase activities measured in membrane-free cell extract (soluble) and membrane fraction (membrane-bound). Activities with standard deviations from at least duplicate experiments. The dashed line indicates the average background activity that was determined in the soluble fraction of *E. coli pntAB-udhA* and *A. tumefaciens pntAB-sTH* double mutants.

grew about 9% slower and attained 16% lower biomass yields. While these physiological data suggest some functional relevance of the membrane-bound transhydrogenase during growth on glucose, ^{13}C -based flux analyses demonstrated clearly that there was an almost unaltered catabolic overproduction of NADPH (data not shown). Thus, we can exclude a major role of the membrane-bound transhydrogenase in *A. tumefaciens*, *R. sphaeroides*, *S. meliloti* and *Z. mobilis*, but not in *P. versutus*.

Discussion

How bacteria balance catabolic formation with anabolic consumption of the redox cofactor NADPH has not yet been seriously addressed, presumably because it is a complicated property that concerns the entire network. Thus, techniques of systems biology are necessary that became available only recently. By combining ^{13}C -flux data with in vitro characterization of cofactor specificities for key enzymes, we address this question here for seven bacterial species by taking a network approach. With the possible exception of *P. fluorescens*, catabolic and anabolic NADPH rates were not balanced during batch growth on glucose as the sole carbon source. As the only investigated species, *E. coli* produced insufficient NADPH from glucose catabolism, thus required significant additional formation of NADPH via the energy-coupling transhydrogenase PntAB, as was shown previously (179). The other five species, in contrast, produced significantly more NADPH during catabolism than was required for anabolism. Thus, they must feature NADPH imbalance avoiding or reoxidation mechanisms for NADPH to prevent an imbalance that would preclude sustained growth.

The most well-known valve-like mechanism is the soluble transhydrogenase, which has been shown to fulfill this function in *E. coli* (179) and, upon heterologous expression, also in *S. cerevisiae* (63). Since none of the five ‘overproducing’ species exhibited significant soluble transhydrogenase activity, they must rely on a different mechanism. An obvious possibility is that the catabolic enzymes do not exhibit the assumed cofactor specificity, and this was investigated in detail. Although we found several catabolic reactions to accept both cofactors, most prominently the dehydrogenases of the oxidative PP pathway, even the unlikely exclusive use of NAD^+ in the oxidative PP pathway would not prevent significant overproduction of NADPH in *P. versutus*. Since this organism features very high membrane-bound and also some soluble transhydrogenase activity, this remains the most likely explanation for the redox balancing, although we did not provide direct evidence for this hypothesis.

For *A. tumefaciens*, *R. sphaeroides*, *S. meliloti* and *Z. mobilis*, an overproduction of NADPH could principally be avoided assuming almost exclusive specificities for NADH in

the glucose-6P dehydrogenase of the ED pathway. Absent genes or absent activities of transhydrogenases for *Z. mobilis* and *S. meliloti*, respectively, render this cofactor unspecificity the most likely explanation. Significant in vitro activities of the potentially reversible membrane-bound transhydrogenase were detected in *A. tumefaciens* and *R. sphaeroides*, and mutants in the encoding gene exhibited a small, but significant growth phenotype. The NADPH balance in these mutants, however, was identical to the parent within the resolution of the analysis, indicating that either these enzymes play no role in redox balancing, or are efficiently supplemented by alternative mechanisms. The most relevant redox balancing mechanism for these four species thus appears to be the cofactor unspecificity of several catabolic enzymes, possibly supported by putative redox cycles, NADH kinases, or possibly higher than anticipated NADPH demand for thioredoxin reduction. It has not escaped our notice that both NADPH/NADP⁺ and NADH/NAD⁺ ratios might vary among species and thus significantly affect the in vivo specificity of dehydrogenases in general. To obtain precise information on the in vivo specificities one would additionally require kinetic characterization of at least the PP pathway dehydrogenases in all seven species, which was beyond the scope of this work.

Nevertheless, a highly unexpected key finding was that, except for *E. coli*, none of the investigated species contained NADPH-specific dehydrogenases in the oxidative PP pathway. This finding contrasts with the textbook view of the PP pathway as a main NADPH producing pathway. The lack of high NADPH specificity, in particular in the glucose-6P dehydrogenase may be related to the fact that this enzyme is also required for the ED pathway, which is the main or even exclusive catabolic pathway of glucose in all species investigated except *E. coli*. In *Z. mobilis*, the very low biomass yield of 3% and high ethanol production directly links the demand of NADH for the alcohol dehydrogenase to the regeneration of NADH by glucose-6P- and glyceraldehyde-3P dehydrogenase. Since the genes for transhydrogenases are absent, both of these dehydrogenases operate primarily or even exclusively with NADH in vivo. The unspecificity of the key enzyme glucose-6P dehydrogenase appears to be a major mechanism to avoid an NADPH overproduction in a number of species. With respect to redox balances, the general role of the PP pathway has to be reconsidered for modeling species other than *E. coli*.

Chapter 4

Transhydrogenase expression in *Escherichia coli* is substrate dependent

Tobias Fuhrer, Matthias Heinemann and Uwe Sauer

Institute of Molecular Systems Biology, ETH Zürich, Zürich, Switzerland

manuscript in preparation

Dr. Matthias Heinemann supervised the data analysis and contributed to the writing.
Prof. Dr. Uwe Sauer designed the project, supervised the work and contributed to the writing.

Abstract

A soluble and a membrane-bound transhydrogenase enable *Escherichia coli* to uncouple catabolic NADPH formation from anabolic NADPH consumption by catalyzing the interconversion of reducing equivalents NAD(H) and NADP(H). Their exact function and regulation remained unclear, despite some evidence that the NADPH balance might affect their regulation. Here, we wanted to test whether the transhydrogenase expression correlates with the NADPH balance. Therefore, we systematically perturbed NADPH metabolism using 7 different substrates and 23 mutants with different deleted metabolic genes, which were predicted to resemble extreme cases in NADPH production. Transcriptional regulation was evident with up to 3-fold up and 5-fold down-regulation but the experimentally determined transhydrogenase expression patterns derived from promoter-GFP fusion plasmids did not correlate with the predicted transhydrogenase fluxes. Instead, the expression data revealed that the gluconeogenic substrates used in the screen (acetate and succinate) exhibited similar expression patterns for both transhydrogenases, while the expression patterns obtained on glycolytic substrates were remarkably different. During growth on glucose, *E. coli* exhibited diauxic growth behavior where the membrane-bound transhydrogenases was strongly induced after the acetate switch, most likely as response to dropping pH. The observed expression of UdhA during NADPH underproduction conditions requires an efficient mechanism to prevent its detrimental activity under these conditions, presumably by allosteric inhibition.

Introduction

For each nutritional condition, the about 60 reactions of central carbon metabolism (131) provide building blocks and energy at appropriate rates and stoichiometries to fuel about 300 anabolic reactions. Additionally, redox equivalents must be appropriately balanced between several producing and large numbers of consuming reactions. Aerobically, the primary role of the redox cofactor NADH is respiratory ATP generation via oxidative phosphorylation (84). Anaerobically, it is primarily a catabolic byproduct that must be reoxidized through formation of reduced end products such as ethanol or lactate. The chemically very similar redox cofactor NADPH, in contrast, serves the different function of driving anabolic reductions. To fulfill these rather distinct functions, the two redox couples are generally maintained far away from their thermodynamic equilibria, with the NADPH-to-NADP⁺ ratio in a more reduced state than the NADH-to-NAD⁺ ratio (89).

For most microbes during growth on glucose, the major NADPH-generating reactions are the oxidative pentose phosphate (PP) pathway, Entner-Doudoroff (ED) pathway and isocitrate dehydrogenase in the tricarboxylic acid (TCA) cycle (Fig. 1). The precise formation rate of NADPH, depends on the actual carbon fluxes through these catabolic pathways. These flux distributions vary significantly with environmental conditions. Typical catabolic flux patterns on substrates like acetate and glucose, for example in *Escherichia coli*, lead to situations with high and low NADPH formation, respectively (179).

The anabolic demand for NADPH, in contrast, is coupled to the rate of biomass formation (138) and, to a varying extent, to the reduction of thioredoxin that is required to maintain an appropriate redox state (9). Thus, in the absence of reactions that reoxidize NADPH at the expense of NAD⁺, the catabolic fluxes through the NADPH-generating reactions must be perfectly balanced with the requirements for NADPH in about 100 anabolic reactions. This situation is indeed found in yeasts (16, 22).

studies it was shown that, during growth on glucose, the membrane-bound transhydrogenase PntAB provides a significant portion of the required NADPH (70, 179) (**Chapter 3**). Under conditions of excess NADPH formation, mutant data strongly suggested that the soluble transhydrogenase UdhA functions as a valve to reoxidize the surplus of NADPH by reducing NAD^+ (179).

Despite their important role in linking the fundamental processes of catabolism and anabolism, it is still unclear if and how the two transhydrogenases are regulated, as there is only some evidence that expression of PntAB or UdhA may correlate with NADPH balance (179). The main depository databases for microarray data provided first evidence that both transhydrogenases are not constitutively expressed in *E. coli* but can vary significantly (56, 61, 191). However, microarray data, which related expression to directly the NADPH balance, were not available up to date. To test whether the transhydrogenases PntAB and UdhA of *E. coli* are transcriptionally regulated, we investigate their expression profiles during exponential growth on different carbon substrates via promoter-GFP fusion plasmids. Specifically, we test the hypothesis whether or not their expression levels are controlled by the cellular demand for NADPH oxidation or NADP^+ reduction.

Materials and Methods

Strains, media and growth conditions

All strains used here (Table 1) were transformed with the promoter-less low-copy plasmid pUA139 that contains the green fluorescent protein variant *gfpmut2* or with variants of pUA139 carrying the intergenic region upstream of *udhA* (pPEC3876-98156187) or *pntAB* (pPEC3876-98154949) cloned upstream of *gfpmut2* (36, 236). Precultures were grown in 96-well deep well plates with LB and kanamycin. All growth experiments were conducted in 96-well plates sealed with gas-permeable membranes (ABgene Gas Permeable Adhesive Seals). The strains were cultivated in 200 μ l minimal (M9) medium supplemented with a single carbon source at 800 rpm and 37°C (BioLector, m2p-labs GmbH, Aachen, Germany).

The M9 medium contained per liter of deionized water: 7.52 g $\text{Na}_2\text{HPO}_4 \cdot 2\text{H}_2\text{O}$, 3.0 g KH_2PO_4 , 0.5 g NaCl and 2.5 g $(\text{NH}_4)_2\text{SO}_4$. The following components were sterilized separately and then added (per liter of final medium): 1 ml 0.1 M CaCl_2 , 1 ml 1 M MgSO_4 , 0.6 ml 100 mM FeCl_3 , 2 mL of vitamin solution (filter sterilized) and 10 ml M9 trace salts solution. The vitamins solution contained (per 50 mL): 25 mg of each biotin, cyanocobalamin, niacin, calcium pantothenate, pyridoxine HCl and thiamine HCl. The M9 trace salts solution contained (per liter): 0.18 g $\text{ZnSO}_4 \cdot 7\text{H}_2\text{O}$, 0.12 g $\text{CuCl}_2 \cdot 2\text{H}_2\text{O}$, 0.12 g $\text{MnSO}_4 \cdot \text{H}_2\text{O}$ and 0.18 g $\text{CoCl}_2 \cdot 6\text{H}_2\text{O}$. Different carbon sources used were at equal C-molar concentration: acetate (60 mM), succinate (30 mM), glucose (20 mM), gluconate (20 mM), lactate (40 mM), xylose (24 mM) and glycerol (40 mM).

Data recording and analysis

Over the entire batch growth phase of 12 to 24 hours in a BioLector 96-well plate incubator (m2p-labs GmbH, Aachen, Germany), online data were recorded for light scattering and fluorescence signal to follow biomass formation and GFP expression (174). Both signals were recorded every 7.5 min for each well and biomass was followed by light scatter (excitation and emission at 620 and 650 nm respectively). GFP was excited at 486 nm and fluorescent emission recorded at 510 nm. In preliminary experiments, we found that the light scatter signal correlates linearly with biomass in the range of OD 0.02-20. Background

light scatter signal due to the growth medium was subtracted for each well individually before inoculation. Datasets were exported from the BioLector V1.0 software to MATLAB[®] to determine growth rates and promoter activity (i.e. normalized GFP expression defined as $\Delta\text{fluorescence}/\Delta t/\text{light scatter signal}$) (236).

The fluorescence raw data was processed with a correction function to subtract first the fluorescence background signal caused by biomass and second the fluorescence reference signal from the promoter-less plasmid. The biomass correction function was determined from fluorescence data of the wild-type strain containing no plasmid. The integrated promoter activity over the entire growth experiment was obtained by integrating the normalized GFP expression over total time using trapezoidal numerical integration with MATLAB[®]. For integrated promoter activity restricted to a specific growth phase, integration was done only within a time window specified by the light scatter signal.

Computational prediction of NADPH production

The seven investigated carbon sources enter metabolism at different points, thus cause most likely different metabolic situations of catabolic NADPH formation. Since this NADPH formation is, with the exception of glucose (179) unknown, we estimated intracellular fluxes on these substrates by using a previously published reaction network of *E. coli* central carbon metabolism that contained 98 reactions and 60 metabolites (186). To accommodate for all substrates used, the network was extended with the uptake reactions for gluconate, glycerol and xylose, which were ATP dependent or energy independent based on literature (30, 152, 193). In addition the extracellular conversion of glucose into gluconate was included such that the final network contained 110 reactions and 70 metabolites (75).

For the wild-type on glucose, fluxes were predicted using the multi-objective optimality (MOP) principle, which is based on a previously determined optimal trade-off between the contradicting objectives to minimize intracellular flux, maximize ATP yield and maximize biomass yield (187). The relative weights (optimal trade-off values compared to the maximal ATP and biomass production possible using them as the sole objective functions) were determined to be 17 and 67% for ATP and biomass respectively. For the present study, these relative weights were assumed to valid also for the wild-type grown on other substrates. The

relative value of 67% for biomass was shown to be true comparing experimentally determined biomass yields with predicted values. As for glucose, predicted values for the other substrates were calculated from the maximal ATP and biomass production when used as sole objective functions.

Fluxes for in silico mutants of each reaction of the network were then predicted for every single substrate and mutant combination (7 substrates * 110 reactions) by flux balance analysis using the minimization of metabolic adjustment (MOMA) principle (62, 190). The above wild-type flux estimates were used as reference solution. Finally, we selected the most abundant 23 mutants exhibiting significant transhydrogenase fluxes for GFP expression analysis (Table 1, 3).

Correlation between integrated promoter activity and transhydrogenase fluxes

As a measure for correlation we defined *dist* as follows:

$$dist = \text{abs}[\ln(IPA_{rel}) - \ln(THflux_{rel})]$$

where IPA_{rel} and $THflux_{rel}$ were the changes of integrated promoter activity and normalized transhydrogenase flux respectively relative to the wild-type for each substrate. Integrated promoter activity values were averages from triplicate with standard deviations (Appendix). Transhydrogenase fluxes were predicted by FBA and normalized on the carbon uptake (Appendix).

Table 1 - Bacterial strains and plasmids used in this study

Strain or plasmid	Relevant phenotype or genotype	Source
Strains		
<i>E. coli</i> BW25113	<i>lacI^r rrnB3 ΔlacZ4787 hsdR514 Δ(araBAD)567 Δ(rhaBAD)568 rph-1</i>	(39)
JW0422	<i>E. coli</i> BW25113 derivative, <i>ΔcyoA::Kan^R</i>	(12)
JW0711	<i>E. coli</i> BW25113 derivative, <i>ΔsdhC::Kan^R</i>	(12)
JW0717	<i>E. coli</i> BW25113 derivative, <i>ΔsucC::Kan^R</i>	(12)
JW1595	<i>E. coli</i> BW25113 derivative, <i>ΔpntA::Kan^R</i>	(12)
JW1692	<i>E. coli</i> BW25113 derivative, <i>ΔppsA::Kan^R</i>	(12)
JW1840	<i>E. coli</i> BW25113 derivative, <i>Δedd::Kan^R</i>	(12)
JW1841	<i>E. coli</i> BW25113 derivative, <i>Δzwf::Kan^R</i>	(12)
JW2011	<i>E. coli</i> BW25113 derivative, <i>Δgnd::Kan^R</i>	(12)
JW2278	<i>E. coli</i> BW25113 derivative, <i>ΔnuoG::Kan^R</i>	(12)
JW2294	<i>E. coli</i> BW25113 derivative, <i>Δpta::Kan^R</i>	(12)
JW2385	<i>E. coli</i> BW25113 derivative, <i>Δglk::Kan^R</i>	(12)
JW2447	<i>E. coli</i> BW25113 derivative, <i>ΔmaeB::Kan^R</i>	(12)
JW3349	<i>E. coli</i> BW25113 derivative, <i>Δrpe::Kan^R</i>	(12)
JW3366	<i>E. coli</i> BW25113 derivative, <i>ΔpckA::Kan^R</i>	(12)
JW3712	<i>E. coli</i> BW25113 derivative, <i>ΔatpA::Kan^R</i>	(12)
JW3890	<i>E. coli</i> BW25113 derivative, <i>ΔtpiA::Kan^R</i>	(12)
JW3928	<i>E. coli</i> BW25113 derivative, <i>Δppc::Kan^R</i>	(12)
JW3985	<i>E. coli</i> BW25113 derivative, <i>Δpgi::Kan^R</i>	(12)
JW4030	<i>E. coli</i> BW25113 derivative, <i>Δacs::Kan^R</i>	(12)
JW4115	<i>E. coli</i> BW25113 derivative, <i>ΔfrdA::Kan^R</i>	(12)
JW5129	<i>E. coli</i> BW25113 derivative, <i>ΔmgsA::Kan^R</i>	(12)
JW5238	<i>E. coli</i> BW25113 derivative, <i>ΔsfcA::Kan^R</i>	(12)
JW5551	<i>E. coli</i> BW25113 derivative, <i>ΔudhA::Kan^R</i>	(12)
Plasmids		
pUA139	Kan ^R	(236)
pPEC3876-98154949	Kan ^R , pUA139 derivative, contains pntA promoter region	(236)
pPEC3876-98156187	Kan ^R , pUA139 derivative, contains sthA promoter region	(236)

Results

Systematic perturbation of NADPH metabolism through single gene knockouts and different substrates

To systematically investigate genetic regulation of the two transhydrogenases, we aimed at perturbing NADPH metabolism by growing *E. coli* on different substrates and then deleting those central metabolic enzymes that cause the greatest effect on the NADPH balance in each particular condition. Since the intracellular fluxes were, with the exception of glucose, not known, we predicted the transhydrogenase fluxes in all 110 in silico metabolic mutants of the network by flux balance analysis for growth on the different substrates. Based on earlier work (186, 187), we chose the MOP principle to calculate the wild-type fluxes for each substrates (Appendix). For each combination of the 110 mutants and 7 substrates, we then calculated the flux distributions by the MOMA approach using wild-type solutions as reference. In addition, we predicted fluxes directly with 5 alternative objective functions (maximize ATP, maximize biomass, minimize overall intracellular flux, maximize ATP per fluxunit and maximize biomass per fluxunit, data not shown).

Since many mutants exhibited redundant flux distributions, we selected a set of 23 non-redundant mutants with most extreme fluxes through transhydrogenases (Table 1, Fig. 2) based on the above flux predictions. The same 23 mutants were also found by the predictions with the 5 alternative objective functions. Acetate and gluconate were the only substrates where significant transhydrogenase flux from NADPH to NADH (i.e. NADPH overproduction) was predicted for wild-type and most mutants (Fig. 2). The opposite transhydrogenase flux was obtained for glucose, glycerol, lactate and xylose because the catabolic NADPH formation was insufficient. Matching catabolic NADPH formation and anabolic demands and thus no need for transhydrogenase fluxes was estimated for wild-type and most mutants during growth on succinate.

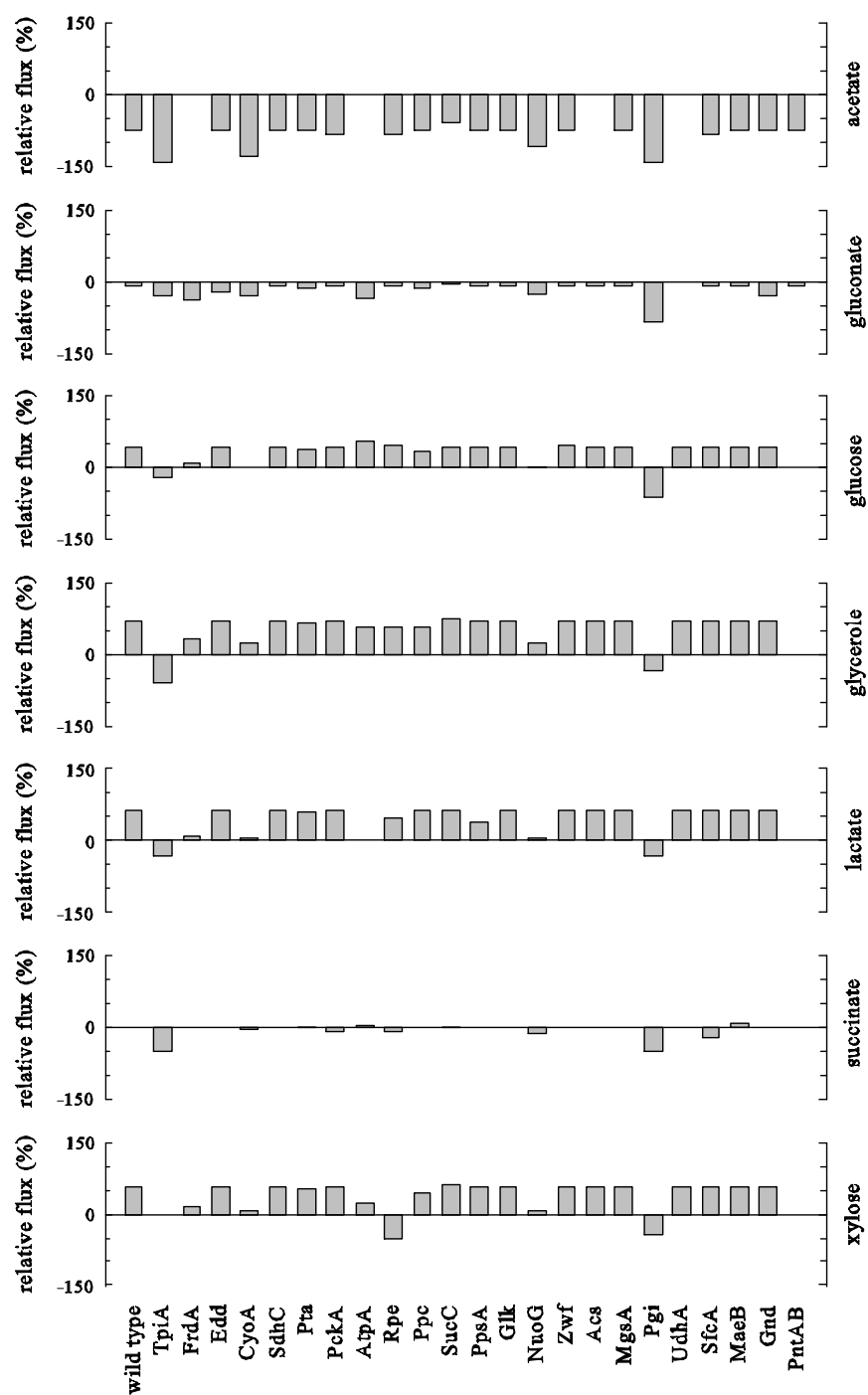


Figure 2 - Predicted relative transhydrogenase fluxes (+, NADH towards NADPH and -, NADPH towards NADH, normalized to substrate uptake) based on FBA using the MOMA objective function.

Effect of putative promoter regions upstream of *pntAB* and *udhA*

Having established different conditions of intracellular NADPH metabolism (Fig. 2), we next asked whether they correlate with transhydrogenase expression. To quantify transhydrogenase expression, we used GFP reporter plasmids with *gfpmut2* cloned behind the upstream intergenic regions of the *E. coli* *pntA* or *udhA* genes that potentially contain the putative promoter regions (236). The fluorescence intensity time course was recorded online together with biomass (light scatter). The promoter activity was defined as the fluorescence increase over time normalized to biomass, which is shown for the example for BW25113 wild-type during growth on glucose in Figure 3.

The biomass recording (Fig. 3, upper row) indicated that wild-type *E. coli* exhibited a diauxic growth behavior on glucose independent of the plasmid. The fluorescence signal in contrast, was almost absent in the strain containing the empty plasmid pUA139, but gave very different dynamic profiles in the strains harboring plasmid with putative promoter regions of *udhA* and *pntAB* (Fig. 3, middle row). From the fluorescence signal, we then determined the promoter activity time course and the integrated promoter activity (Fig. 3, bottom row). This integrated promoter activity quantifies the overall promoter activity from the intergenic region upstream of *udhA* or *pntAB* during the entire growth experiment (Fig. 3, bottom row, values in the insets). These results clearly demonstrated that the GFP reporter plasmids were useful to monitor expression of the transhydrogenases UdhA and PntAB, which was specific due to the different upstream intergenic regions present in the plasmids.

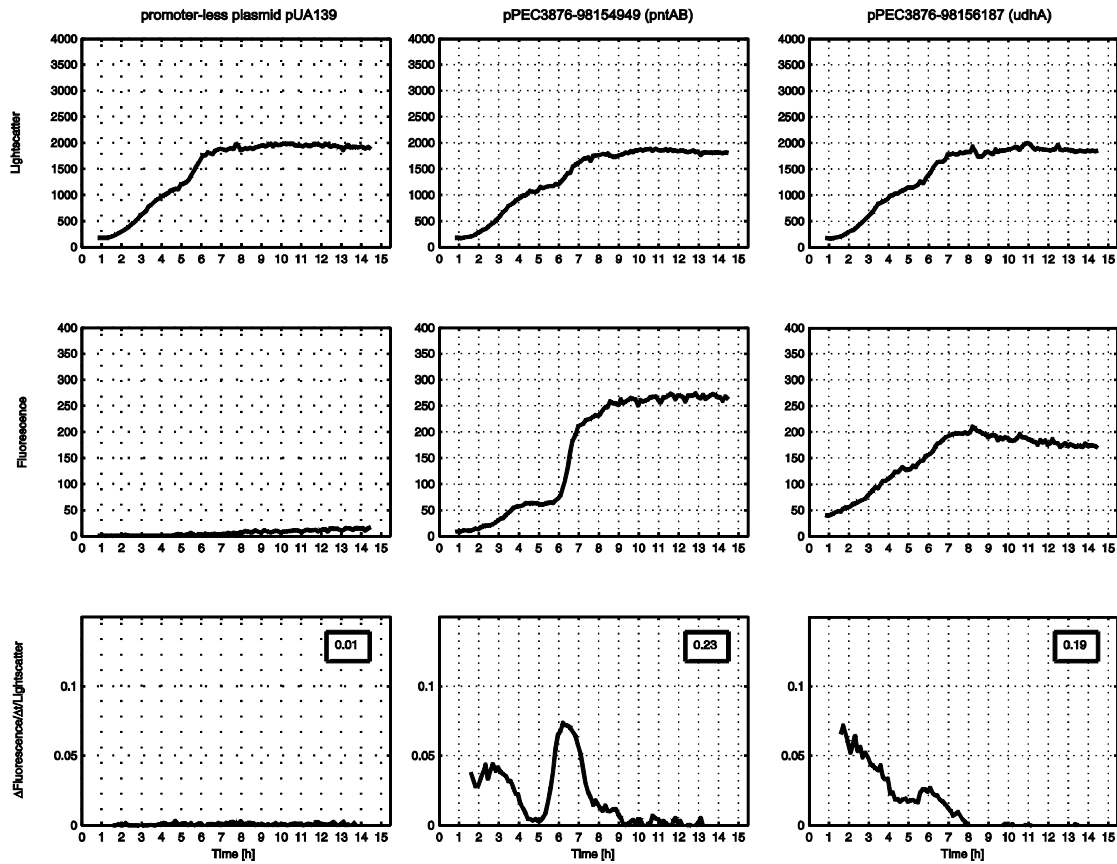


Figure 3 - Time courses of light scatter (biomass, top row), fluorescence (middle row) and promoter activity ($\Delta\text{fluorescence}/\Delta\text{time}/\text{light scatter}$, bottom row) for *E. coli* BW25113 wild-type during growth on glucose minimal medium. The *E. coli* BW25113 wild-type strain harbors the empty plasmid pUA139 (left column) or the pUA139 derivatives containing the intergenic region upstream of *pntAB* and *udhA* (middle and right column respectively). Integrated promoter activity is indicated in the insets, which reflects the total amount of GFP formed per cell (area below the curve).

Do transhydrogenase promoter activities correlate with NADPH balance?

To answer this question, we calculated the correlation *dist* as the absolute distance between the relative changes of both predicted transhydrogenase fluxes and integrated promoter activity for each substrate and mutant combination (Fig. 4A and 4B). A *dist* value of zero would result from a perfect correlation where both integrated promoter activity and predicted flux through a transhydrogenase increase or decrease by e.g. 50 % compared to the wild-type. Values close to zero still indicated a good correlation if the relative changes were in the same direction (both up or both down).

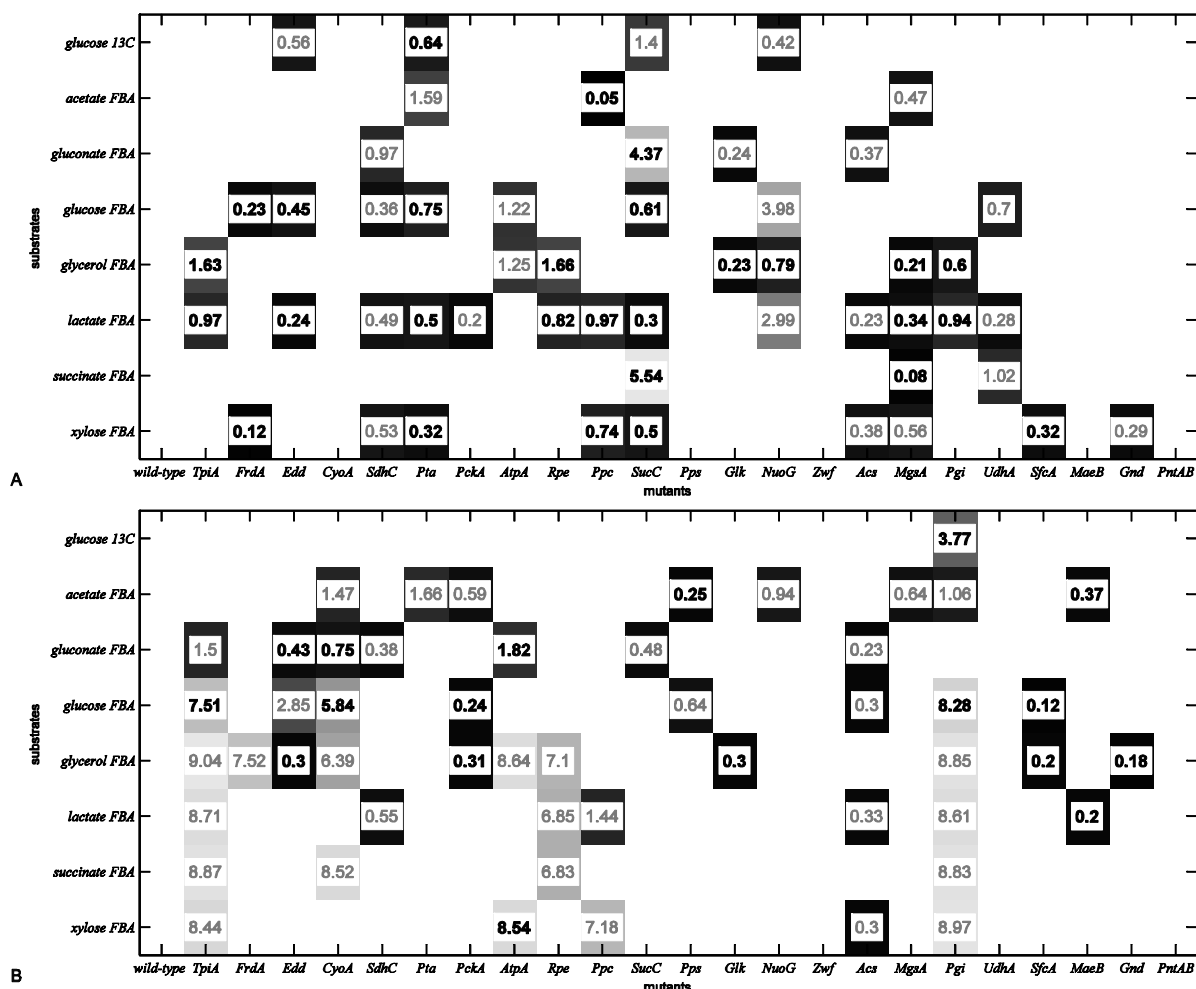


Figure 4 - Correlation (bold, black font) and anti-correlation (grey font) heat map of predicted transhydrogenase fluxes and integrated promoter activity (*pntAB*, A and *udhA*, B). Qualitatively, correlation is indicated for changes in same direction (both up or both down) and anti-correlation for changes in opposite direction (one up the other down). Quantitatively, black and light grey squares indicated good correlation (small *dist* values) and bad correlation (large *dist* values) respectively. Only correlation values were plotted, which were based on significant changes in integrated promoter activity (threshold = two times standard deviations of raw data).

For *pntAB*, only about half of the comparisons between integrated promoter activity and predicted transhydrogenase fluxes indicated a correlation (green background in Fig. 4A) and had also small *dist* values. For *udhA*, the majority of comparisons between integrated promoter activity and predicted transhydrogenase fluxes revealed an anti-correlation (red background in Fig. 4B). Moreover, the *dist* values covered a higher range than for *pntAB*

(maximal values up to 9 in comparison to about 4 for *pntAB*). Since there was no majority of correlations (green backgrounds) with small *dist* values for both *pntAB* and *udhA*, we concluded that there was no correlation between catabolic NADPH over- or underproduction and expression of transhydrogenase in *E. coli* in general.

Clustering promoter activity data

Since expression of *pntAB* or *udhA* is obviously not correlated with and thus regulated via the NADPH balance, we investigated next whether integrated promoter activities correlate with any other feature in the dataset. For this purpose, we clustered the integrated promoter activities, i.e. the area under the $\Delta\text{fluorescence}/\Delta\text{time}/\text{lightscatter}$ curve in Figure 3, bottom (complete dataset in Appendix) by calculating the pairwise correlation distances of the observations using MATLAB[®] (see Appendix for details). The clustering was performed in the typical way using data arranged in a matrix where the rows represent observations and columns contain many variables measured for every observation.

First, we searched for expression patterns that are specific for the two transhydrogenases and for the different substrates. Therefore, all combinations of substrates and PntAB or UdhA were set as observations containing the corresponding integrated promoter activities for all mutants as variables (Fig. 5). Here, we found that for all mutants the expression patterns of both transhydrogenases were very similar on the two gluconeogenic substrates acetate and succinate but that these expression patterns were very different from all other substrates. The finding of these two clusters relates to the metabolic network topology, where succinate and acetate enter carbon metabolism via TCA cycle / glyoxylate shunt whereas all other substrates are degraded by one of the three main catabolic pathways (EMP, PP and/or ED pathway) (Fig. 1). In the group of the non-gluconeogenic substrates, we found that both *pntAB* and *udhA* expression patterns on glucose were different from the other substrates while *pntAB* expression patterns for the remaining four substrates gluconate, glycerol, lactate and xylose clustered close together. From these results we concluded that transhydrogenase expression might be dependent on the nature of substrate, independent of the specific transhydrogenase.

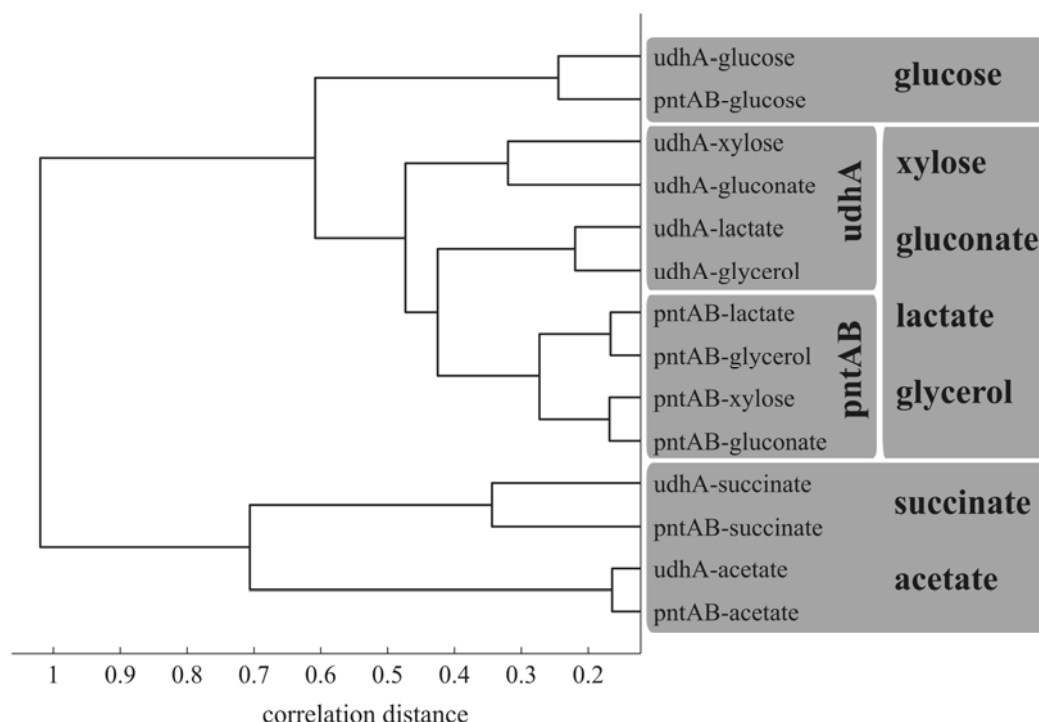


Figure 5 - Hierarchical cluster tree, leaves correspond to the observations (all *pntAB* or *udhA* and substrate combinations). X-axis values are a measure for correlation distance based on the variables (integrated promoter activities for each mutant).

Second, we tried to identify mutant specific expression patterns on all substrates for both transhydrogenases. Therefore, all mutants were set as observations and the integrated promoter activities for either PntAB or UdhA on all substrates were set as variables (Fig. 6). For both transhydrogenases, the mutants clustered into three groups. The mutants that clustered together in the three groups were largely identical for *udhA* and *pntAB* expression: Fig. 6, upper group: Pgi, NuoG, SucC, AtpA and SdhC; middle group: Rpe, MgsA and TpiA; lower group: Acs, Edd, Zwf, FrdA, Gnd, SfcA, Pps, MaeB and UdhA plus the wild-type. For some mutants, however, *pntAB* and *udhA* expression patterns belonged to different clusters (Ppc, Glk, Pta, PckA and CyoA). Interestingly, *ppc* and *pck*, which have opposite functions in glycolysis and gluconeogenesis during growth on e.g. glucose and acetate respectively, were identified as such “switching” mutants. Thus, their different response in expression of transhydrogenases provides further evidence that the nature of substrate indeed might be important.

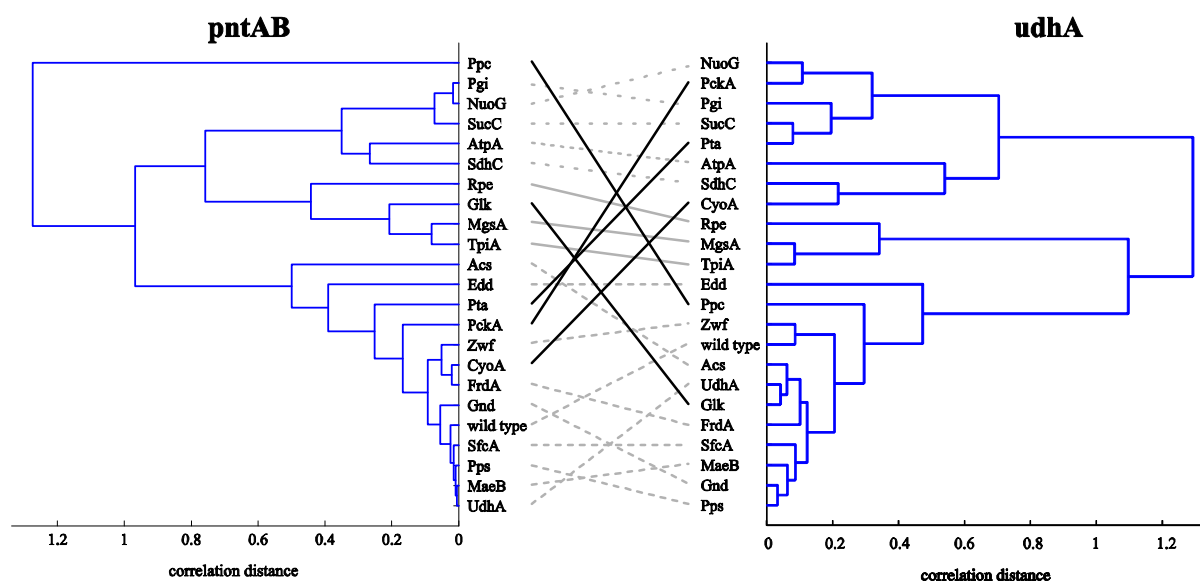


Figure 6 - Hierarchical cluster tree, leaves correspond to the observations (all mutants) for *pntAB* (left) and *udhA* (right). X-axis values are a measure for correlation distance based on the variables (integrated promoter activities for each substrate). Horizontal lines connect and sort equal genes into three groups (grey dotted, solid and dashed lines). Genes that are not in the same group for both *pntAB* and *udhA* expression are connected by black solid lines. Abbreviations: phosphoenolpyruvate carboxylase, Ppc; phosphoglucosomerase, Pgi; NADH dehydrogenase I subunit, NuoG; Succinyl-CoA synthetase beta-subunit, SucC; membrane-bound ATP synthase alpha-subunit, AtpA; succinate dehydrogenase membrane anchor subunit, SdhC; ribulose-5P epimerase, Rpe; glucokinase, Glk; methylglyoxal synthase, MgsA; triosephosphate isomerase, TpiA; acetyl-CoA synthetase, Acs; 6P-gluconate dehydratase, Edd; phosphotransacetylase, Pta; phosphoenolpyruvate carboxykinase, PckA; glucose-6P dehydrogenase, Zwf; cytochrome o oxidase subunit II, CyoA; Fumarate reductase flavoprotein subunit, FrdA; 6P-gluconate dehydrogenase, Gnd; NAD⁺-dependent malic enzyme, SfcA; phosphoenolpyruvate synthase, Pps; NADP⁺-dependent malic enzyme, MaeB and soluble transhydrogenase, UdhA.

Induced *pntAB* expression after switch from glucose to acetate

From both clustering analyses, we obtained indications that the nature of the substrates (glycolytic or gluconeogenic) might affect expression of *pntAB* and *udhA*. To provide further evidence for this conclusion, we compared the time courses of promoter activity on glucose and acetate. These two substrates are particularly interesting because during growth on glucose, *E. coli* wild-type typically accumulates acetate in the first growth phase, which is then taken up again in the second growth phase (29, 48). Thus, there is a switch from glycolytic to a gluconeogenic substrate during one growth experiment. On acetate as sole

carbon source, any effect related to this switch on the expression of transhydrogenases is expected to be absent.

To verify the above statement, we analyzed the time courses of the promoter activities during growth on glucose and acetate in detail. In Figure 7 it can be seen that the *pntAB* promoter was active ($\Delta\text{fluorescence}/\Delta\text{time}/\text{lightscatter}$, bottom row) during the first exponential growth phase in the wild-type grown on glucose. During the second growth phase on acetate, the *pntAB* promoter was active again with the same maximal promoter activity levels. In contrast, the *pntAB* promoter was less active in the second growth phase or completely absent in the acetyl-CoA synthetase (*Acs*) and phosphotransacetylase (*Pta*) mutants respectively. In these two mutants the secretion or uptake of acetate is impaired, as confirmed by the absent second growth phase (Fig. 7, top row). *Pta* encodes acetyl phosphotransferase, which is required for the acetate production by *E. coli* but also can convert acetyl-P back to acetyl-CoA (59, 159). This explains why no second growth phase was observed in the *Pta* mutant, which presumably accumulated only little acetate as was shown previously (29, 48). *Acs* encodes acetyl-CoA synthetase, which was shown to be a high-affinity but low-capacity uptake pathway for acetate (25, 116). Here the situation was different, acetate presumably was secreted but the uptake was impaired, which also led to the absent second growth phase. Unlike for *pntAB*, the expression of *udhA* was not affected in the *Acs* and *Pta* mutants; only the *UdhA* mutant itself exhibited an increased expression of *udhA* (Appendix).

During growth on acetate as sole carbon source, the integrated promoter activities of *pntAB* were similar to the values obtained after the diauxic shift (entire growth phase for *Acs* mutant) on glucose but the maximal promoter activity levels attained were about 3 times lower. In contrast, the levels and thus the integrated promoter activity originating from the *udhA* reporter plasmid were about two fold higher compared to growth on glucose, at least for the wild-type and the *PntAB* mutant. The *UdhA* and the *Pta* mutants did not grow at all on acetate and *Acs* only poorly (data not shown). To conclude, after the diauxic shift during growth on glucose, promoter activities of *PntAB* but not *UdhA* were higher than during growth on acetate as sole carbon source.

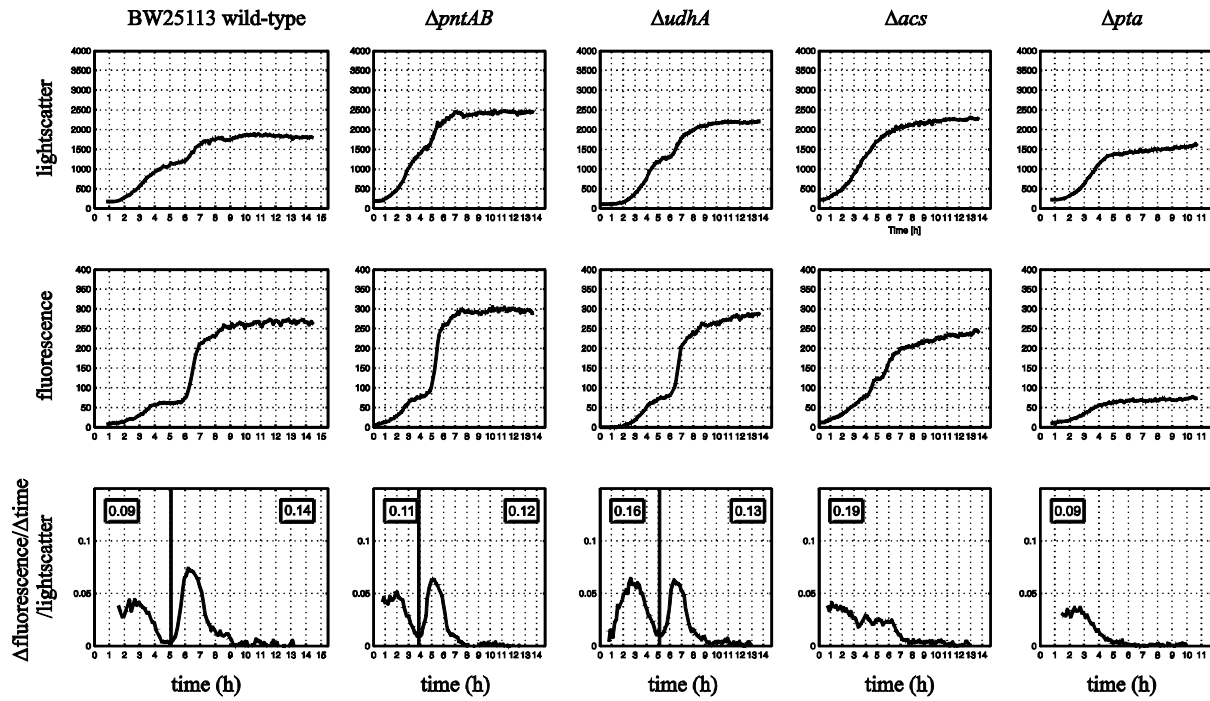


Figure 7 - Time courses of light scatter (biomass, top row), fluorescence (middle row) and promoter activity from the *pntAB* reporter plasmid ($\Delta \text{fluorescence} / \Delta \text{time} / \text{light scatter}$, bottom row) for *E. coli* BW25113 wild-type and *PntAB*, *UdhA*, *Acs* and *Pta* mutants during growth on glucose minimal medium. Integrated promoter activity is indicated in the insets, which reflects the total amount of GFP formed per cell (area below the curve left and right of the vertical line). The vertical line splits the time course in two phases observed in the top row (biomass).

Discussion

Our primary hypothesis that expression of transhydrogenases in *E. coli* would be regulated in response to the NADPH balance of the cell was obviously wrong. The basis for this conclusion was the fact that we could not observe a correlation between transhydrogenase expression levels and predicted transhydrogenase fluxes in mutants with systematically perturbed NADPH metabolism. Both transhydrogenases were clearly expressed at different levels in the acquired dataset and we clustered the integrated promoter activities to identify possible regulatory principles. This analysis revealed that the gluconeogenic substrates acetate and succinate caused similar expression patterns for both *udhA* and *pntAB*, while the expression patterns were completely different for all the other five substrates tested. This finding is consistent with wild-type microarray data where transcript levels of both *pntAB* and *udhA* were similar to each other on the gluconeogenic substrates succinate and acetate but together significantly different from glucose (119). We observed the same type of response to the nature of substrate not only for the wild-type, but for 23 different metabolic mutants on seven different substrates. For two of these mutants, *PckA* and *Ppc*, transhydrogenase expression clustered into opposed groups, which provided further evidence that gluconeogenic and glycolytic substrates cause different expression patterns. There may be of course other regulatory mechanisms present, which grouped the other mutants into the three distinct clusters.

In contrast to acetate, growth on glucose caused distinguishable expression dynamics in the two growth phases as consequence of the diauxic shift. *PntAB* was not only expressed during growth on glucose but was induced again after entering the second growth phase where *E. coli* typically consumes the previously secreted acetate (29, 48). Interestingly, the *UdhA* mutation did not have any effect during the second growth phase on glucose, which provides evidence that *PntAB* has to take over the NADPH balancing function after the acetate switch. The maximal *pntAB* promoter activity attained in the second growth phase of the wild-type on glucose was about 3 times higher than the one observed on acetate as sole carbon source. To conclude here, *pntAB* was strongly induced during growth on glucose only when the cell consumed the secreted acetate and the promoter activity levels were

significantly higher than the ones obtained during growth on acetate as sole carbon source. One explanation for that may be the pH in the medium as a major difference between the conditions, where *E. coli* cells grew on glucose secreted acetate and where *E. coli* cells grew on sodium acetate. Starting pH was always about 6.5, but it dropped during growth on glucose to about 4.5 due to acetate excretion (measured in glucose batch cultures, data not shown).

We see that transhydrogenases are transcriptionally regulated. Their response seems to be a function of substrates and pH, at least for PntAB. Until today, no regulator is known. What could be the link between pH and regulation of *pntAB* expression? It was shown for *E. coli* cells growing at neutral pH on glucose that exposure to acetate induces the RpoS (σ^S) mediated stress response, probably due to elevated acetyl-CoA levels, and that enhanced acid tolerance results from that response (10, 110). Furthermore, a recent transcriptome analysis revealed significantly increased RpoS, Dps, KatE and GrxB levels in cells grown on acetate compared to glucose (119). Dps, KatE and GrxB are related to oxidative stress, GrxB is a glutathione-dependent oxidoreductase (217). This substrate-dependent response might be mediated via sigma factor σ^{70} because the intergenic region upstream of *pntAB* contains a putative σ^{70} binding site (32). The housekeeping σ^{70} was shown to induce transcription of *acs* when switching from acetogenic substrates (any substrates that causes excretion of acetate) to acetate itself (115). In the absence of functional σ^{70} , cells could not reuse secreted acetate and absent expression of *acs* was shown on the enzyme activity, protein and transcript levels (115). These findings indicated that indeed *pntAB* could undergo similar regulation like *acs* and could therefore be controlled by σ^{70} . Overall, the results provide circumstantial evidence for regulatory mechanisms where accumulation of acetyl-CoA and/or pH stress might induce an oxidative stress like response during the second growth phase on glucose.

The soluble transhydrogenase UdhA was significantly expressed at various NADPH underproduction conditions (Appendix) despite its known function to counterbalance NADPH overproduction (179). An active UdhA during NADPH underproduction where PntAB is assumed to provide part of the NADPH would result in an energy-dissipating cycle, which is a disadvantage for the cell. *E. coli* might therefore require a regulatory mechanism to prevent UdhA activity under NADPH underproduction conditions, presumably allosteric

regulation since intracellular cofactor concentrations were found to be rather stable despite extremely different NADPH production rates (see **Chapter 5**).

To summarize, our data show that there is no apparent mechanism that relates transhydrogenase expression with the NADPH balance of the cell. Gluconeogenic and glycolytic substrates led to distinguishable expression patterns, which provide first evidence for regulatory mechanisms related to the nature of substrates. The observed expression levels for PntAB during pH and/or oxidative stress-like conditions points to a yet unknown regulatory mechanism besides its contribution to the NADPH formation during growth on glycolytic substrates. In addition, both transhydrogenases were also present at NADPH balance conditions where their activity would be detrimental to the cell. Therefore, the cell requires a general mechanism to prevent their activity, presumably by allosteric regulation.

Acknowledgements

We thank m2p-labs GmbH, 52074 Aachen, Germany, for providing the BioLector prototype that was used in this study; Robert Schütz and Ari Rantanen who assisted in the FBA-based transhydrogenase predictions and GFP data analysis, respectively.

Chapter 5

Pentose phosphate pathway flux in *Escherichia coli* is limited by the levels of glucose-6P- and 6P-gluconate dehydrogenase

Tobias Fuhrer, Stefan Christen and Uwe Sauer

Institute of Molecular Systems Biology, ETH Zürich, Zürich, Switzerland

manuscript in preparation

Stefan Christen did the purification and kinetic characterization of glucose-6P- and 6P-gluconate dehydrogenase.

Prof. Dr. Uwe Sauer designed the project, supervised the work and contributed to the writing.

Abstract

Despite its important role in providing the reducing equivalent NADPH and metabolic precursors for biomass production, regulation of flux through the pentose phosphate pathway remained obscure in *Escherichia coli*. Based on experimentally determined in vitro kinetic parameters of glucose-6P- and 6P-gluconate dehydrogenase and in vivo intracellular metabolite concentrations in mutants of initial glucose catabolism, we elucidated the kinetic properties of the oxidative pentose phosphate pathway in *Escherichia coli*. Of all metabolites and cofactors of the two dehydrogenases, only glucose-6P and 6P-gluconate accumulated 10-fold when flux was forced through the oxidative pentose phosphate pathway in a phosphoglucisomerase mutant. Both dehydrogenases were fully saturated at these 10-fold elevated concentrations and overexpression of 6P-gluconate dehydrogenase provided indirect evidence that at least this reaction was limited by the enzyme level. Out of 22 metabolites of central carbon metabolism and cofactors tested, 6 exhibited inhibitory effects on the two dehydrogenases with ATP and fructose-1,6-P as the strongest effectors. Overall, these results provide evidence that the abundance of the two dehydrogenases limits the oxidative pentose phosphate pathway flux, at least in mutants that rely exclusively on this pathway. NADH/NAD⁺ and NADPH/NADP⁺ redox ratios were surprisingly stable in both mutants and wild-type despite radically different flux distributions.

Introduction

In addition to energy, nutrients and the carbon backbone building blocks for biomass production, microorganisms require a continuous regeneration of the cofactor NADPH for anabolic reduction reactions. During batch growth of *Escherichia coli* on glucose minimal medium, about 63, 22 and 8 % of the total NADPH are required for protein, lipids and RNA synthesis, respectively (60, 138). The precise NADPH requirements depend on the biomass composition that varies with growth rate and conditions (42, 60). During maximum growth of *E. coli* in glucose minimal medium at 37°C at a rate of 0.67 h⁻¹, about 15.8 mmol NADPH are needed to produce 1 g cell dry weight (60), which corresponds to a net flux of NADPH into biomass of 10.6 mmol g⁻¹ h⁻¹.

This NADPH requirement must be fulfilled by NADPH regenerating reactions of the central carbon metabolism. These are glucose-6P- and 6P-gluconate dehydrogenase in the pentose phosphate (PP) pathway, isocitrate dehydrogenase in the tricarboxylic acid (TCA) cycle, NADPH-dependent malic enzyme and the membrane-bound transhydrogenase. During growth on glucose, these reactions provide about 35-45, 20-30, 0-5 and 25-45 % of the required NADPH respectively (65, 76, 153, 179). Other potential NADPH regeneration mechanisms were discussed already in **Chapter 3** and were not considered to be important under the conditions investigated here.

The importance for NADPH regeneration of glucose-6P-, 6P-gluconate and isocitrate dehydrogenase during growth on glucose is intuitively comprehensible because they are directly involved in glucose catabolism. Why and how cells choose to regenerate part of their NADPH from NADH through the energy dependent membrane-bound transhydrogenase and when the PP pathway is used instead is much less clear. Is there any stoichiometric or energetic reason to prefer one of the two pathways? In principle, higher PP pathway fluxes could substitute for the membrane-bound transhydrogenase, and this is perfectly feasible as fluxes in an *E. coli* Pgi mutant illustrate (179). This also the normal situation in other bacteria as shown in **Chapter 3** where glucose is mainly degraded through the glucose-6P dehydrogenase reaction and Entner-Doudoroff pathway (76). Suddenly increased PP pathway fluxes were described as a metabolic response to oxidative stress to supply NADPH for

reducing reactions of the stress response such as glutathione or ferredoxin reductase and peroxidase (78, 85). In this case, glucose-6P dehydrogenase is induced by the superoxide or nitric oxide-generating agents. This transcriptional regulation is mediated via the SoxRS regulatory system but does not involve NADPH itself (78, 85). Besides the well established PP pathway induction by oxidative stress, however, only indirect evidence is available for transcriptional or post-transcriptional regulation of glucose-6P- and 6P-gluconate dehydrogenase in *E. coli* (14, 171).

Growth rate dependent regulation of both glucose-6P- and 6P-gluconate dehydrogenase expression was postulated based on enzyme activities during growth on different substrates such as glucose and acetate (224). However, the choice of carbon substrates not only causes *E. coli* to have different growth rates but also completely different flux distributions with e.g. almost absent PP pathway fluxes on acetate (see **Chapter 4**). If anything, the lower the growth rates, the more NADPH per g biomass is needed based on the growth rate dependent biomass composition of *E. coli* (60). If at all, one would then expect a higher relative PP pathway flux at lower growth rates on glucose given the role of PP pathway in providing NADPH. This was observed at 30°C and the relative contribution of the PP pathway to the NADPH production was then also higher at 30°C compared to 37°C (75). In addition, data from chemostat experiments demonstrated that the lower the dilution rate, the higher the PP pathway was, at least over a broad range (136).

Genetic regulation of the PP pathway to provide NADPH was so far only shown for oxidative stress conditions but not for the metabolic demand of NADPH. In the absence of genetic regulation during oxidative stress conditions, allosteric regulation and kinetic properties of the PP pathway enzymes might be of importance but have not been considered in detail so far. Allosteric effectors are able to fine-tune the enzyme activities without participating in the reaction. They are even necessary to modulate flux when assuming constant substrate, product and enzyme concentrations. For the PP pathway enzymes, only a few metabolites and nucleotides were tested for their effect on the glucose-6P- and 6P-gluconate dehydrogenases by different authors (17, 28, 45, 146, 177, 214). A broad comparative screen for allosteric effectors is still missing.

The two enzymes of the PP pathway involving NADPH, glucose-6P- and 6P-gluconate dehydrogenase, were kinetically characterized in *Corynebacterium glutamicum* and intracellular metabolite concentrations were measured at different conditions (133). Under these conditions, the $\text{NADP}^+/\text{NADPH}$ ratio was altered by expressing cofactor specific glutamate dehydrogenases and the authors concluded that the in vivo activity of glucose-6P dehydrogenase was primarily regulated by the $\text{NADP}^+/\text{NADPH}$ concentration ratio (133). However, the authors did not significantly alter the carbon substrate concentrations under the published conditions. Therefore the conclusion that the $\text{NADP}^+/\text{NADPH}$ concentration ratio regulates the in vivo glucose-6P dehydrogenase activity is not surprising based on the kinetic properties and also does not resemble conditions of altered PP pathway flux.

For *E. coli*, kinetics of PP pathway enzymes were partially addressed by the work of Chassagnole *et al*, where rate laws were assumed and used within a broad kinetic model of the central carbon metabolism (31). However, the authors used kinetic parameters from the seventies and were not able to close the cofactor balance, which indicates either wrong cofactor concentrations or kinetic rate law and/or parameters. To conclude, the kinetic parameters of this key enzyme and also 6P-gluconate dehydrogenase were only partially characterized in *E. coli* over thirty years ago and the question of kinetic limitation of the PP pathway was never properly addressed with reliable intracellular metabolite concentrations (185). Together with a broad screen for allosteric effectors, reevaluation and determination of kinetic parameters presented in this work enabled us to use experimentally determined metabolite concentrations and finally investigate the kinetic properties of the oxidative PP pathway.

Here, we wanted to identify the limiting step of PP pathway flux. For this purpose we compare intracellular metabolite concentrations of the *E. coli* wild-type strain with a phosphoglucoisomerase mutant, which degrades all carbon through the PP pathway. The prediction of reaction velocities by the use of kinetic rate laws for glucose-6P- and 6P-gluconate dehydrogenase and the intracellular concentrations will identify potential kinetic limitation. In particular, we focus on the two dehydrogenases since they involve NADPH as cofactor, which might be the key to characterize the kinetic properties of the PP pathway.

Materials and Methods

Strains, media and growth conditions

In this study, *E. coli* MG1655 (Deutsche Sammlung von Mikroorganismen und Zellkulturen GmbH) and its Pgi and Zwf-EDP mutants were used (179). Aerobic batch cultures were grown at 37°C and 250 rpm in 500 mL baffled flasks with 50 mL of M9 minimal medium that contained per liter of deionized water: 7.52 g Na₂HPO₄•2H₂O, 3.0 g KH₂PO₄, 0.5 g NaCl and 2.5 g (NH₄)₂SO₄. The following components were sterilized separately and then added (per liter of final medium): 1 ml 0.1 M CaCl₂, 1 ml 1 M MgSO₄, 0.6 ml 100 mM FeCl₃, 2 mL of vitamin solution (filter sterilized) and 10 ml M9 trace salts solution. The vitamins solution contained (per 50 mL): 25 mg of each biotin, cyanocobalamin, niacin, calcium pantothenate, pyridoxine HCl and thiamine HCl. The M9 trace salts solution contained (per liter): 0.18 g ZnSO₄•7H₂O, 0.12 g CuCl₂•2H₂O, 0.12 g MnSO₄•H₂O and 0.18 g CoCl₂•6H₂O.

Sampling and extraction of intracellular metabolites for LC-MS/MS analysis

There are many different approaches considering quenching and separation of the cell pellet (130, 160). Separation of quenched bacterial cells from the medium by centrifugation causes loss of intracellular metabolite to a varying extent, which often can be recovered from the supernatant. To avoid loss of metabolites, *E. coli* cells grown on glucose minimal medium were harvested at mid-exponential growth phase by rapid centrifugation of 1 ml cell broth aliquots in a table-top centrifuge at 15,000 rpm and room temperature for 15 sec. Pellets and supernatants were subsequently frozen in liquid N₂ until further processing. Alternatively, 0.75 ml *E. coli* cell broth was directly frozen in liquid N₂ for whole cell broth extraction. Cell pellets were extracted three times with 0.5 ml 10 mM ammonium acetate buffer (pH 7.2) in 60% ethanol at 70°C for 1 min and the pooled supernatants of this extraction were completely dried in a speed-vac at 30°C and 0.14 bar and resuspended in 100 µl of 10 mM ammonium acetate buffer (pH 7.2). To test for increased recoveries for NADH and NADPH or NAD⁺ and NADP⁺ at basic or acidic conditions, respectively, cell pellets were alternatively extracted three times with 0.5 ml 2 M formate (pH 1.8) or 2 M NH₃ (pH 11.9) in 60% ethanol

at 70°C for 1 min and the pooled supernatants were completely dried in a speed-vac at 30°C and 0.14 bar and resuspended in 100 µl of extraction solution used. Whole cell broths were extracted 2 times with 0.75 ml of 0.2 M NaOH (final pH 12) or 0.2 M HCL (final pH 1.5) at 70°C for 1 min and compared to whole cell broth extractions done with 2 times 0.75 ml of 10 mM ammonium acetate buffer (pH 7.2) in 60% ethanol at 70°C and 1 min. Pooled supernatants were completely dried in a speed-vac at 30°C and 0.14 bar and resuspended in 100 µl of extraction solution used.

Metabolite quantification by LC-MS/MS method

All measurements were carried out on an Agilent 1100 Series HPLC system coupled with an Applied Biosystems / MDS SCIEX 4000 Q TRAPTM. Data were recorded and analyzed with Analyst Software Version 1.4.2 Build 1228. Chromatographic separation was achieved on a Phenomenex Hydro RP 150 mm x 2.1 mm x 4 µm column at 40°C using an adapted version of a published protocol (123). Briefly, the injected volume was 8 µl, and the mobile phase at a flow rate of 200 µl/min was directly introduced into the mass spectrometer via electro spray ionization (ESI). The gradient profile was linear with two phases (Table 1), where solution A was 10 mM tributylamine and 15 mM acetate in H₂O (pH 4.95) and solution B was 100 % methanol. Multiple reaction monitoring (MRM) settings were optimized individually for each metabolite except 6P-gluconolactone for which the MRM settings were adapted from 6P-gluconate (123).

Table 1 - Gradient profile applied for the LC-MS/MS method

Step	Total time (min)	Eluent A (vol.%)	Eluent B (vol.%)
1	0	100	0
2	15	45	55
3	27	34	66
4	28	0	100
5	33	0	100
6	35	100	0
7	55	100	0

Overexpression and purification of PP pathway enzymes

E. coli strains harboring over-expression plasmids for His-tagged PP pathway enzymes were obtained from the ASKA clone collection (111). These plasmids were transformed individually into the Pgi mutant and the mutants were grown in M9 minimal medium as described above in the presence of 0, 1, 10 and 100 μ M IPTG. Over-expression of the His-tagged glucose-6P- and 6P-gluconate dehydrogenase for kinetic characterization was performed in 50 ml LB medium containing 0.1 mM IPTG and 20 μ g/ml chloramphenicol at 250 rpm and 37°C. Bacterial cells were harvested by centrifugation at 4°C and washed twice in 0.9% NaCl and 10 mM MgSO₄. Cells were concentrated 10-fold in extraction buffer (100 mM Tris-HCl, pH 7.5, 5 mM MgCl₂, 1 mM dithiothreitol and Complete™ EDTA-free protease inhibitor cocktail (Roche)) and disrupted by passage through a french press at 4°C. Cell-free extracts were obtained by centrifugation at 23,100 x g and 30 min at 4°C.

His-tagged glucose-6P- and 6P-gluconate dehydrogenase were purified from cell-free extracts by HiTrap™ affinity columns from Amersham Biosciences following the manufacturer's instructions and active enzyme was obtained after dialysis using Spectra/Por® Float-A-Lyzer® membranes with a molecular weight cut-off of 25 kD. To determine the kinetic parameters, reduction of NAD⁺/NADP⁺ was monitored spectrophotometrically at 340 nm in 1 ml buffer (100 mM Tris-HCL, pH 7.5, 10 mM MgCl₂) at 30°C. Protein concentrations of the extracts were determined by the biuret assay (82). For the inhibitor screen, all metabolite solutions were prepared at a pH of 7.2 and stored at -30°C. Their impact on the enzyme activity was tested with 20 μ l of 8 or 12-fold diluted pure glucose-6P- or 6P-gluconate dehydrogenase respectively in 100 mM Tris-HCL (pH 7.5) and 10 mM MgCl₂ at different NADP⁺ and substrate concentrations.

Enzymatic characterization of glucose-6P- and 6P-gluconate dehydrogenase

Glucose-6P- and 6P-gluconate dehydrogenase were considered as sequential two-substrate (ordered Bi-Bi) and (ordered Bi-Ter) reactions respectively that are described by the complete raete equations (Appendix). From the complete rate equation, the following equation for the initial forward velocity in the absence of products can be derived, which was used for both glucose-6P- and 6P-gluconate dehydrogenase (189):

$$v = \frac{V_{\max} [A][B]}{K_{iA} K_{mB} + K_{mB} [A] + K_{mA} [B] + [A][B]} \quad (1)$$

A and B are the cofactor NADP^+ and glucose-6P or 6P-gluconate. K_M and K_i are the Michaelis-Menten and dissociation constants. When the oxidized cofactor is kept constant, equation 1 can be linearized and primary Lineweaver-Burk plots are applied to determine Michaelis-Menten and dissociation constants:

$$\frac{1}{v} = \frac{K_{iA} K_{mB}}{V_{\max} [A][B]} + \frac{K_{mA}}{V_{\max} [A]} + \frac{K_{mB}}{V_{\max} [B]} + \frac{1}{V_{\max}} \quad (2)$$

Where the slope (Sl) of the function $1/v$ versus $1/[A]$ is described by:

$$Sl = \frac{K_{iA} K_{mB}}{V_{\max} [B]} + \frac{K_{mA}}{V_{\max}} \quad (3)$$

and the axis intercept (AI) by:

$$AI = \frac{K_{mB}}{V_{\max} [B]} + \frac{1}{V_{\max}} \quad (4)$$

The slopes and intercepts were plotted against $1/[B]$ in secondary Lineweaver-Burk plots to obtain the values for K_{MA} , K_{MB} and K_{iA} . The obtained values for K_{MA} , K_{MB} and K_{iA} were confirmed by using nonlinear regression with equation 1.

Competitive and uncompetitive inhibition of NADP^+ or substrate binding by NADPH, product or any other inhibitor was then determined with only one substrate varied at different NADPH concentration. A general rate law of mixed-type inhibition describes this experiment (189):

$$v = \frac{V_{\max} [S]}{\left(1 + \frac{[I]}{K_{ic}}\right) K_m + \left(1 + \frac{[I]}{K_{iu}}\right) [S]} \quad (5)$$

which can be linearized similarly as equation 1:

$$\frac{1}{v} = \frac{K_m}{V_{\max}} \left(1 + \frac{[I]}{K_{ic}}\right) \frac{1}{[S]} + \frac{1}{V_{\max}} \left(1 + \frac{[I]}{K_{iu}}\right) \quad (6)$$

Where the slope (Sl) of the function $1/v$ versus $1/[S]$ is described by:

$$Sl = \frac{K_m}{K_{ic} V_{\max}} [I] + \frac{K_m}{V_{\max}} \quad (7)$$

and the axis intercept (AI) by:

$$AI = \frac{1}{K_{ic} V_{\max}} [I] + \frac{1}{V_{\max}} \quad (8)$$

The slopes and intercepts were plotted against $1/[I]$ to obtain the values for K_{ic} and K_{iu} . The obtained values for K_{ic} and K_{iu} were confirmed by using nonlinear regression with equation 5.

For the rate predictions using intracellular metabolite concentrations, the rate laws describing the forward reaction in the presence of both educts and products were used that were previously published for glucose-6P dehydrogenase in *C. glutamicum* and *E. coli* (31, 133). Only the forward reaction with NADPH inhibition was simulated since the 6P-gluconolactone produced reacts rapidly further to 6P-gluconate and in addition is very instable (18):

$$V_{G6PDH} = \frac{V_{\max} [\text{NADP}^+][\text{G6P}]}{K_{i,\text{NADP}^+} K_{m,\text{G6P}} \left(1 + \frac{[\text{NADPH}]}{K_{ic,\text{NADPH},\text{NADP}^+}} \right) + K_{m,\text{G6P}} [\text{NADP}^+] + K_{m,\text{NADP}^+} [\text{G6P}] \left(1 + \frac{[\text{NADPH}]}{K_{ic,\text{NADPH},\text{NADP}^+}} \right) + [\text{NADP}^+][\text{G6P}]} \quad (9)$$

6P-gluconate dehydrogenase was assumed to be irreversible due to the CO_2 production. The same rate law was assumed to include inhibition by NADPH (similar to equation 9) and alternatively following previously proposed rate law including inhibition by ATP was adapted (31, 133):

$$V_{6PGDH} = \frac{V_{\max} [\text{NADP}^+][6\text{PG}]}{K_{i,\text{NADP}^+} K_{m,6\text{PG}} \left(1 + \frac{[\text{NADPH}]}{K_{ic,\text{NADPH},\text{NADP}^+}} \right) + K_{m,6\text{PG}} [\text{NADP}^+] + K_{m,\text{NADP}^+} [6\text{PG}] \left(1 + \frac{[\text{NADPH}]}{K_{ic,\text{NADPH},\text{NADP}^+}} \right) + [\text{NADP}^+][6\text{PG}]} \quad (10)$$

$$V_{6PGDH} = \frac{V_{\max} [6\text{PG}][\text{NADP}^+]}{([6\text{PG}] + K_{m,6\text{PG}})([\text{NADP}^+] + K_{m,\text{NADP}^+} (1 + \frac{[\text{NADPH}]}{K_{ic,\text{NADPH},\text{NADP}^+}})(1 + \frac{[\text{ATP}]}{K_{ic,\text{ATP},\text{NADP}^+}}))} \quad (11)$$

Further rate laws were tested, which also included inhibition by NADPH of binding of the substrates (competitive and uncompetitive) for both enzymes (Appendix equations I and III). In addition, inhibition by ribulose-5P of binding of the NADP^+ (competitive and uncompetitive) and of the 6P-gluconate (competitive) was considered (Appendix equation IV). Simultaneous inhibition by more than one metabolite was considered by including the inhibitory fraction ($[I]/K_i$) into the same inhibitory term (Appendix equation II and V) (189).

Results

The main metabolic reactions for NADPH regeneration, the two dehydrogenases of the PP pathway and the membrane-bound transhydrogenase PntAB, regenerate each about 40% of the NADPH in *E. coli* during exponential batch growth on glucose. There does not seem to be any fundamental energetic or stoichiometric reason for the cell to prefer the one or the other pathway. While maximum theoretical biomass yields would only be obtained with exclusive use of PntAB because loss of CO₂ is precluded (212), more realistic objective functions for such flux balance analysis (186) show that both pathways are used equally or even the PP pathway exclusively (Appendix). Similarly, estimating the energy cost per NADPH regenerated through either pathway revealed basically identical energetics (Appendix). Since there is no fundamental stoichiometric or energetic reason to use the PP pathway, regulation and/or the kinetic properties of the PP pathway enzymes must be responsible for maintaining a particular flux. Besides the known transcriptional regulation during oxidative stress conditions and some indirect evidence on possible genetic regulation there is no known regulatory mechanisms for the PP pathway (14, 78, 85, 171). Thus, we hypothesized that the kinetics of the PP pathway dehydrogenases might determine the in vivo PP pathway usage.

Determination of intracellular metabolite concentrations

To investigate whether the NADP⁺/NADPH or substrate/product ratios could possibly be involved in the PP pathway regulation, we determined intracellular concentrations of redox cofactors and PP pathway metabolites in *E. coli* wild-type during aerobic batch growth on glucose. In addition to the wild-type, we also investigated two mutants with completely inactive and exclusively active PP pathway, Zwf-EDP and Pgi mutants, respectively.

We tested different sampling and extraction procedures for their impact on the quality of LC-MS/MS spectra and the recovery of metabolites of interest. Direct whole cell broth extraction with ammonium acetate buffer or NaOH and HCL solution led to severe loss of metabolites, probably because of medium salts and pH (data not shown) (170). Both extreme pH and medium salts might catalyze degradation of unstable metabolites during extraction.

To improve recovery, we then tested rapid centrifugation and extracted the pellets subsequently under neutral (ammonium acetate buffer pH 7.2), basic and acidic conditions (NH_3 and formate solution). NH_3 turned out to be very harmful for all metabolites and gave also unreliable LC-MS/MS spectra. Formate was less harmful but recovery of metabolites still was worse than extraction with ammonium acetate buffer (data not shown).

Since we considered this as the currently best method, all concentrations were determined after rapid centrifugation of cells and extraction with ammonium acetate buffer by LC-MS/MS quantification (Fig. 1 and Table 2). Less than 10% of total metabolite amounts were detected in the supernatant after rapid centrifugation except for ATP and ADP where the supernatant concentrations were significant. For these two metabolites, the amounts detected in the supernatant were added to the amounts of extraction to give the final metabolite concentrations. Most prominent, 10-fold changes were observed between the wild-type and the Pgi mutant for the concentrations of glucose-6P and 6P-gluconate while the intermediate 6P-gluconolactone pool was not affected (Fig. 1). In the Zwf-EDP mutant, the concentrations of 6P-gluconolactone, 6P-gluconate and pentoses were significantly reduced, which is in agreement with absent flux through PP pathway. Remaining pentoses were assumed to be formed by backward flux through lower PP pathway to provide precursors for biomass. For the involved redox cofactor NADP^+ , absolute concentrations of the reduced and oxidized form were stable, which also resulted in a stable NADPH reduction charge despite drastically different fluxes through the PP pathway (Table 2). Therefore, a regulatory role of the redox cofactor concentrations and/or the NADPH reduction charge can be excluded. The energy charge was strongly reduced in the Pgi mutant but only slightly increased in the Zwf-EDP mutant (Table 2).

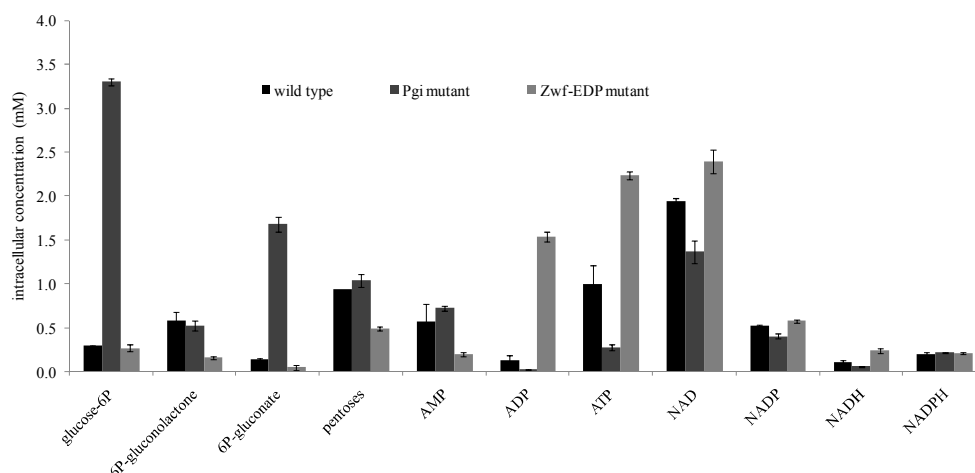


Figure 1 - Intracellular metabolite concentrations determined by LC-MS/MS method for *E. coli* wild-type, Pgi and Zwf-EDP mutant. All measurements are triplicate extractions with ammonium acetate buffer.

Table 2 - Ratios of intracellular metabolite concentration

	wild-type	Pgi mutant	Zwf-EDP mutant
energy charge ^a	0.63	0.28	0.76
NADH reduction charge	0.05	0.04	0.09
NADPH reduction charge	0.27	0.35	0.26
6PGon ^b /G6P	2.01	0.16	0.59
6PG/6PGon	0.24	3.24	0.26

^a energy charge = $([ATP] + \frac{1}{2}[ADP])/([ATP] + [ADP] + [AMP])$, NAD(P)H reduction charge = $[NAD(P)H]/([NAD(P)H] + [NAD(P)^+])$

^b Abbreviations: glucose-6P (G6P), 6P-gluconolactone (6PGon) and 6P-gluconate (6PG)

To determine the thermodynamic feasibility of the determined intracellular metabolite and cofactor concentrations, we calculated the Gibbs reaction energies for glucose-6P- and 6P-gluconate dehydrogenase, 6P-gluconolactonase and the two transhydrogenases using the software anNET (Fig. 2) (117, 234). The Gibbs reaction energies obtained based on the intracellular concentrations have to be negative for the PP pathway enzymes to occur spontaneously in the direction for glucose-6P towards ribulose-5P, which was the case for all

three enzyme in the wild-type and both Pgi and Zwf-EDP mutant (Fig. 2). Both dehydrogenases of the PP pathway exhibited more negative Gibbs energies of reaction in the Pgi mutant and the opposite was observed for the reaction catalyzed by the 6P-gluconolactonase (Figure 2), which is in agreement with limiting enzyme capacity in the dehydrogenase steps but not the lactonase reaction. To conclude, we verified our obtained intracellular concentrations to be thermodynamically feasible and found that the cofactor concentrations are not involved in the regulation of PP pathway flux. Are then only the metabolite concentrations controlling the PP pathway flux through kinetic and/or allosteric regulation?

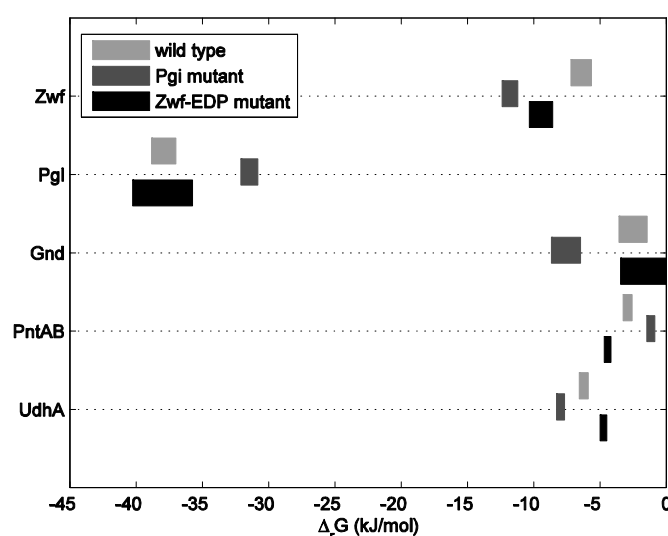


Figure 2 - Gibbs reaction energies of transhydrogenases and oxidative PP enzymes in wild type *E. coli* and Pgi and Zwf-EDP mutants. Glucose-6P dehydrogenase (Zwf), 6P-gluconolactonase (Pgl), 6P-gluconate dehydrogenase (Gnd), membrane-bound (PntAB) and soluble transhydrogenase (UdhA). Bars represent the range of Gibbs reaction energies obtained based on the metabolite concentration ranges.

In vitro kinetic characterization of glucose-6P- and 6P-gluconate dehydrogenases

Next, we wanted to relate the in vivo metabolite and cofactor concentrations to the enzyme properties to determine their impact on controlling the PP pathway flux. For this purpose and also to identify potential allosteric regulators that could modulate PP pathway fluxes, we determined the kinetic parameters of glucose-6P- and 6P-gluconate

dehydrogenase. Both dehydrogenases were purified as His-tagged proteins from crude cell extracts of *E. coli* K12 strain AG1 (111) to a specific activity of 187'000 and 54'500 U g⁻¹ (Fig. 3). The purity obtained was high because no other proteins eluted from the His-Tag column and no inclusion bodies were observed after centrifugation by analyzing the pellet on SDS PAGE gels (Fig. 3).

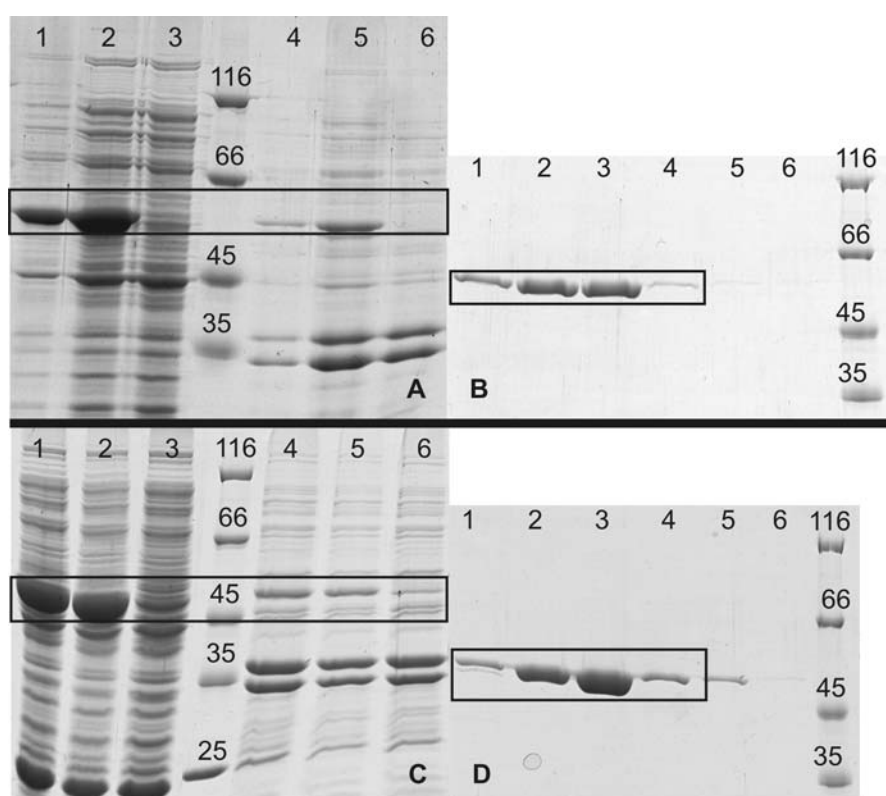


Figure 3 - Coomassie Blue stained SDS-PAGE of crude cell extracts containing overexpressed glucose-6P dehydrogenase (A) and 6P-gluconate dehydrogenases (C) with His-tag. Overexpression was induced by different concentrations of IPTG (0.1, 1 and 0 mM in lanes 1, 2 and 3 respectively in A and C). Corresponding cell pellets after centrifugation (0.1, 1 and 0 mM in lanes 4, 5 and 6 respectively in A and C). SDS-PAGE of elution fractions after HisTrap purification of glucose-6P dehydrogenase (B) and 6P-gluconate dehydrogenases (D). The enzymes were eluted with different imidazole concentrations (100 - 200, 200, 200 - 300 and 300 mM at lanes 1, 2, 3 and 4 respectively, wash fractions with 500 mM imidazole at lanes 5 and 6).

Initial reaction velocities at different starting conditions were determined using a second order polynome fit and the kinetic parameters were obtained from secondary Lineweaver-Burk plots (Table 3). The main kinetic parameters (K_M of substrates and K_i of NADPH) were confirmed by non-linear regression fits with Sigma-Plot using the corresponding rate laws

and were in the range of previously reported *E. coli* values from various sources (17, 28, 146, 177). Consistent with previous in vitro data obtained with crude extracts (**chapter 3**), both purified enzymes did not exhibit any detectable activity with NAD^+ and were therefore considered to be specific for NADP^+ . Product inhibition of glucose-6P dehydrogenase by 6P-gluconolactone could not be investigated because of the instability of the lactone (132).

Table 3 - Kinetic parameters of purified enzymes [μM]

	glucose-6P dehydrogenase	6P-gluconate dehydrogenase
K_M		
NADP ⁺	23	9
glucose-6P	136	-
6P-gluconate	-	19
K_i		
NADP ⁺	90	19
NADPH inhibition		
K_{ic,NADP^+}	35	20
$K_{ic,\text{glucose-6P}}$	100	-
$K_{ic,6\text{P-gluconate}}$	-	130
$K_{m,6\text{P-gluconate}}$	-	190
product inhibition		
$K_{m,6\text{PG,NADP}^+}$	4250	-
$K_{ic,6\text{PG,G6P}}$	2000	-
$K_{ic,\text{R5P,NADP}^+}$	-	311
$K_{m,\text{R5P,NADP}^+}$	-	1160
$K_{ic,\text{R5P, 6PG}}$	-	250

Errors were below 20% and absolute values were confirmed by non-linear regression fits with the corresponding rate laws.

To identify potential allosteric effectors of both dehydrogenases, we screened 21 metabolites of central carbon metabolism for their impact on the initial reaction velocities (Table 4). The assay concentrations of metabolic substrates, NADP^+ , glucose-6P and 6P-gluconate were chosen to be in the range of the corresponding K_M values to observe

inhibitory effects on the initial reaction rates (Table 4). Inhibitory concentrations of metabolites were chosen to resemble typical *in vivo* concentrations (117).

Generally, none of the investigated metabolites affected the glucose-6P dehydrogenase reaction velocity significantly in the physiological concentrations range (125 or 300 μ M) tested (Table 4). The only two exceptions were citrate and 6P-gluconate. In the former case, the 25% inhibition at 125 μ M glucose-6P concentration was not seen at 5 mM glucose-6P (<5% inhibition, data not shown). Intracellular citrate concentrations did not change in the Pgi or Zwf-EDP mutant (data not shown) and in the Pgi mutant the glucose-6P was close to a level where the inhibition of citrate might be absent. Therefore, we considered potential inhibition by citrate as not relevant under the tested conditions. The other relevant inhibitor of glucose-6P dehydrogenase was 6P-gluconate, which was analyzed in detail (Table 3). These values are relatively high because 6P-gluconate is not the direct product of glucose-6P dehydrogenase but the product of the fast 6P-gluconolactonase reaction.

In contrast to glucose-6P dehydrogenase, 6P-gluconate dehydrogenase activity was significantly inhibited by several effectors, most prominently by four intermediates of the EMP pathway, two pentose phosphates and ATP (Table 4). This inhibition at the physiological 6P-gluconate concentration range of 13 to 84% was abolished at a 6P-gluconate concentration of 5 mM. The sole exception was the by far strongest inhibition through fructose-1,6-bisP, which was effective at both concentrations. Since the intracellular concentrations of glyceraldehyde-3P, 3P-glycerate and PEP were significantly lower in the Pgi mutant than in the wild-type (far below the concentrations used for the screen) and thus did not exhibit any effect under these conditions, we did not determine the corresponding inhibition constants. We determined the inhibition constant only for ribulose-5P, while we used published inhibition constants for ATP and FBP (45, 133).

Table 4 - Relative in vitro reaction rates in the presence of potential inhibitors^a

	glucose-6P dehydrogenase		6P-gluconate dehydrogenase	
	25 μ M	25 μ M	20 μ M	20 μ M
	NADP ⁺	NADP ⁺	NADP ⁺	NADP ⁺
	125 μ M G6P	300 μ M G6P	40 μ M 6PG	5 mM 6PG
<i>EMP pathway</i>				
2 mM glucose-6P	- ^b	-	96	-
1 mM fructose-6P	105	-	94	-
2 mM fructose-1,6-bisP	98	-	16	72
1 mM glyceraldehyde-3P	95	-	60	92
4 mM 3P-glycerate	96	-	62	96
2 mM PEP	107	-	69	95
2 mM pyruvate	98	-	95	-
<i>PP pathway</i>				
0.6 mM ribose-5P	-	102	60	99
0.6 mM erythrose-4P	-	119	87	96
0.5 mM ribulose-5P	-	98	39	96
1 mM 6P-gluconate	-	80	-	-
<i>TCA cycle</i>				
5 mM malate	103	-	92	-
2.5 mM oxaloacetate	106	-	93	-
2.5 mM oxalate	109	-	111	-
5 mM isocitrate	98	-	83	-
5 mM α -ketoglutarate	87	-	98	-
5 mM citrate	75	-	95	-
<i>Cofactors</i>				
1 mM ATP	-	101	59	93
1 mM ADP	-	109	95	-
0.5 mM NAD ⁺	104	-	99	-
0.5 mM NADH	103	-	101	-

^a normalized to the velocities of the purified enzyme without inhibitors, standard deviations were generally below 5%

^b not determined

Prediction of in vivo reaction rates using different rate laws

To quantify the impact of changing metabolite concentrations on the PP pathway flux by kinetic regulation, we then predicted the in vivo reaction rates of the PP pathway dehydrogenases in wild-type and the Pgi and Zwf-EDP mutants based on the experimentally determined enzyme kinetics and intracellular metabolite concentrations. The reaction rates of glucose-6P- and 6P-gluconate dehydrogenases were plotted versus a range of substrate concentrations that are physiologically relevant (Fig. 4 and 5). To investigate whether inhibition by cofactors plays a relevant role, we tested different rate laws with and without different inhibition terms of the cofactors. Specifically, we used equations 1, 9 and Appendix equations I and II or 1, 10, 11, Appendix III, IV and V with the experimentally determined kinetic parameters (Table 3).

For glucose-6P dehydrogenase independent of the chosen rate law, the enzyme was not saturated in the wild-type and the Zwf-EDP mutant (Fig. 4) because the in vivo glucose-6P concentrations were about 0.3 mM. In the Pgi mutant with about 10-fold higher glucose-6P concentration, the enzyme was fully saturated, independent of the assumed rate law. Since the concentrations of NADP^+ and NADPH were rather constant for all three strains, they did not have a significant impact on the predicted rates within one assumed rate law (Equations 9 and Appendix equation I) (Fig. 4). Mixed-type inhibition by 6P-gluconate was included additionally, which gave basically the same behavior as the previous rate laws except for the Pgi mutant where 6P-gluconate accumulated and therefore significantly reduced the apparent V_{max} (Appendix equation II). Rate laws that include inhibition by NADPH reduced the apparent V_{max} by about 30-50% in the wild-type and also the mutants. This explains why the previously determined intracellular net fluxes (75, 179) were about 50% of determined crude cell extract activities of glucose-6P dehydrogenase (4.9 and 2.0 $\text{mmol g}^{-1} \text{h}^{-1}$ respectively) in the wild-type measured at optimal conditions (saturated and no inhibitory effects) and thus provides evidence that inhibition by NADPH is important.

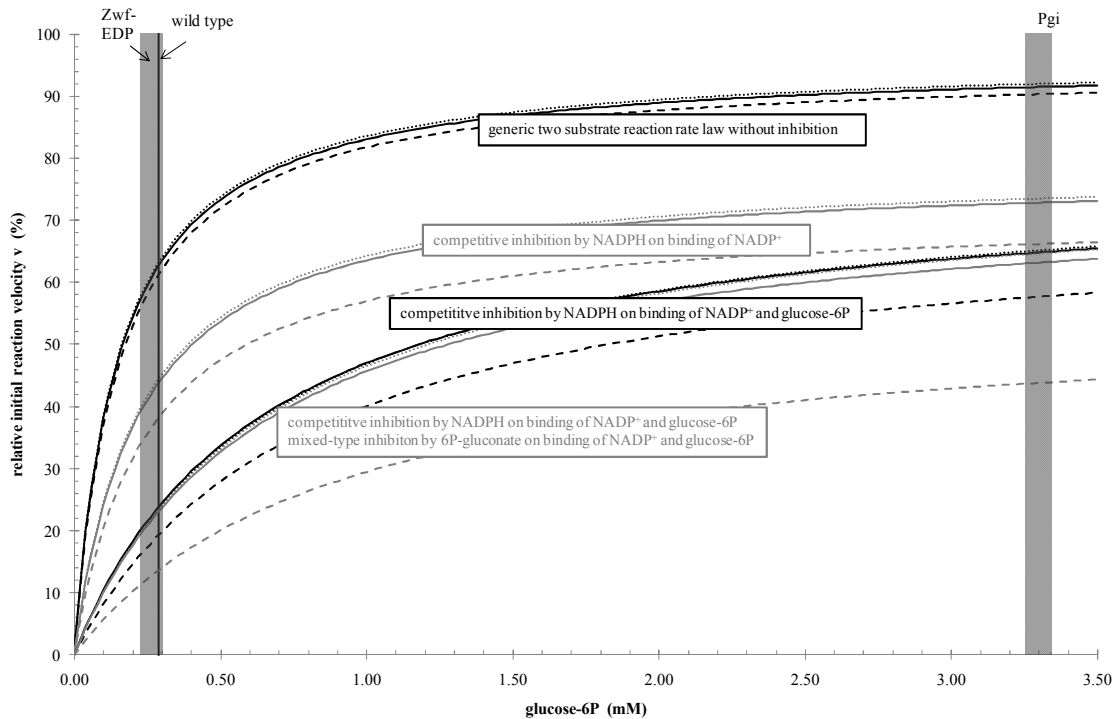


Figure 4 - Dependency of the relative reaction velocity of glucose-6P dehydrogenase on the glucose-6P concentration as a consequence of different rate laws (equations 1, 9, Appendix equations I and II). V_{\max} was set arbitrarily to 100%. Vertical black or grey bars indicate the in vivo glucose-6P concentration range of different strains (Fig. 2). The slightly varying NADP^+ and NADPH concentrations were taken into account for wild-type (solid line), Pgi mutant (dashed line) and Zwf-EDP mutant (dotted line).

For 6P-gluconate dehydrogenase, the same type of basic rate laws were tested as for glucose-6P dehydrogenase (equations 1, 10 and Appendix equations III) (Fig. 5). As we observed an inhibitory effect for ATP, we tested the additional rate law that includes an inhibition constant for ATP (equation 11 and the competitive inhibition constant for ATP 1.3 mM) (133). Product inhibition by ribulose-5P was investigated in detail (Table 3) and we included the inhibition constants with appropriate rate law for simulation (Appendix equation IV). Simultaneous inhibition by both NADPH and ribulose-5P had then the strongest effect on the apparent V_{\max} (Fig. 5, rate law Appendix equation V). Inhibition by fructose-1,6-P was assumed to be uncompetitive based on previously published data (45). Since maximal inhibition of 60% was observed with fructose-1,6-P concentrations above 0.2 mM (45), we

could define $V_{max,apparent} \approx 0.4 * V_{max}$ because intracellular concentrations of fructose-1,6-P were above 0.2 mM in wild-type and both mutants under the conditions investigated (data not shown). We did not need to use a rate law for the allosteric inhibition by fructose-1,6-P but just considered the reduced V_{max} . The other observed inhibitory effects by the EMP pathway intermediates, glyceraldehyde-3P, 3P-glycerate and PEP were not included for simulation because intracellular in vivo concentrations were significantly lower in the Pgi mutant compared to the tested inhibitory concentrations (data not shown). That means that a rate law considering the corresponding inhibitory terms would yield similar initial reaction velocities as a rate law without the inhibitory terms.

In contrast to glucose-6P dehydrogenase, the 6P-gluconate dehydrogenase was much closer to saturation already in the wild-type, and this was largely independent of the assumed rate law (Fig. 5). Again, the concentration of 6P-gluconate was roughly 10-fold higher in the Pgi mutant, which was fully saturating the enzyme. The rate laws including only competitive inhibition by NADPH and/or ATP (equation 10 and 11) allowed for at least 60% of V_{max} . As observed already for glucose-6P dehydrogenases, the concentrations of $NADP^+$ and NADPH were rather constant for all three strains and did not have a significant impact on the predicted rates within any assumed rate law. Additional noncompetitive inhibition by NADPH, product inhibition by ribulose-5P had a strong effect with maximal rates of about 60% (Fig. 5) (Appendix equations III, IV and V). As observed for the glucose-6P dehydrogenase, the determined intracellular net fluxes were about half the crude cell extract activities of 6P-gluconate dehydrogenase (3.1 and 1.9 mmol g⁻¹ h⁻¹ respectively) in the wild-type measured at saturated conditions (75, 179).

Overall, the results reveal that the strongest effect on the kinetic behavior of glucose-6P- and 6P-gluconate dehydrogenases in the Pgi mutant compared to the wild-type was caused by the about 10-fold increase of glucose-6P and 6P-gluconate. As a consequence both enzymes were fully saturated in the Pgi mutant, which pointed to limiting enzyme levels. In the wild-type, if at all, only the 6P-gluconate dehydrogenase level might be limiting because the enzyme was close to saturation and its V_{max} was additionally reduced by Fructose-1,6-P. In general, the inhibition by cofactors and products reduced the maximal reaction velocities for

both dehydrogenase in wild-type and the Pgi mutant providing further evidence for limiting enzyme levels.

To proof that the attainable V_{max} is indeed limiting the PP pathway, we tried to overexpress glucose-6P- and 6P-gluconate dehydrogenases in the wild-type and the Pgi mutant. Due to the severe growth defects observed during overexpression on glucose minimal medium, only the Pgi mutant showed reproducible effects. Among all PP pathway enzymes overexpressed, only overexpressing 6P-gluconate dehydrogenase did not reduce growth and glucose uptake rate compared to the Pgi mutant without plasmid. We concluded that this was due to a at least partly released limitation in the PP pathway, which provided indirect evidence that 6P-gluconate dehydrogenases levels inside the cells were limiting in the Pgi mutant.

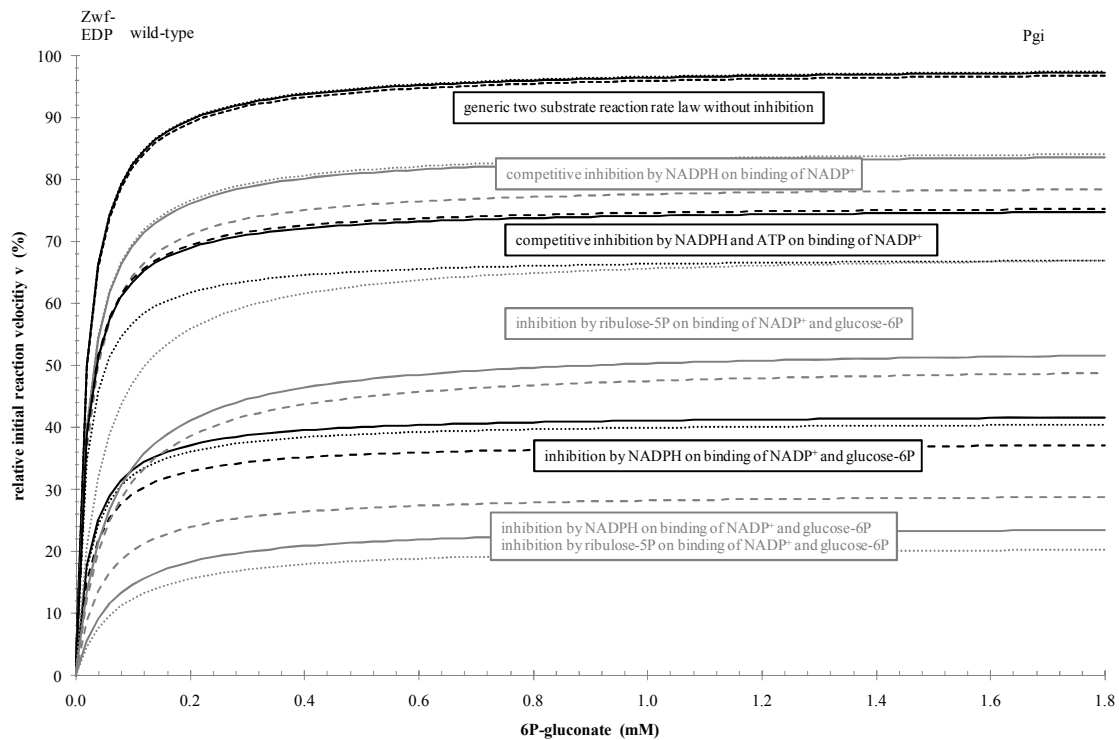


Figure 5 - Dependency of the relative reaction velocity of 6P-gluconate dehydrogenase on the 6P-gluconate concentration as a consequence of different rate laws (equations 1, 10, 11, Appendix III, IV and V). V_{max} was set arbitrarily to 100%. Vertical grey bars indicate the in vivo 6P-gluconate concentration range of different strains (Fig. 2). The slightly varying $NADP^+$ and NADPH concentrations were taken into account for wild-type (solid line), Pgi mutant (dashed line) and Zwf-EDP mutant (dotted line).

Discussion

About 25% of the glucose flux is channeled through glucose-6P dehydrogenase in wild-type *E. coli*. In a Pgi mutant, all of the glucose is degraded through glucose-6P dehydrogenase and about 90% of it also through 6P-gluconate dehydrogenase while the growth rate is significantly decreased from 0.67 h^{-1} to 0.18 h^{-1} (179). Obviously, the PP pathway in the Pgi mutant cannot support the glucose catabolic rate of the wild-type, although the PP pathway flux increased by about 50% compared to the wild-type (from 2.0 to $2.9\text{ mmol g}^{-1}\text{ h}^{-1}$) (179). Why does the PP pathway flux not increase further?

The glucose-6P dehydrogenase operated at non-saturated conditions in the wild-type, thus allowing for potentially higher flux into PP pathway. In contrast to glucose-6P dehydrogenase, the 6P-gluconate dehydrogenase was already close to saturation in the wild-type, indicating that PP pathway was limited by the maximal reaction velocity of at least this enzyme. Taking into account different rate laws for inhibition by NADPH and 6P-gluconate for glucose-6P dehydrogenase and by NADPH, ribulose-5P, ATP or fructose-1,6-P for 6P-gluconate dehydrogenase, the apparent V_{max} corresponded well to the known wild-type net fluxes through PP pathway. This provides direct evidence that both dehydrogenases might limit PP pathway flux.

Since glucose-6P dehydrogenase was not saturated in the wild-type, we asked whether this would still be the case in the Pgi mutant, which has to catabolize all glucose through PP pathway. The intracellular concentration of glucose-6P increased about 10-fold in the Pgi mutant, such that glucose-6P dehydrogenase was now fully saturated like in the wild-type, independent of the type of inhibition. 6P-gluconate dehydrogenase in the Pgi mutant was also fully saturated hence the PP pathway flux was therefore limited in both reactions. The inability to fully restore growth of a Pgi mutant by overexpressing glucose-6P dehydrogenase observed by others (26, 69) is thus now explainable by the saturated 6P-gluconate dehydrogenase, which presumably would have to be overexpressed too. At least for the Pgi mutant, overexpressing 6P-gluconate during growth on glucose minimal medium did not

have a negative effect on growth and glucose uptake rate, while overexpressing all other enzymes of the PP pathway impaired physiological performance. Although this needs further investigation, the finding provided indirect evidence for limiting 6P-gluconate dehydrogenase in at least the Pgi mutant.

To which extent also 6P-gluconolactonase controls the PP pathway flux, remains unclear. The 6P-gluconolactonase has to keep the concentration of 6P-gluconolactone as low as possible for two main reasons: Firstly, glucose-6P dehydrogenase is a reversible reaction operating close at the thermodynamical equilibrium. Therefore, accumulating 6P-gluconolactone would disable PP pathway flux (18). Secondly, 6P-gluconolactone is a highly reactive, electrophilic compound that reacts with nucleophilic, basic amino acids such as arginine or lysine (53). The Gibbs energies of reaction determined based on the intracellular concentrations of the wild-type and mutants provide further evidence. In fed-batch cultures, overexpression of Pgl enabled a higher biomass yield and the authors proposed the Pgl to be limiting the PP pathway, which contrasts with the above findings (221).

Despite radically different NADPH metabolism in the Pgi and Zwf-EDP mutants, the intracellular concentrations of NADP^+ and NADPH did not change significantly. Thus, there is apparently no accumulation of NADPH even when it is significantly overproduced in the Pgi mutant, relative to the anabolic requirement. Presumably the soluble transhydrogenase (179) reoxidizes efficiently the surplus of NADPH. The carbon metabolism drastically changed in both Pgi and Zwf-EDP mutants but the redox ratio of $\text{NADPH}/\text{NADP}^+$ and NADH/NAD^+ , in contrast to the energy charge, remained remarkably stable because both functional anabolism and catabolism rely on stable redox ratios.

In general, our experimentally determined kinetic parameters were in the range of the few previously obtained values from different sources. For the glucose-6P dehydrogenase, the K_M values for glucose-6P and NADP^+ of 0.136 and 0.023 mM compare well with the previously determined values in the range of 0.070-0.145 mM and 0.010-0.015 mM, respectively (17, 28, 146, 177). The enzyme was reported to be specific for NADP^+ with a 100-fold higher K_M for NAD^+ than for NADP^+ (17) and found to be inhibited by NADPH ($K_{ic,\text{NADPH},\text{NADP}^+} = 0.01$ mM, $K_{ic,\text{NADPH},\text{G6P}} = 0.04$ mM, $K_{iu,\text{NADPH},\text{G6P}} = 0.18$ mM) (146, 177). We were not able to detect activity with NAD^+ at all, which confirmed specificity for NADP^+ and our own values

for the inhibition constants differed significantly (Table 3). Galactose-6P, glucose, glucose-1P, 6P-gluconate, ribose-5P, phosphoenolpyruvate, fructose-1P, fructose-1,6-bisP, 3P-glycerate, ATP, AMP, ADP, GTP, acetyl-CoA and CoA were tested by different authors and did not exhibit an inhibitory effect (17, 146, 177). With our broader screen for potential inhibitors, we confirmed these findings and could further exclude metabolites from EMP and PP pathway (Table 3). The only possible effect that we found was inhibition by citrate. However, the intracellular concentration of citrate was significantly lower than the one used for the inhibitory screen (5 mM) and also similar for wild-type, Pgi and Zwf-EDP mutant (0.31, 0.35 and 0.22 mM respectively). Thus, the inhibitory effect would be small in wild-type and both mutants, and is therefore not relevant for reaction velocities.

For 6P-gluconate dehydrogenase, the K_M for 6P-gluconate and NADP^+ of 0.019 and 0.009 compare well with previously determined values in the range of 0.01-0.1 mM and 0.017-0.033 mM, respectively (45, 214). The enzyme was reported to be specific for NADP^+ (214) and found to be inhibited by NADPH ($K_{ic,\text{NADPH},\text{NADP}^+} = 0.049$ mM) (214). We were not able to detect activity with NAD^+ at all, which confirmed specificity for NADP^+ and our own values for the inhibition constants were in the same range (Table 3). The enzyme is inhibited by several compounds of central carbon metabolism; i.e. fructose-1,6-bisP, ribulose-5P and ATP at 1 mM (45). We observed these inhibition effects and determined the so far unknown product inhibition constants for ribulose-5P (Table 3 and 4). For ATP, we used a previously published rate law and inhibition constant (31, 133) and for fructose-1,6-bisP we included non-competitive inhibition by limiting the $V_{\text{max,apparent}}$ to $0.4 \cdot V_{\text{max}}$ (45).

Overall, our results indicate that there is no fundamental (stoichiometric or energetic) reason to generate NADPH by the PP pathway. The PP pathway appears to operate in a rather robust and unregulated fashion based on the kinetic properties of the two dehydrogenases, while 6P-gluconolactonase keeps the first dehydrogenase thermodynamically feasible. The PP pathway appears to operate with saturated 6P-gluconate dehydrogenase in wild-type and both saturated dehydrogenases in the Pgi mutant. This provided evidence that PP pathway might be limited by their abundance, which was shown to be true for 6P-gluconate dehydrogenase in the Pgi mutant. Active transcriptional upregulation of PP pathway only takes place under conditions of suddenly increased demand of NADPH (i.e. oxidative stress).

(78, 85)) but apparently not when metabolic mutants lead to altered NADPH balance or intracellular glucose-6P concentration.

Acknowledgements

We thank Joerg Büscher for his expertise and assistance in sample preparation and LC-MS/MS operation and Mario Klimacek for his critical comments on the kinetic characterization and rate predictions.

Conclusions and Outlook

The previously established method of metabolic flux ratio analysis was successfully applied to characterize metabolic network topologies of less well studied or even not sequenced species of different genera. We aimed at determining whether model species such as *E. coli* and *B. subtilis* are good representatives of microbial glucose catabolism in general. The determined metabolic flux ratios quantified relative usage of pathways and it was found that except for the two model species *B. subtilis* and *E. coli*, the ED pathway was the predominant route for glucose degradation, which contrasts with the generally held textbook view that the EMP pathway is the major route. Estimating then intracellular carbon fluxes from these ^{13}C ratios revealed a wide range of catabolic carbon throughput with extremely high glucose uptake rate in *Z. mobilis* and slow catabolism in *S. meliloti* or *R. sphaeroides* (ten times higher and three times lower respectively than e.g. in *E. coli*). Except in *Z. mobilis*, overflow metabolism was absent and PP pathway was used exclusively as an anaplerotic pathway. These findings demonstrate that, although widely used in the laboratory, *E. coli* and *B. subtilis* do not represent microbial glucose catabolism qualitatively and quantitatively.

Since their metabolic fluxes differed so widely, balancing of the redox cofactor NADPH must vary significantly because generation of NADPH is coupled to glucose catabolism but finally must be balanced to match the comparatively stable anabolic demands for NADPH. Therefore, we focused on the NADPH metabolism in these diverse species and aimed at elucidating NADPH metabolism quantitatively. Based on the net fluxes determined in **Chapter 2**, we quantified NADPH metabolism in these diverse species using cofactor specificities of potential NADPH regenerating enzymes in the central carbon metabolism. With some exceptions, most species exhibited significant NADPH overproduction and experimentally determined unspecific dehydrogenases in the PP pathway were principally able to avoid the NADPH overproduction. However, in three cases, transhydrogenase activity was detected and therefore could counter-balance an overproduction.

For at least *Z. mobilis* and *S. meliloti* with absent transhydrogenases, we concluded that a NADPH overproduction must be avoided by NADH specific PP pathway dehydrogenases. Of course, the in vitro determined cofactor specificities provide only indirect evidence for the

actual specificity inside the cell. The question how dual cofactor specific enzymes perform *in vivo* is still a general challenge in the field of enzyme kinetics. A possible, although work intensive approach to resolve this issue is the kinetic characterization in the cellular matrix i.e. assay buffer representing exactly the chemical composition of the cytosol. Therefore one needs to quench and extract cells with subsequent protein removal by low cut-off filters. Full analysis of the extract with current tools for metabolite and ion detection would include GC-MS, LC-MS/MS, GC-TOF for metabolites and different variations of atom absorption spectrometry (AAS), optic emission spectrometry or ion chromatographies for cations and anions. Once determined, one could use the composition to prepare synthetic enzymes buffers resembling perfectly the cytosolic environment and do inhibitor / activator studies under “real” conditions.

Because *E. coli* seemed to be exceptional having cofactor specific dehydrogenases and two isoforms of transhydrogenases, we focused on a more detailed investigation of its NADPH metabolism. The soluble and membrane-bound transhydrogenases of *E. coli* play an important role in its NADPH metabolism because *E. coli* does obviously not have any other NADPH balancing mechanisms such as dual cofactor specificity of the PP pathway dehydrogenases. Therefore, any carbon flux redistribution will affect the NADPH balance and require appropriate transhydrogenase activity in one or the other direction. However, by analyzing 23 metabolic mutants on 7 different substrates, we show that there is no transcriptional regulation related to the NADPH balance. Instead, expression data rather provided evidence that the membrane-bound transhydrogenase is induced under specific stress conditions not mediated via the NADPH pool. The soluble transhydrogenase UdhA seemed to be expressed also during NADPH underproduction conditions and with higher levels in the UdhA mutant. For both transhydrogenases, there might be a regulation at the transcriptional level related to the carbon source, if at all. But how the redox balance is handled in the case of metabolic mutants remains an open question.

The question what actually might induce PntAB and UdhA at the transcriptional level depending on the carbon source or at stress conditions could be answered by fishing for proteins binding to immobilized promoter region of the transhydrogenases with established methods of quantitative proteomics (87, 161, 162). Further open questions relate to the

regulation of UdhA, specifically how UdhA present at NADPH underproduction conditions could be prevented from oxidizing NADPH. Since UdhA is known to be a homo octamer or heptamer in its active form, the decay of the UdhA complex is of interest and could be investigated by different approaches such as blue native gels (201, 202) or crosslinking experiments (77, 163). Furthermore, the kinetic characterization and an allosteric effector screen would provide more insight into the role of UdhA in *E. coli*. We actually purified UdhA by size exclusion chromatography from *E. coli* cells overexpressing UdhA from an inducible plasmid, performed an inhibitor screen and an initial kinetic characterization (see Appendix for details). While the kinetic characterization needs further improvement due to analytical issues, the inhibitor screen provided first evidence that intermediates of lower EMP pathway have an inhibitory and adenosine phosphates an activation effect (Appendix). To conclude, UdhA seems to be expressed also during NADPH underproduction conditions and thus not regulated by the NADPH balance. First steps into the kinetic characterization were done and provided evidence for allosteric and/or kinetic regulation by metabolites other than reducing equivalents to be responsible for the in vivo activity of UdhA.

Besides the addressed regulation of transhydrogenases, we also examined the PP pathway as it accounts for a significant part of NADPH production in *E. coli*. Specifically, we were interested in the reason why obviously flux through PP pathway was limited in a Pgi mutant and how flux might be controlled in general. Therefore, we determined the kinetic properties of the PP pathway in *E. coli* in detail by comparing the wild-type and its Pgi and Zwfd mutants on the level of intracellular metabolite concentrations and analysis of the kinetic properties of the glucose-6P- and 6P-gluconate dehydrogenase. The NADPH to NADP⁺ ratio was found to be surprisingly constant but PP pathway metabolite concentrations increased about 10-fold in the Pgi mutant compared to the wild-type such that the dehydrogenases were saturated. Therefore, the PP pathway was not regulated by the redox balance, which is actually in agreement with the fact that elevated PP pathway during oxidative stress response via SoxRS system does not involve NADPH itself. Constant NADPH to NADP⁺ ratio further explain why no correlation of transhydrogenase flux and expression was observed, since the cell can only indirectly respond to changing fluxes when metabolite concentrations are altered.

References

1. **Ahmed, H., T. J. Ettema, B. Tjaden, A. C. Geerling, J. van der Oost, and B. Siebers.** 2005. The semi-phosphorylative Entner-Doudoroff pathway in hyperthermophilic archaea - a re-evaluation. *Biochem. J.* **390**:529-540.
2. **Al Zaid Siddiquee, K., M. J. Arauzo-Bravo, and K. Shimizu.** 2004. Metabolic flux analysis of pykF gene knockout *Escherichia coli* based on ¹³C-labeling experiments together with measurements of enzyme activities and intracellular metabolite concentrations. *Appl. Microbiol. Biotechnol.* **63**:407-417.
3. **Althage, M., T. Bizouarn, B. Kindlund, J. Mullins, J. Alander, and J. Rydstrom.** 2004. Cross-linking of transmembrane helices in proton-translocating nicotinamide nucleotide transhydrogenase from *Escherichia coli*: implications for the structure and function of the membrane domain. *Biochim. Biophys. Acta* **1659**:73-82.
4. **Althage, M., T. Bizouarn, and J. Rydstrom.** 2001. Identification of a region involved in the communication between the NADP(H) binding domain and the membrane domain in proton pumping *Escherichia coli* transhydrogenase. *Biochemistry* **40**:9968-9976.
5. **Anderlund, M., T. L. Nissen, J. Nielsen, J. Villadsen, J. Rydstrom, B. Hahn-Hagerdal, and M. C. Kielland-Brandt.** 1999. Expression of the *Escherichia coli* pntA and pntB genes, encoding nicotinamide nucleotide transhydrogenase, in *Saccharomyces cerevisiae* and its effect on product formation during anaerobic glucose fermentation. *Appl. Environ. Microbiol.* **65**:2333-2340.
6. **Andersen, K. B., and K. von Meyenburg.** 1977. Charges of nicotinamide adenine nucleotides and adenylate energy charge as regulatory parameters of the metabolism in *Escherichia coli*. *J. Biol. Chem.* **252**:4151-4156.
7. **Arkblad, E. L., C. Betsholtz, D. Mandoli, and J. Rydstrom.** 2001. Characterization of a nicotinamide nucleotide transhydrogenase gene from the green alga *Acetabularia acetabulum* and comparison of its structure with those of the corresponding genes in mouse and *Caenorhabditis elegans*. *Biochim. Biophys. Acta* **1520**:115-123.
8. **Arkblad, E. L., S. Tuck, N. B. Pestov, R. I. Dmitriev, M. B. Kostina, J. Stenvall, M. Tranberg, and J. Rydstrom.** 2005. A *Caenorhabditis elegans* mutant lacking functional nicotinamide nucleotide transhydrogenase displays increased sensitivity to oxidative stress. *Free Radic. Biol. Med.* **38**:1518-1525.
9. **Arner, E. S., and A. Holmgren.** 2000. Physiological functions of thioredoxin and thioredoxin reductase. *Eur. J. Biochem.* **267**:6102-6109.
10. **Arnold, C. N., J. McElhanon, A. Lee, R. Leonhart, and D. A. Siegele.** 2001. Global analysis of *Escherichia coli* gene expression during the acetate-induced acid tolerance response. *J. Bacteriol.* **183**:2178-2186.
11. **Arthur, L. O., L. A. Bulla, Jr., G. S. Julian, and L. K. Nakamura.** 1973. Carbohydrate metabolism in *Agrobacterium tumefaciens*. *J. Bacteriol.* **116**:304-313.
12. **Baba, T., T. Ara, M. Hasegawa, Y. Takai, Y. Okumura, M. Baba, K. A. Datsenko, M. Tomita, B. L. Wanner, and H. Mori.** 2006. Construction of *Escherichia coli* K-12 in-frame, single-gene knockout mutants: the Keio collection. *Mol. Syst. Biol.* **2**:2006 0008.
13. **Bailey, J. E.** 1991. Toward a science of metabolic engineering. *Science* **252**:1668-1675.
14. **Baker, H. V., 2nd, and R. E. Wolf, Jr.** 1983. Growth rate-dependent regulation of 6-phosphogluconate dehydrogenase level in *Escherichia coli* K-12: beta-galactosidase expression in gnd-lac operon fusion strains. *J. Bacteriol.* **153**:771-781.
15. **Baker, S. C., S. J. Ferguson, B. Ludwig, M. D. Page, O. M. Richter, and R. J. van Spanning.** 1998. Molecular genetics of the genus *Paracoccus*: metabolically versatile bacteria with bioenergetic flexibility. *Microbiol. Mol. Biol. Rev.* **62**:1046-1078.

16. **Bakker, B. M., K. M. Overkamp, A. J. van Maris, P. Kotter, M. A. Luttik, J. P. van Dijken, and J. T. Pronk.** 2001. Stoichiometry and compartmentation of NADH metabolism in *Saccharomyces cerevisiae*. *FEMS Microbiol. Rev.* **25**:15-37.
17. **Banerjee, S., and D. G. Fraenkel.** 1972. Glucose-6-phosphate dehydrogenase from *Escherichia coli* and from a "high-level" mutant. *J. Bacteriol.* **110**:155-160.
18. **Bauer, H. P., T. Srihari, J. C. Jochims, and H. W. Hofer.** 1983. 6-phosphogluconolactonase. Purification, properties and activities in various tissues. *Eur. J. Biochem.* **133**:163-168.
19. **Bizouarn, T., M. Althage, A. Pedersen, A. Tigerstrom, J. Karlsson, C. Johansson, and J. Rydstrom.** 2002. The organization of the membrane domain and its interaction with the NADP(H)-binding site in proton-translocating transhydrogenase from *Escherichia coli*. *Biochim. Biophys. Acta* **1555**:122-127.
20. **Bizouarn, T., O. Fjellstrom, M. Axelsson, T. V. Korneenko, N. B. Pestov, M. V. Ivanova, M. V. Egorov, M. Shakhparonov, and J. Rydstrom.** 2000. Interactions between the soluble domain I of nicotinamide nucleotide transhydrogenase from *Rhodospirillum rubrum* and transhydrogenase from *Escherichia coli*. Effects on catalytic and H⁺-pumping activities. *Eur. J. Biochem.* **267**:3281-3288.
21. **Bizouarn, T., O. Fjellstrom, J. Mueller, M. Axelsson, A. Bergkvist, C. Johansson, B. Goran Karlsson, and J. Rydstrom.** 2000. Proton translocating nicotinamide nucleotide transhydrogenase from *Escherichia coli*. Mechanism of action deduced from its structural and catalytic properties. *Biochim. Biophys. Acta* **1457**:211-228.
22. **Blank, L. M., F. Lehmbeck, and U. Sauer.** 2005. Metabolic-flux and network analysis in fourteen hemiascomycetous yeasts. *FEMS Yeast Res.* **5**:545-558.
23. **Blank, L. M., and U. Sauer.** 2004. TCA cycle activity in *Saccharomyces cerevisiae* is a function of the environmentally determined specific growth and glucose uptake rates. *Microbiology* **150**:1085-1093.
24. **Boonstra, B., C. E. French, I. Wainwright, and N. C. Bruce.** 1999. The *udhA* gene of *Escherichia coli* encodes a soluble pyridine nucleotide transhydrogenase. *J. Bacteriol.* **181**:1030-1034.
25. **Brown, T. D., M. C. Jones-Mortimer, and H. L. Kornberg.** 1977. The enzymic interconversion of acetate and acetyl-coenzyme A in *Escherichia coli*. *J. Gen. Microbiol.* **102**:327-336.
26. **Canonaco, F., T. A. Hess, S. Heri, T. Wang, T. Szyperski, and U. Sauer.** 2001. Metabolic flux response to phosphoglucose isomerase knock-out in *Escherichia coli* and impact of overexpression of the soluble transhydrogenase UdhA. *FEMS Microbiol. Lett.* **204**:247-252.
27. **Carugo, O., and P. Argos.** 1997. NADP-dependent enzymes. I: Conserved stereochemistry of cofactor binding. *Proteins* **28**:10-28.
28. **Cavalieri, R. L., and H. Z. Sable.** 1973. Enzymes of pentose biosynthesis. II. Evidence that the proposed control of glucose 6-phosphate dehydrogenase by reduced diphosphopyridine nucleotide is an instrumental artifact. *J. Biol. Chem.* **248**:2815-2817.
29. **Chang, D. E., S. Shin, J. S. Rhee, and J. G. Pan.** 1999. Acetate metabolism in a pta mutant of *Escherichia coli* W3110: importance of maintaining acetyl coenzyme A flux for growth and survival. *J. Bacteriol.* **181**:6656-6663.
30. **Charrier, V., E. Buckley, D. Parsonage, A. Galinier, E. Darbon, M. Jaquinod, E. Forest, J. Deutscher, and A. Claiborne.** 1997. Cloning and sequencing of two enterococcal glpK genes and regulation of the encoded glycerol kinases by phosphoenolpyruvate-dependent, phosphotransferase system-catalyzed phosphorylation of a single histidyl residue. *J. Biol. Chem.* **272**:14166-14174.
31. **Chassagnole, C., N. Noisommit-Rizzi, J. W. Schmid, K. Mauch, and M. Reuss.** 2002. Dynamic modeling of the central carbon metabolism of *Escherichia coli*. *Biotechnol. Bioeng.* **79**:53-73.
32. **Clarke, D. M., T. W. Loo, S. Gillam, and P. D. Bragg.** 1986. Nucleotide sequence of the *pntA* and *pntB* genes encoding the pyridine nucleotide transhydrogenase of *Escherichia coli*. *Eur. J. Biochem.* **158**:647-653.
33. **Conrad, R., and H. G. Schlegel.** 1977. Different degradation pathways for glucose and fructose in *Rhodopseudomonas capsulata*. *Arch. Microbiol.* **112**:39-48.
34. **Conrad, R., and H. G. Schlegel.** 1977. Influence of aerobic and phototrophic growth conditions on the distribution of glucose and fructose carbon into the Entner-Doudoroff and Embden-Meyerhof pathways in *Rhodopseudomonas sphaeroides*. *J. Gen. Microbiol.* **101**:277-290.

35. **Conway, T.** 1992. The Entner-Doudoroff pathway: history, physiology and molecular biology. *FEMS Microbiol. Rev.* **9**:1-27.
36. **Cormack, B. P., R. H. Valdivia, and S. Falkow.** 1996. FACS-optimized mutants of the green fluorescent protein (GFP). *Gene* **173**:33-38.
37. **Cornish-Bowden, A.** 2004. Fundamentals of enzyme kinetics. Portland Press, London.
38. **Csonka, L. N., and D. G. Fraenkel.** 1977. Pathways of NADPH formation in *Escherichia coli*. *J. Biol. Chem.* **252**:3382-3391.
39. **Datsenko, K. A., and B. L. Wanner.** 2000. One-step inactivation of chromosomal genes in *Escherichia coli* K-12 using PCR products. *Proc. Natl. Acad. Sci. U. S. A.* **97**:6640-6645.
40. **Dauner, M., J. E. Bailey, and U. Sauer.** 2001. Metabolic flux analysis with a comprehensive isotopomer model in *Bacillus subtilis*. *Biotechnol. Bioeng.* **76**:144-156.
41. **Dauner, M., and U. Sauer.** 2000. GC-MS analysis of amino acids rapidly provides rich information for isotopomer balancing. *Biotechnol. Prog.* **16**:642-649.
42. **Dauner, M., and U. Sauer.** 2001. Stoichiometric growth model for riboflavin-producing *Bacillus subtilis*. *Biotechnol. Bioeng.* **76**:132-143.
43. **Dauner, M., T. Storni, and U. Sauer.** 2001. *Bacillus subtilis* metabolism and energetics in carbon-limited and excess-carbon chemostat culture. *J. Bacteriol.* **183**:7308-7317.
44. **De Graaf, A. A., K. Striegel, R. M. Wittig, B. Laufer, G. Schmitz, W. Wiechert, G. A. Sprenger, and H. Sahm.** 1999. Metabolic state of *Zymomonas mobilis* in glucose-, fructose-, and xylose-fed continuous cultures as analysed by ^{13}C - and ^{31}P -NMR spectroscopy. *Arch. Microbiol.* **171**:371-385.
45. **de Silva, A. O., and D. G. Fraenkel.** 1979. The 6-phosphogluconate dehydrogenase reaction in *Escherichia coli*. *J. Biol. Chem.* **254**:10237-10242.
46. **del Castillo, T., J. L. Ramos, J. J. Rodriguez-Herva, T. Fuhrer, U. Sauer, and E. Duque.** 2007. Convergent peripheral pathways catalyze initial glucose catabolism in *Pseudomonas putida*: genomic and flux analysis. *J. Bacteriol.* **189**:5142-5152.
47. **Dietrichs, D., and J. R. Andreessen.** 1990. Purification and comparative studies of dihydrolipoamide dehydrogenases from the anaerobic, glycine-utilizing bacteria *Peptostreptococcus glycinophilus*, *Clostridium cylindrosporum*, and *Clostridium sporogenes*. *J. Bacteriol.* **172**:243-251.
48. **Dittrich, C. R., G. N. Bennett, and K. Y. San.** 2005. Characterization of the acetate-producing pathways in *Escherichia coli*. *Biotechnol. Prog.* **21**:1062-1067.
49. **Doan, T., P. Servant, S. Tojo, H. Yamaguchi, G. Lerondel, K. Yoshida, Y. Fujita, and S. Aymerich.** 2003. The *Bacillus subtilis* ywK gene encodes a malic enzyme and its transcription is activated by the YufL/YufM two-component system in response to malate. *Microbiology* **149**:2331-2343.
50. **Doelle, H. W., L. Kirk, R. Crittenden, H. Toh, and M. B. Doelle.** 1993. *Zymomonas mobilis*--science and industrial application. *Crit. Rev. Biotechnol.* **13**:57-98.
51. **Driscoll, B. T., and T. M. Finan.** 1993. NAD^+ -dependent malic enzyme of *Rhizobium meliloti* is required for symbiotic nitrogen fixation. *Mol. Microbiol.* **7**:865-873.
52. **Driscoll, B. T., and T. M. Finan.** 1997. Properties of NAD^+ - and NADP^+ -dependent malic enzymes of *Rhizobium* (*Sinorhizobium*) *meliloti* and differential expression of their genes in nitrogen-fixing bacteroids. *Microbiology* **143**:489-498.
53. **Duffieux, F., J. Van Roy, P. A. Michels, and F. R. Oppendoes.** 2000. Molecular characterization of the first two enzymes of the pentose-phosphate pathway of *Trypanosoma brucei*. Glucose-6-phosphate dehydrogenase and 6-phosphogluconolactonase. *J. Biol. Chem.* **275**:27559-27565.
54. **Dunn, M. F.** 1998. Tricarboxylic acid cycle and anaplerotic enzymes in rhizobia. *FEMS Microbiol. Rev.* **22**:105-123.
55. **Dunn, M. F., G. Araiza, and T. M. Finan.** 2001. Cloning and characterization of the pyruvate carboxylase from *Sinorhizobium meliloti* Rm1021. *Arch. Microbiol.* **176**:355-363.
56. **Edgar, R., M. Domrachev, and A. E. Lash.** 2002. Gene Expression Omnibus: NCBI gene expression and hybridization array data repository. *Nucleic Acids Res.* **30**:207-210.
57. **Eisenberg, R. C., S. J. Butters, S. C. Quay, and S. B. Friedman.** 1974. Glucose uptake and phosphorylation in *Pseudomonas fluorescens*. *J. Bacteriol.* **120**:147-153.
58. **Eisenberg, R. C., and W. J. Dobrogosz.** 1967. Gluconate metabolism in *Escherichia coli*. *J. Bacteriol.* **93**:941-949.

59. **el-Mansi, E. M., and W. H. Holms.** 1989. Control of carbon flux to acetate excretion during growth of *Escherichia coli* in batch and continuous cultures. *J. Gen. Microbiol.* **135**:2875-2883.
60. **Emmerling, M., M. Dauner, A. Ponti, J. Fiaux, M. Hochuli, T. Szyperski, K. Wüthrich, J. E. Bailey, and U. Sauer.** 2002. Metabolic flux responses to pyruvate kinase knockout in *Escherichia coli*. *J. Bacteriol.* **184**:152-164.
61. **Faith, J. J., M. E. Driscoll, V. A. Fusaro, E. J. Cosgrove, B. Hayete, F. S. Juhn, S. J. Schneider, and T. S. Gardner.** 2008. Many Microbe Microarrays Database: uniformly normalized Affymetrix compendia with structured experimental metadata. *Nucleic Acids Res.* **36**:D866-870.
62. **Fell, D. A., and J. R. Small.** 1986. Fat synthesis in adipose tissue. An examination of stoichiometric constraints. *Biochem. J.* **238**:781-786.
63. **Fiaux, J., Z. P. Cakar, M. Sonderegger, K. Wüthrich, T. Szyperski, and U. Sauer.** 2003. Metabolic-flux profiling of the yeasts *Saccharomyces cerevisiae* and *Pichia stipitis*. *Eukaryot. Cell* **2**:170-180.
64. **Fillinger, S., S. Boschi-Muller, S. Azza, E. Dervyn, G. Branlant, and S. Aymerich.** 2000. Two glyceraldehyde-3-phosphate dehydrogenases with opposite physiological roles in a nonphotosynthetic bacterium. *J. Biol. Chem.* **275**:14031-14037.
65. **Fischer, E., and U. Sauer.** 2003. Metabolic flux profiling of *Escherichia coli* mutants in central carbon metabolism using GC-MS. *Eur. J. Biochem.* **270**:880-891.
66. **Fischer, E., and U. Sauer.** 2003. A novel metabolic cycle catalyzes glucose oxidation and anaplerosis in hungry *Escherichia coli*. *J. Biol. Chem.* **278**:46446-46451.
67. **Fischer, E., N. Zamboni, and U. Sauer.** 2004. High-throughput metabolic flux analysis based on gas chromatography-mass spectrometry derived ^{13}C constraints. *Anal. Biochem.* **325**:308-316.
68. **Fishov, I., A. Zaritsky, and N. B. Grover.** 1995. On microbial states of growth. *Mol. Microbiol.* **15**:789-794.
69. **Flores, S., R. de Anda-Herrera, G. Gosset, and F. G. Bolivar.** 2004. Growth-rate recovery of *Escherichia coli* cultures carrying a multicopy plasmid, by engineering of the pentose-phosphate pathway. *Biotechnol. Bioeng.* **87**:485-494.
70. **Fong, S. S., A. Nanchen, B. O. Palsson, and U. Sauer.** 2006. Latent pathway activation and increased pathway capacity enable *Escherichia coli* adaptation to loss of key metabolic enzymes. *J. Biol. Chem.* **281**:8024-8033.
71. **Forster, J., I. Famili, P. Fu, B. O. Palsson, and J. Nielsen.** 2003. Genome-scale reconstruction of the *Saccharomyces cerevisiae* metabolic network. *Genome Res.* **13**:244-253.
72. **Fraenkel, D. G.** 1996. Glycolysis, p. 189-198. *In* F. C. Neidhardt, R. Curtiss III, J. L. Ingraham, C. C. Lin, K. B. Low, B. Magasanik, W. S. Reznikoff, M. Riley, M. Schaechter, and H. E. Umberger (ed.), *Escherichia coli* and *Salmonella typhimurium*: Cellular and molecular biology. ASM press, Washington, D.C.
73. **French, C. E., B. Boonstra, K. A. Bufton, and N. C. Bruce.** 1997. Cloning, sequence, and properties of the soluble pyridine nucleotide transhydrogenase of *Pseudomonas fluorescens*. *J. Bacteriol.* **179**:2761-2765.
74. **Fuhrer, T., L. Chen, U. Sauer, and D. Vitkup.** 2007. Computational Prediction and Experimental Verification of the Gene Encoding the $\text{NAD}^+/\text{NADP}^+$ -Dependent Succinate Semialdehyde Dehydrogenase in *Escherichia coli*. *J. Bacteriol.* **189**:8073-8078.
75. **Fuhrer, T., E. Fischer, and U. Sauer.** 2005. Experimental identification and quantification of glucose metabolism in seven bacterial species. *J. Bacteriol.* **187**:1581-1590.
76. **Fuhrer, T., and U. Sauer.** 2007. Different biochemical mechanisms ensure network-wide balancing of reducing equivalents in microbial metabolism. Submitted.
77. **Gingras, A. C., M. Gstaiger, B. Raught, and R. Aebersold.** 2007. Analysis of protein complexes using mass spectrometry. *Nat. Rev. Mol. Cell. Biol.* **8**:645-654.
78. **Giro, M., N. Carrillo, and A. R. Krapp.** 2006. Glucose-6-phosphate dehydrogenase and ferredoxin-NADP(H) reductase contribute to damage repair during the soxRS response of *Escherichia coli*. *Microbiology* **152**:1119-1128.
79. **Gober, J. W., and E. R. Kashket.** 1986. Effects of K^+ on the proton motive force of *Bradyrhizobium* sp. strain 32H1. *J. Bacteriol.* **166**:618-622.

80. **Gombert, A. K., M. Moreira dos Santos, B. Christensen, and J. Nielsen.** 2001. Network identification and flux quantification in the central metabolism of *Saccharomyces cerevisiae* under different conditions of glucose repression. *J. Bacteriol.* **183**:1441-1451.
81. **Gonzalez, J. E., G. M. York, and G. C. Walker.** 1996. *Rhizobium meliloti* exopolysaccharides: synthesis and symbiotic function. *Gene* **179**:141-146.
82. **Gornall, A., W. Bardawill, and M. David.** 1949. Determinations of serum proteins by means of the Biuret reaction. *J. Biol. Chem.* **177**:751-766.
83. **Gosselin, I., O. Wattraint, D. Riboul, J. Barbotin, and J. Portais.** 2001. A deeper investigation on carbohydrate cycling in *Sinorhizobium meliloti*. *FEBS Lett.* **499**:45-49.
84. **Gottschalk, G.** 1986. Bacterial metabolism. Springer-Verlag, New York, NY.
85. **Greenberg, J. T., J. H. Chou, P. A. Monach, and B. Demple.** 1991. Activation of oxidative stress genes by mutations at the *soxQ/cfxB/marA* locus of *Escherichia coli*. *J. Bacteriol.* **173**:4433-4439.
86. **Gunnarsson, N., U. H. Mortensen, M. Sosio, and J. Nielsen.** 2004. Identification of the Entner-Doudoroff pathway in an antibiotic-producing *actinomycete* species. *Mol. Microbiol.* **52**:895-902.
87. **Gygi, S. P., B. Rist, S. A. Gerber, F. Turecek, M. H. Gelb, and R. Aebersold.** 1999. Quantitative analysis of complex protein mixtures using isotope-coded affinity tags. *Nature Biotechnol.* **17**:994-999.
88. **Harayama, S., M. Kok, and E. L. Neidle.** 1992. Functional and evolutionary relationships among diverse oxygenases. *Annu. Rev. Microbiol.* **46**:565-601.
89. **Harold, F.** 1986. The Vital Force: A Study of Bioenergetics. Freeman and Company, New York, NY.
90. **Harris, D. M., J. A. Diderich, Z. A. van der Krogt, M. A. Luttik, L. M. Raamsdonk, R. A. Bovenberg, W. M. van Gulik, J. P. van Dijken, and J. T. Pronk.** 2006. Enzymic analysis of NADPH metabolism in beta-lactam-producing *Penicillium chrysogenum*: presence of a mitochondrial NADPH dehydrogenase. *Metabolic Eng.* **8**:91-101.
91. **Heijnen, J. J.** 2005. Approximative kinetic formats used in metabolic network modeling. *Biotechnol. Bioeng.* **91**:534-545.
92. **Heinemann, M., A. Kummel, R. Ruinatscha, and S. Panke.** 2005. In silico genome-scale reconstruction and validation of the *Staphylococcus aureus* metabolic network. *Biotechnol. Bioeng.* **92**:850-864.
93. **Hickman, J. W., R. D. Barber, E. P. Skaar, and T. J. Donohue.** 2002. Link between the membrane-bound pyridine nucleotide transhydrogenase and glutathione-dependent processes in *Rhodobacter sphaeroides*. *J. Bacteriol.* **184**:400-409.
94. **Hoek, J. B., and J. Rydstrom.** 1988. Physiological roles of nicotinamide nucleotide transhydrogenase. *Biochem. J.* **254**:1-10.
95. **Holms, H.** 2001. Flux analysis: a basic tool of microbial physiology. *Adv. Microb. Physiol.* **45**:271-340.
96. **Hong, S. H., S. J. Park, S. Y. Moon, J. P. Park, and S. Y. Lee.** 2003. In silico prediction and validation of the importance of the Entner-Doudoroff pathway in poly(3-hydroxybutyrate) production by metabolically engineered *Escherichia coli*. *Biotechnol. Bioeng.* **83**:854-863.
97. **Horecker, B. L.** 2002. The pentose phosphate pathway. *J. Biol. Chem.* **277**:47965-47971.
98. **Hua, Q., C. Yang, T. Baba, H. Mori, and K. Shimizu.** 2003. Responses of the central metabolism in *Escherichia coli* to phosphoglucose isomerase and glucose-6-phosphate dehydrogenase knockouts. *J. Bacteriol.* **185**:7053-7067.
99. **Hurley, J. H., R. Chen, and A. M. Dean.** 1996. Determinants of cofactor specificity in isocitrate dehydrogenase: structure of an engineered NADP⁺ → NAD⁺ specificity-reversal mutant. *Biochemistry* **35**:5670-5678.
100. **Irigoyen, J. J., M. Sanchezdiaz, and D. W. Emerich.** 1990. Carbon metabolism enzymes of *Rhizobium meliloti* cultures and bacteroids and their distribution within Alfalfa nodules. *Appl. Environ. Microb.* **56**:2587-2589.
101. **Iwakura, M., M. Tokushige, H. Katsuki, and S. Muramatsu.** 1978. Studies on regulatory functions of malic enzymes. V. Comparative studies of malic enzymes in bacteria. *J. Biochem. (Tokyo)* **83**:1387-1394.
102. **Kabus, A., T. Georgi, V. F. Wendisch, and M. Bott.** 2007. Expression of the *Escherichia coli* pntAB genes encoding a membrane-bound transhydrogenase in *Corynebacterium glutamicum* improves L-lysine formation. *Appl. Microbiol. Biotechnol.* **75**:47-53.

References

103. **Kashket, E. R.** 1981. Proton motive force in growing *Streptococcus lactis* and *Staphylococcus aureus* cells under aerobic and anaerobic conditions. *J. Bacteriol.* **146**:369-376.
104. **Kawai, S., C. Fukuda, T. Mukai, and K. Murata.** 2005. MJ0917 in archaeon *Methanococcus jannaschii* is a novel NADP⁺ phosphatase/NAD⁺ kinase. *J. Biol. Chem.* **280**:39200-39207.
105. **Kawai, S., S. Mori, T. Mukai, W. Hashimoto, and K. Murata.** 2001. Molecular characterization of *Escherichia coli* NAD⁺ kinase. *Eur. J. Biochem.* **268**:4359-4365.
106. **Kell, D. B., P. John, and S. J. Ferguson.** 1978. The protonmotive force in phosphorylating membrane vesicles from *Paracoccus denitrificans*. Magnitude, sites of generation and comparison with the phosphorylation potential. *Biochem. J.* **174**:257-266.
107. **Kersters, K., and J. De Ley.** 1968. The occurrence of the Entner-Doudoroff pathway in bacteria. *Ant. Van Leeuwenhoek* **34**:393-408.
108. **Kim, S., and S. B. Lee.** 2005. Identification and characterization of *Sulfolobus solfataricus* D-gluconate dehydratase: a key enzyme in the non-phosphorylated Entner-Doudoroff pathway. *Biochem. J.* **387**:271-280.
109. **Kinoshita, S., T. Kakizono, K. Kadota, K. Das, and H. Taguchi.** 1985. Purification of 2 alcohol dehydrogenases from *Zymomonas mobilis* and their properties. *Appl. Microbiol. Biot.* **22**:249-254.
110. **Kirkpatrick, C., L. M. Maurer, N. E. Oyelakin, Y. N. Yoncheva, R. Maurer, and J. L. Slonczewski.** 2001. Acetate and formate stress: opposite responses in the proteome of *Escherichia coli*. *J. Bacteriol.* **183**:6466-6477.
111. **Kitagawa, M., T. Ara, M. Arifuzzaman, T. Ioka-Nakamichi, E. Inamoto, H. Toyonaga, and H. Mori.** 2005. Complete set of ORF clones of *Escherichia coli* ASKA library (a complete set of *Escherichia coli* K-12 ORF archive): unique resources for biological research. *DNA Res.* **12**:291-299.
112. **Klamt, S., S. Schuster, and E. D. Gilles.** 2002. Calculability analysis in underdetermined metabolic networks illustrated by a model of the central metabolism in purple nonsulfur bacteria. *Biotechnol. Bioeng.* **77**:734-751.
113. **Klapa, M. I., S. M. Park, A. J. Sinskey, and G. Stephanopoulos.** 1999. Metabolite and isotopomer balancing in the analysis of metabolic cycles: I. Theory. *Biotechnol. Bioeng.* **62**:375-391.
114. **Krieger, C. J., P. Zhang, L. A. Mueller, A. Wang, S. Paley, M. Arnaud, J. Pick, S. Y. Rhee, and P. D. Karp.** 2004. MetaCyc: a multiorganism database of metabolic pathways and enzymes. *Nucleic Acids Res.* **32**:D438-442.
115. **Kumari, S., E. J. Simel, and A. J. Wolfe.** 2000. sigma(70) is the principal sigma factor responsible for transcription of *acs*, which encodes acetyl coenzyme A synthetase in *Escherichia coli*. *J. Bacteriol.* **182**:551-554.
116. **Kumari, S., R. Tishel, M. Eisenbach, and A. J. Wolfe.** 1995. Cloning, characterization, and functional expression of *acs*, the gene which encodes acetyl coenzyme A synthetase in *Escherichia coli*. *J. Bacteriol.* **177**:2878-2886.
117. **Kummel, A., S. Panke, and M. Heinemann.** 2006. Putative regulatory sites unraveled by network-embedded thermodynamic analysis of metabolome data. *Mol. Syst. Biol.* **2**:2006 0034.
118. **Lessie, T. G., and P. V. Phibbs, Jr.** 1984. Alternative pathways of carbohydrate utilization in pseudomonads. *Annu. Rev. Microbiol.* **38**:359-388.
119. **Liu, M., T. Durfee, J. E. Cabrera, K. Zhao, D. J. Jin, and F. R. Blattner.** 2005. Global transcriptional programs reveal a carbon source foraging strategy by *Escherichia coli*. *J. Biol. Chem.* **280**:15921-15927.
120. **Lowry, O. H., J. V. Passonneau, and M. K. Rock.** 1961. The stability of pyridine nucleotides. *J. Biol. Chem.* **236**:2756-2759.
121. **Lowry, O. H., J. V. Passonneau, D. W. Schulz, and M. K. Rock.** 1961. The measurement of pyridine nucleotides by enzymatic cycling. *J. Biol. Chem.* **236**:2746-2755.
122. **Ludovico, P., F. Sansonetty, and M. Corte-Real.** 2001. Assessment of mitochondrial membrane potential in yeast cell populations by flow cytometry. *Microbiology* **147**:3335-3343.
123. **Luo, B., K. Groenke, R. Takors, C. Wandrey, and M. Oldiges.** 2007. Simultaneous determination of multiple intracellular metabolites in glycolysis, pentose phosphate pathway and tricarboxylic acid cycle by liquid chromatography-mass spectrometry. *J. Chromatogr. A* **1147**:153-164.
124. **Lynch, W. H., and M. Franklin.** 1978. Effect of temperature on uptake of glucose, gluconate, and 2-ketogluconate by *Pseudomonas fluorescens*. *Can. J. Microbiol.* **24**:56-62.

125. **Madigan, M. T., J. M. Martinko, and J. Parker.** 2000. Brock Biology of Microorganisms. Prentice Hall, Upper Saddle River.
126. **Maharjan, R. P., P. L. Yu, S. Seeto, and T. Ferenci.** 2005. The role of isocitrate lyase and the glyoxylate cycle in *Escherichia coli* growing under glucose limitation. Research in Microbiology **156**:178-183.
127. **Maloy, S. R., and W. D. Nunn.** 1982. Genetic regulation of the glyoxylate shunt in *Escherichia coli* K-12. J. Bacteriol. **149**:173-180.
128. **Martinez-Drets, G., A. Gardiol, and A. Arias.** 1977. 6-Phospho-D-gluconate: NAD⁺ 2-oxidoreductase (decarboxylating) from slow-growing rhizobia. J. Bacteriol. **130**:1139-1143.
129. **Marx, A., A. A. deGraaf, W. Wiechert, L. Eggeling, and H. Sahm.** 1996. Determination of the fluxes in the central metabolism of *Corynebacterium glutamicum* by nuclear magnetic resonance spectroscopy combined with metabolite balancing. Biotechnol. Bioeng. **49**:111-129.
130. **Mashego, M. R., K. Rumbold, M. De Mey, E. Vandamme, W. Soetaert, and J. J. Heijnen.** 2007. Microbial metabolomics: past, present and future methodologies. Biotechnol. Lett. **29**:1-16.
131. **Michal, G.** 1999. Biochemical pathways. Spektrum Akademischer Verlag GmbH, Heidelberg.
132. **Moir, R. D., and G. B. Stokes.** 1988. A spectrophotometric assay for 6-phosphogluconolactonase involving the use of immobilized enzymes to prepare the labile 6-phosphoglucono-delta-lactone substrate. Biochem. J. **256**:69-73.
133. **Moritz, B., K. Striegel, A. A. De Graaf, and H. Sahm.** 2000. Kinetic properties of the glucose-6-phosphate and 6-phosphogluconate dehydrogenases from *Corynebacterium glutamicum* and their application for predicting pentose phosphate pathway flux in vivo. Eur. J. Biochem. **267**:3442-3452.
134. **Murai, T., M. Tokushige, J. Nagai, and H. Katsuki.** 1971. Physiological functions of NAD⁺- and NADP⁺-linked malic enzymes in *Escherichia coli*. Biochem. Biophys. Res. Commun. **43**:875-881.
135. **Nanchen, A., T. Fuhrer, and U. Sauer.** 2006. Determination of Metabolic Flux Ratios From 13C-Experiments and Gas Chromatography-Mass Spectrometry Data: Protocol and Principles. Methods. Mol. Biol. **358**:177-198.
136. **Nanchen, A., A. Schicker, and U. Sauer.** 2006. Nonlinear dependency of intracellular fluxes on growth rate in miniaturized continuous cultures of *Escherichia coli*. Appl. Environ. Microbiol. **72**:1164-1172.
137. **Naylor, C. E., S. Gover, A. K. Basak, M. S. Cosgrove, H. R. Levy, and M. J. Adams.** 2001. NADP⁺ and NAD⁺ binding to the dual coenzyme specific enzyme *Leuconostoc mesenteroides* glucose 6-phosphate dehydrogenase: different interdomain hinge angles are seen in different binary and ternary complexes. Acta. Crystallogr. D. Biol. Crystallogr. **57**:635-648.
138. **Neidhardt, F. C., J. L. Ingraham, and M. Schaechter.** 1990. Physiology of the Bacterial Cell: a Molecular Approach. Sinauer Associates Inc., Sunderland, MA.
139. **Niebisch, A., and M. Bott.** 2001. Molecular analysis of the cytochrome bc1-aa3 branch of the *Corynebacterium glutamicum* respiratory chain containing an unusual diheme cytochrome c1. Arch. Microbiol. **175**:282-294.
140. **Nipkow, A., B. Sonnleitner, and A. Fiechter.** 1985. Effect of carbon-dioxide on growth of *Zymomonas mobilis* in continuous culture. Appl. Microbiol. Biotechnol. **21**:287-291.
141. **Nissen, T. L., M. Anderlund, J. Nielsen, J. Villadsen, and M. C. Kielland-Brandt.** 2001. Expression of a cytoplasmic transhydrogenase in *Saccharomyces cerevisiae* results in formation of 2-oxoglutarate due to depletion of the NADPH pool. Yeast **18**:19-32.
142. **Noguchi, Y., Y. Nakai, N. Shimba, H. Toyosaki, Y. Kawahara, S. Sugimoto, and E. Suzuki.** 2004. The energetic conversion competence of *Escherichia coli* during aerobic respiration studied by 31P NMR using a circulating fermentation system. J. Biochem. (Tokyo) **136**:509-515.
143. **Ogata, H., S. Goto, K. Sato, W. Fujibuchi, H. Bono, and M. Kanehisa.** 1999. KEGG: Kyoto Encyclopedia of Genes and Genomes. Nucleic Acids Res. **27**:29-34.
144. **Oh, Y. K., B. O. Palsson, S. M. Park, C. H. Schilling, and R. Mahadevan.** 2007. Genome-scale reconstruction of metabolic network in *Bacillus subtilis* based on high-throughput phenotyping and gene essentiality data. J. Biol. Chem. **282**:28791-28799.
145. **Olausson, T., O. Fjellstrom, J. Mueller, and J. Rydstrom.** 1995. Molecular biology of nicotinamide nucleotide transhydrogenase--a unique proton pump. Biochim. Biophys. Acta **1231**:1-19.

146. **Orthner, C. L., and L. I. Pizer.** 1974. An evaluation of regulation of the hexose monophosphate shunt in *Escherichia coli*. *J. Biol. Chem.* **249**:3750-3755.
147. **Osman, Y. A., T. Conway, S. J. Bonetti, and L. O. Ingram.** 1987. Glycolytic flux in *Zymomonas mobilis*: enzyme and metabolite levels during batch fermentation. *J. Bacteriol.* **169**:3726-3736.
148. **Outten, C. E., and V. C. Culotta.** 2003. A novel NADH kinase is the mitochondrial source of NADPH in *Saccharomyces cerevisiae*. *EMBO J.* **22**:2015-2024.
149. **Overkamp, K. M., B. M. Bakker, H. Y. Steensma, J. P. van Dijken, and J. T. Pronk.** 2002. Two mechanisms for oxidation of cytosolic NADPH by *Kluyveromyces lactis* mitochondria. *Yeast* **19**:813-824.
150. **Park, S. M., M. I. Klapa, A. J. Sinskey, and G. Stephanopoulos.** 1999. Metabolite and isotopomer balancing in the analysis of metabolic cycles: II. Applications. *Biotechnol. Bioeng.* **62**:392-401.
151. **Peekhaus, N., and T. Conway.** 1998. What's for dinner? Entner-Doudoroff metabolism in *Escherichia coli*. *J. Bacteriol.* **180**:3495-3502.
152. **Peekhaus, N., S. Tong, J. Reizer, M. H. Saier, Jr., E. Murray, and T. Conway.** 1997. Characterization of a novel transporter family that includes multiple *Escherichia coli* gluconate transporters and their homologues. *FEMS Microbiol. Lett.* **147**:233-238.
153. **Perrenoud, A., and U. Sauer.** 2005. Impact of global transcriptional regulation by ArcA, ArcB, Cra, Crp, Cya, Fnr, and Mlc on glucose catabolism in *Escherichia coli*. *J. Bacteriol.* **187**:3171-3179.
154. **Petersen, S., A. A. de Graaf, L. Eggeling, M. Mollney, W. Wiechert, and H. Sahm.** 2000. In vivo quantification of parallel and bidirectional fluxes in the anaplerosis of *Corynebacterium glutamicum*. *J. Biol. Chem.* **275**:35932-35941.
155. **Ponce, E., M. Garcia, and M. E. Munoz.** 2005. Participation of the Entner-Doudoroff pathway in *Escherichia coli* strains with an inactive phosphotransferase system (PTS- Glc+) in gluconate and glucose batch cultures. *Can. J. Microbiol.* **51**:975-982.
156. **Portais, J. C., and A. M. Delort.** 2002. Carbohydrate cycling in micro-organisms: what can ¹³C-NMR tell us? *FEMS Microbiol. Rev.* **26**:375-402.
157. **Portais, J. C., P. Tavernier, I. Gosselin, and J. N. Barbotin.** 1999. Cyclic organization of the carbohydrate metabolism in *Sinorhizobium meliloti*. *Eur. J. Biochem.* **265**:473-480.
158. **Price, N. D., J. L. Reed, and B. O. Palsson.** 2004. Genome-scale models of microbial cells: evaluating the consequences of constraints. *Nat. Rev. Microbiol.* **2**:886-897.
159. **Pruss, B. M., and A. J. Wolfe.** 1994. Regulation of acetyl phosphate synthesis and degradation, and the control of flagellar expression in *Escherichia coli*. *Mol. Microbiol.* **12**:973-984.
160. **Rabinowitz, J. D.** 2007. Cellular metabolomics of *Escherichia coli*. *Expert Rev Proteomics* **4**:187-198.
161. **Ranish, J. A., E. C. Yi, D. M. Leslie, S. O. Purvine, D. R. Goodlett, J. Eng, and R. Aebersold.** 2003. The study of macromolecular complexes by quantitative proteomics. *Nat. Genet.* **33**:349-355.
162. **Ranish, J. A., N. Yudkovsky, and S. Hahn.** 1999. Intermediates in formation and activity of the RNA polymerase II preinitiation complex: holoenzyme recruitment and a postrecruitment role for the TATA box and TFIIB. *Genes Dev.* **13**:49-63.
163. **Rappsilber, J., S. Siniossoglou, E. C. Hurt, and M. Mann.** 2000. A generic strategy to analyze the spatial organization of multi-protein complexes by cross-linking and mass spectrometry. *Anal. Chem.* **72**:267-275.
164. **Reed, J. L., T. D. Vo, C. H. Schilling, and B. O. Palsson.** 2003. An expanded genome-scale model of *Escherichia coli* K-12 (iJR904 GSM/GPR). *Genome Biol.* **4**:R54.
165. **Reid, M. F., and C. A. Fewson.** 1994. Molecular characterization of microbial alcohol dehydrogenases. *Crit. Rev. Microbiol.* **20**:13-56.
166. **Revelles, O., M. Espinosa-Urgel, T. Fuhrer, U. Sauer, and J. L. Ramos.** 2005. Multiple and interconnected pathways for L-lysine catabolism in *Pseudomonas putida* KT2440. *J. Bacteriol.* **187**:7500-7510.
167. **Riondet, C., R. Cachon, Y. Wache, G. Alcaraz, and C. Divies.** 1999. Changes in the proton-motive force in *Escherichia coli* in response to external oxidoreduction potential. *Eur. J. Biochem.* **262**:595-599.
168. **Romano, A. H., and T. Conway.** 1996. Evolution of carbohydrate metabolic pathways. *Res. Microbiol.* **147**:448-455.

169. **Ronimus, R. S., and H. W. Morgan.** 2003. Distribution and phylogenies of enzymes of the Embden-Meyerhof-Parnas pathway from archaea and hyperthermophilic bacteria support a gluconeogenic origin of metabolism. *Archaea* **1**:199-221.
170. **Rover Junior, L., J. C. Fernandes, G. de Oliveira Neto, L. T. Kubota, E. Katekawa, and S. H. Serrano.** 1998. Study of NADH stability using ultraviolet-visible spectrophotometric analysis and factorial design. *Anal. Biochem.* **260**:50-55.
171. **Rowley, D. L., A. J. Pease, and R. E. Wolf, Jr.** 1991. Genetic and physical analyses of the growth rate-dependent regulation of *Escherichia coli* zwf expression. *J. Bacteriol.* **173**:4660-4667.
172. **Russell, J. B.** 2007. The energy spilling reactions of bacteria and other organisms. *J. Mol. Microbiol. Biotechnol.* **13**:1-11.
173. **Sakuraba, H., R. Kawakami, and T. Ohshima.** 2005. First archaeal inorganic polyphosphate/ATP-dependent NAD kinase, from hyperthermophilic archaeon *Pyrococcus horikoshii*: cloning, expression, and characterization. *Appl. Environ. Microbiol.* **71**:4352-4358.
174. **Samorski, M., G. Muller-Newen, and J. Buchs.** 2005. Quasi-continuous combined scattered light and fluorescence measurements: a novel measurement technique for shaken microtiter plates. *Biotechnol. Bioeng.* **92**:61-68.
175. **Sanchez, A. M., J. Andrews, I. Hussein, G. N. Bennett, and K. Y. San.** 2006. Effect of overexpression of a soluble pyridine nucleotide transhydrogenase (UdhA) on the production of poly(3-hydroxybutyrate) in *Escherichia coli*. *Biotechnol. Prog.* **22**:420-425.
176. **Sanford, K., P. Soucaille, G. Whited, and G. Chotani.** 2002. Genomics to fluxomics and physiomics - pathway engineering. *Curr. Opin. Microbiol.* **5**:318-322.
177. **Sanwal, B. D.** 1970. Regulatory mechanisms involving nicotinamide adenine nucleotides as allosteric effectors. 3. Control of glucose 6-phosphate dehydrogenase. *J. Biol. Chem.* **245**:1626-1631.
178. **Sauer, U.** 2004. High-throughput phenomics: experimental methods for mapping fluxomes. *Curr. Opin. Biotech.* **15**:58-63.
179. **Sauer, U., F. Canonaco, S. Heri, A. Perrenoud, and E. Fischer.** 2004. The soluble and membrane-bound transhydrogenases UdhA and PntAB have divergent functions in NADPH metabolism of *Escherichia coli*. *J. Biol. Chem.* **279**:6613-6619.
180. **Sauer, U., V. Hatzimanikatis, J. E. Bailey, M. Hochuli, T. Szyperski, and K. Wüthrich.** 1997. Metabolic fluxes in riboflavin-producing *Bacillus subtilis*. *Nature Biotechnol.* **15**:448-452.
181. **Sauer, U., D. R. Lasko, J. Fiaux, M. Hochuli, R. Glaser, T. Szyperski, K. Wüthrich, and J. E. Bailey.** 1999. Metabolic flux ratio analysis of genetic and environmental modulations of *Escherichia coli* central carbon metabolism. *J. Bacteriol.* **181**:6679-6688.
182. **Sazanov, L. A., and J. B. Jackson.** 1994. Proton-translocating transhydrogenase and NAD⁺- and NADP⁺-linked isocitrate dehydrogenases operate in a substrate cycle which contributes to fine regulation of the tricarboxylic acid cycle activity in mitochondria. *FEBS Lett.* **344**:109-116.
183. **Schafer, A., A. Tauch, W. Jager, J. Kalinowski, G. Thierbach, and A. Puhler.** 1994. Small mobilizable multi-purpose cloning vectors derived from the *Escherichia coli* plasmids pK18 and pK19: selection of defined deletions in the chromosome of *Corynebacterium glutamicum*. *Gene* **145**:69-73.
184. **Schilling, C. H., M. W. Covert, I. Famili, G. M. Church, J. S. Edwards, and B. O. Palsson.** 2002. Genome-scale metabolic model of *Helicobacter pylori* 26695. *J. Bacteriol.* **184**:4582-4593.
185. **Schomburg, I., A. Chang, C. Ebeling, M. Gremse, C. Heldt, G. Huhn, and D. Schomburg.** 2004. BRENDA, the enzyme database: updates and major new developments. *Nucleic Acids Res.* **32**:D431-433.
186. **Schuetz, R., L. Kuepfer, and U. Sauer.** 2007. Systematic evaluation of objective functions for predicting intracellular fluxes in *Escherichia coli*. *Mol. Syst. Biol.*:doi:10.1038 (in press).
187. **Schuetz, R., L. Kuepfer, D. Vitkup, M. Heinemann, and U. Sauer.** 2008. Understanding multi-objective optimality tradeoffs in metabolic networks. Unpublished.
188. **Scrutton, N. S., A. Berry, and R. N. Perham.** 1990. Redesign of the coenzyme specificity of a dehydrogenase by protein engineering. *Nature* **343**:38-43.
189. **Segel, I. H.** 1975. Enzyme Kinetics. Behaviour and Analysis of Rapid Equilibrium and Steady State Enzyme Systems. John Wiley & Sons, Inc., New York, London, Sydney & Toronto.
190. **Segre, D., D. Vitkup, and G. M. Church.** 2002. Analysis of optimality in natural and perturbed metabolic networks. *Proc. Natl. Acad. Sci. U. S. A.* **99**:15112-15117.

191. **Sherlock, G., T. Hernandez-Boussard, A. Kasarskis, G. Binkley, J. C. Matese, S. S. Dwight, M. Kaloper, S. Weng, H. Jin, C. A. Ball, M. B. Eisen, P. T. Spellman, P. O. Brown, D. Botstein, and J. M. Cherry.** 2001. The Stanford Microarray Database. *Nucleic Acids Res.* **29**:152-155.
192. **Siebers, B., and P. Schonheit.** 2005. Unusual pathways and enzymes of central carbohydrate metabolism in Archaea. *Curr. Opin. Microbiol.* **8**:695-705.
193. **Song, S., and C. Park.** 1998. Utilization of D-ribose through D-xylose transporter. *FEMS Microbiol. Lett.* **163**:255-261.
194. **Sprenger, G. A.** 1996. Carbohydrate metabolism in *Zymomonas mobilis*: A catabolic highway with some scenic routes. *FEMS Microbiol. Lett.* **145**:301-307.
195. **Stafford, D. E., K. S. Yanagimachi, P. A. Lessard, S. K. Rijhwani, A. J. Sinskey, and G. Stephanopoulos.** 2002. Optimizing bioconversion pathways through systems analysis and metabolic engineering. *Proc. Natl. Acad. Sci. U. S. A.* **99**:1801-1806.
196. **Steen, I. H., D. Madern, M. Karlstrom, T. Lien, R. Ladenstein, and N. K. Birkeland.** 2001. Comparison of isocitrate dehydrogenase from three hyperthermophiles reveals differences in thermostability, cofactor specificity, oligomeric state, and phylogenetic affiliation. *J. Biol. Chem.* **276**:43924-43931.
197. **Stephanopoulos, G.** 1999. Metabolic fluxes and metabolic engineering. *Metabolic Eng.* **1**:1-11.
198. **Stephanopoulos, G., A. Aristidou, and J. Nielsen.** 1998. *Metabolic Engineering, Principles and Methodologies.* Academic Press, San Diego, London.
199. **Stournaras, C., P. Maurer, and G. Kurz.** 1983. 6-phospho-D-gluconate dehydrogenase from *Pseudomonas fluorescens*. Properties and subunit structure. *Eur. J. Biochem.* **130**:391-396.
200. **Stowers, M. D.** 1985. Carbon metabolism in *Rhizobium species*. *Annu. Rev. Microbiol.* **39**:89-108.
201. **Swamy, M., Y. Kulathu, S. Ernst, M. Reth, and W. W. Schamel.** 2006. Two dimensional Blue Native-/SDS-PAGE analysis of SLP family adaptor protein complexes. *Immunol. Lett.* **104**:131-137.
202. **Swamy, M., G. M. Siegers, S. Minguet, B. Wollscheid, and W. W. Schamel.** 2006. Blue native polyacrylamide gel electrophoresis (BN-PAGE) for the identification and analysis of multiprotein complexes. *Sci. STKE* **2006**:pl4.
203. **Szyperski, T.** 1995. Biosynthetically directed fractional ¹³C-labeling of proteinogenic amino acids. An efficient analytical tool to investigate intermediary metabolism. *Eur. J. Biochem.* **232**:433-448.
204. **Szyperski, T.** 1998. C-13-NMR, MS and metabolic flux balancing in biotechnology research. *Q. Rev. Biophys.* **31**:41-106.
205. **Tarrio, N., M. Becerra, M. E. Cerdan, and M. I. Gonzalez Siso.** 2006. Reoxidation of cytosolic NADPH in *Kluyveromyces lactis*. *FEMS Yeast Res.* **6**:371-380.
206. **Temple, L. M., A. E. Sage, H. P. Schweizer, and P. V. Phibbs, Jr.** 1998. Carbohydrate metabolism in *Pseudomonas aeruginosa*, p. 35-72, *Biotechnology Handbooks*, vol. 10. Plenum Press, New York.
207. **Teusink, B., J. Passarge, C. A. Reijenga, E. Esgalhado, C. C. van der Weijden, M. Schepper, M. C. Walsh, B. M. Bakker, K. van Dam, H. V. Westerhoff, and J. L. Snoep.** 2000. Can yeast glycolysis be understood in terms of in vitro kinetics of the constituent enzymes? Testing biochemistry. *European Journal of Biochemistry* **267**:5313-5329.
208. **Theobald, U., W. Mailinger, M. Baltes, M. Rizzi, and M. Reuss.** 1997. In vivo analysis of metabolic dynamics in *Saccharomyces cerevisiae*. 1. Experimental observations. *Biotechnol. Bioeng.* **55**:305-316.
209. **Toledano, M. B., C. Kumar, N. Le Moan, D. Spector, and F. Tacnet.** 2007. The system biology of thiol redox system in *Escherichia coli* and yeast: differential functions in oxidative stress, iron metabolism and DNA synthesis. *FEBS Lett.* **581**:3598-3607.
210. **Umemura, K., and H. Kimura.** 2005. Determination of oxidized and reduced nicotinamide adenine dinucleotide in cell monolayers using a single extraction procedure and a spectrophotometric assay. *Anal. Biochem.* **338**:131-135.
211. **van Beilen, J. B., and E. G. Funhoff.** 2007. Alkane hydroxylases involved in microbial alkane degradation. *Appl. Microbiol. Biotechnol.* **74**:13-21.
212. **Varma, A., B. W. Boesch, and B. O. Palsson.** 1993. Stoichiometric interpretation of *Escherichia coli* glucose catabolism under various oxygenation rates. *Appl. Environ. Microbiol.* **59**:2465-2473.
213. **Verho, R., P. Richard, P. H. Jonson, L. Sundqvist, J. Londesborough, and M. Penttila.** 2002. Identification of the first fungal NADP⁺-GAPDH from *Kluyveromyces lactis*. *Biochemistry* **41**:13833-13838.

214. **Veronese, F. M., E. Boccu, and A. Fontana.** 1976. Isolation and properties of 6-phosphogluconate dehydrogenase from *Escherichia coli*. Some comparisons with the thermophilic enzyme from *Bacillus stearothermophilus*. *Biochemistry* **15**:4026-4033.
215. **Vicente, M., and J. L. Canovas.** 1973. Glucolysis in *Pseudomonas putida*: physiological role of alternative routes from the analysis of defective mutants. *J. Bacteriol.* **116**:908-914.
216. **Viikari, L.** 1988. Carbohydrate metabolism in *Z. mobilis*. *Crit. Rev. Biotechnol.* **7**:237-261.
217. **Vlami-Gardikas, A., F. Aslund, G. Spyrou, T. Bergman, and A. Holmgren.** 1997. Cloning, overexpression, and characterization of glutaredoxin 2, an atypical glutaredoxin from *Escherichia coli*. *J. Biol. Chem.* **272**:11236-11243.
218. **Voordouw, G., S. M. van der Vies, and A. P. Themmen.** 1983. Why are two different types of pyridine nucleotide transhydrogenase found in living organisms? *Eur. J. Biochem.* **131**:527-533.
219. **Wagner, T. C., and M. D. Scott.** 1994. Single extraction method for the spectrophotometric quantification of oxidized and reduced pyridine nucleotides in erythrocytes. *Anal. Biochem.* **222**:417-426.
220. **Wang, C. H., I. Stern, C. M. Gilmour, S. Klungsoyr, D. J. Reed, J. J. Bialy, B. E. Christensen, and V. H. Cheldelin.** 1958. Comparative study of glucose catabolism by the radiorespirometric method. *J. Bacteriol.* **76**:207-216.
221. **Wang, Y., S. L. Wu, W. S. Hancock, R. Trala, M. Kessler, A. H. Taylor, P. S. Patel, and J. C. Aon.** 2005. Proteomic profiling of *Escherichia coli* proteins under high cell density fed-batch cultivation with overexpression of phosphogluconolactonase. *Biotechnol. Prog.* **21**:1401-1411.
222. **Wiechert, W.** 2001. ¹³C metabolic flux analysis. *Metabolic Eng.* **3**:195-206.
223. **Wittmann, C., and E. Heinzle.** 2002. Genealogy profiling through strain improvement by using metabolic network analysis: metabolic flux genealogy of several generations of lysine-producing corynebacteria. *Appl. Environ. Microbiol.* **68**:5843-5859.
224. **Wolf, R. E., Jr., D. M. Prather, and F. M. Shea.** 1979. Growth-rate-dependent alteration of 6-phosphogluconate dehydrogenase and glucose 6-phosphate dehydrogenase levels in *Escherichia coli* K-12. *J. Bacteriol.* **139**:1093-1096.
225. **Wood, A. P., and D. P. Kelly.** 1980. Carbohydrate degradation pathways in *Thiobacillus* A2 grown on various sugars. *J. Gen. Microbiol.* **120**:333-345.
226. **Wood, A. P., and D. P. Kelly.** 1977. Heterotrophic growth of *Thiobacillus* A2 on sugars and organic acids. *Arch. Microbiol.* **113**:257-264.
227. **Wood, A. P., D. P. Kelly, and C. F. Thurston.** 1977. Simultaneous operation of three catabolic pathways in the metabolism of glucose by *Thiobacillus* A2. *Arch. Microbiol.* **113**:265-274.
228. **Wood, T.** 1986. Physiological functions of the pentose phosphate pathway. *Cell Biochem. Funct.* **4**:241-247.
229. **Yakunin, A. F., and P. C. Hallenbeck.** 1997. Regulation of synthesis of pyruvate carboxylase in the photosynthetic bacterium *Rhodobacter capsulatus*. *J. Bacteriol.* **179**:1460-1468.
230. **Yamaguchi, M., and C. D. Stout.** 2003. Essential glycine in the proton channel of *Escherichia coli* transhydrogenase. *J. Biol. Chem.* **278**:45333-45339.
231. **Yamaguchi, M., C. D. Stout, and Y. Hatefi.** 2002. The proton channel of the energy-transducing nicotinamide nucleotide transhydrogenase of *Escherichia coli*. *J. Biol. Chem.* **277**:33670-33675.
232. **Yang, C., Q. Hua, T. Baba, H. Mori, and K. Shimizu.** 2003. Analysis of *Escherichia coli* anaplerotic metabolism and its regulation mechanisms from the metabolic responses to altered dilution rates and phosphoenolpyruvate carboxykinase knockout. *Biotechnol. Bioeng.* **84**:129-144.
233. **Zamboni, N., E. Fischer, and U. Sauer.** 2005. FiatFlux - a software for metabolic flux analysis from ¹³C-glucose experiments. *BMC Bioinformatics* **6**:209.
234. **Zamboni, N., A. Kummel, and M. Heinemann.** 2008. anNET: a tool for network-embedded thermodynamic analysis of quantitative metabolome data. Submitted.
235. **Zamboni, N., and U. Sauer.** 2003. Knockout of the high-coupling cytochrome *aa₃* oxidase reduces TCA cycle fluxes in *Bacillus subtilis*. *FEMS Microbiol. Lett.* **226**:121-126.
236. **Zaslaver, A., A. Bren, M. Ronen, S. Itzkovitz, I. Kikoin, S. Shavit, W. Liebermeister, M. G. Surette, and U. Alon.** 2006. A comprehensive library of fluorescent transcriptional reporters for *Escherichia coli*. *Nature Methods* **3**:623-628.

References

- 237. **Zerez, C. R., D. E. Moul, E. G. Gomez, V. M. Lopez, and A. J. Andreoli.** 1987. Negative modulation of *Escherichia coli* NAD⁺ kinase by NADPH and NADH. *J. Bacteriol.* **169**:184-188.
- 238. **Zevenhuizen, L. P.** 1981. Cellular glycogen, beta-1,2-glucan, poly beta-hydroxybutyric acid and extracellular polysaccharides in fast-growing species of rhizobium. *Ant. Van Leeuwenhoek* **47**:481-497.

Appendix

Table of contents

Chapter 2	144
Chapter 3	145
Chapter 4	146
Chapter 5	151
Conclusions and Outlook	161

Chapter 2 – Estimated net fluxes

#	Reaction	Organism										
		<i>A. tumefaciens</i>	<i>B. subtilis</i>	<i>E. coli</i>	<i>P. fluorescens</i>	<i>P. putida</i>	<i>R. sphaeroides</i>	<i>S. mellitii</i>	<i>T. versutus</i>	<i>Z. mobilis</i>		
1	GLC → GCLi	4.48 ± 0.19	4.61 ± 0.09	7.52 ± 0.06	4.81 ± 0.17	7.02 ± 0.53	1.86 ± 0.08	2.41 ± 0.13	18.40 ± 0.20	61.51 ± 0.11		
2	GLCi + ATP → G6P	4.48 ± 0.19	4.61 ± 0.09	7.52 ± 0.06	4.81 ± 0.17	7.02 ± 0.53	1.86 ± 0.08	2.41 ± 0.13	18.40 ± 0.20	61.51 ± 0.11		
3	G6P → F6P	-0.01 ± 0.07	2.67 ± 0.07	5.56 ± 0.08	0.05 ± 0.13	-0.37 ± 0.22	-0.00 ± 0.01	0.03 ± 0.09	-0.60 ± 0.12	0.06 ± 0.01		
4	F6P + ATP → 2 T3P		3.68 ± 0.08	6.26 ± 0.07			-0.10 ± 0.05		-1.14 ± 0.27			
5	2 T3P → F6P + ATP											
6	T3P → PGA + ATP + NADH	4.11 ± 0.19	7.71 ± 0.17	13.14 ± 0.13	0.00 ± 0.13	0.46 ± 0.23	1.56 ± 0.09	0.00 ± 0.09	16.01 ± 0.28	61.12 ± 0.12		
7	PGA → PEP	3.76 ± 0.19	7.25 ± 0.17	12.28 ± 0.14	4.07 ± 0.17	5.86 ± 0.43	1.28 ± 0.08	2.22 ± 0.13	14.65 ± 0.28	60.58 ± 0.14		
8	PEP → PYR + ATP	4.00 ± 0.21	7.38 ± 0.21	9.48 ± 0.21	3.19 ± 0.14	5.00 ± 0.40	1.29 ± 0.08	1.97 ± 0.13	15.00 ± 0.32	59.72 ± 0.16		
9	G6P → 6PG + NADPH	4.47 ± 0.20	1.77 ± 0.06	1.94 ± 0.07	3.42 ± 0.17	5.70 ± 0.49	1.84 ± 0.09	2.38 ± 0.18	18.82 ± 0.23	61.40 ± 0.11		
10	6PG → Ru5P + CO ₂ + NADPH	0.27 ± 0.10	1.77 ± 0.06	1.53 ± 0.07	4.73 ± 0.25	7.36 ± 0.66	0.00 ± 0.09	0.09 ± 0.03	0.00 ± 0.44	0.21 ± 0.03		
11	Ru5P → X5P	0.01 ± 0.07	1.01 ± 0.04	0.71 ± 0.04	0.47 ± 0.06	0.38 ± 0.08	-0.09 ± 0.04	-0.03 ± 0.01	0.00 ± 0.29	-0.04 ± 0.01		
12	Ru5P → R5P	0.26 ± 0.04	0.75 ± 0.03	0.83 ± 0.04	-0.04 ± 0.03	0.51 ± 0.04	0.09 ± 0.04	0.12 ± 0.03	0.55 ± 0.15	0.25 ± 0.03		
13	X5P + R5P → S7P + T3P	0.07 ± 0.04	0.58 ± 0.02	0.45 ± 0.02	0.08 ± 0.02	0.06 ± 0.02	-0.04 ± 0.03	0.02 ± 0.01	-0.08 ± 0.14	0.00 ± 0.00		
14	X5P + E4P → F6P + T3P	-0.05 ± 0.03	0.44 ± 0.02	0.26 ± 0.02	-0.12 ± 0.02	-0.14 ± 0.02	-0.06 ± 0.03	-0.05 ± 0.01	-0.47 ± 0.14	-0.04 ± 0.01		
15	S7P + T3P → E4P + F6P	0.07 ± 0.04	0.58 ± 0.02	0.45 ± 0.02	0.08 ± 0.02	0.06 ± 0.02	-0.04 ± 0.03	0.02 ± 0.01	-0.08 ± 0.14	-0.04 ± 0.01		
16	6PG → T3P + PYR	4.20 ± 0.19			0.40 ± 0.05	6.99 ± 0.67	1.84 ± 0.13	2.28 ± 0.18	18.82 ± 0.50	61.19 ± 0.12		
17	OAA + AcCoA → ICT	5.33 ± 0.37	1.90 ± 0.13	3.23 ± 0.15	2.81 ± 0.32	7.21 ± 0.97	1.82 ± 0.19	2.84 ± 0.30	26.32 ± 0.52	0.31 ± 0.04		
18	ICT → OGA + CO ₂ + NADPH	5.33 ± 0.37	1.90 ± 0.13	3.23 ± 0.15	2.81 ± 0.32	7.21 ± 0.97	1.82 ± 0.19	2.84 ± 0.30	26.32 ± 0.52	0.31 ± 0.04		
19	OGA → MAL + CO ₂ + 1.5 ATP + 2 NADH	4.95 ± 0.37	1.44 ± 0.11	2.27 ± 0.15	2.14 ± 0.33	6.50 ± 0.97	1.66 ± 0.18	2.65 ± 0.31	25.20 ± 0.53			
20	MAL → OAA + NADH	3.62 ± 0.30	1.16 ± 0.08	1.88 ± 0.08	0.47 ± 0.20	3.21 ± 0.65	1.12 ± 0.13	1.96 ± 0.25	19.19 ± 0.41			
21	PYR → AcCoA + CO ₂ + NADH	5.98 ± 0.37	4.70 ± 0.15	8.18 ± 0.15	3.98 ± 0.32	8.39 ± 0.97	2.18 ± 0.19	3.19 ± 0.29	27.12 ± 0.52	1.01 ± 0.1		
22	MAL → PYR + CO ₂ + NADH	1.32 ± 0.13	0.27 ± 0.06	0.39 ± 0.09	1.67 ± 0.24	3.29 ± 0.49	0.55 ± 0.07	0.89 ± 0.10	6.00 ± 0.37	0.00 ± 0.00		
23	PEP + CO ₂ → OAA			2.75 ± 0.10								
24	OAA + ATP → PEP + CO ₂	0.47 ± 0.06	0.43 ± 0.08	0.37 ± 0.01	0.65 ± 0.03	1.12 ± 0.16	0.05 ± 0.02	0.00 ± 0.12	1.17 ± 0.17	0.76 ± 0.07		
25	PYR + ATP + CO ₂ → OAA	2.63 ± 0.15	1.86 ± 0.12		3.84 ± 0.25	5.97 ± 0.59	0.98 ± 0.09	1.11 ± 0.14	10.13 ± 0.36			
26	OAA → PYR + CO ₂			3.60 ± 0.05								
27	AcCoA → Acetate + ATP											
28	2 PYR → Acetoin + 2 CO ₂											
29	Acetoin → 2 AcCoA + 2 NADH											
30	PYR → AcAld + CO ₂											
31	AcAld + NADH → EtOH											
										118.85 ± 0.30		
										118.85 ± 0.30		

Estimated net fluxes in mmol g⁻¹ h⁻¹. grey fields indicated absent reactions compared to the master network.
Reactions 32-42 were not used in any net flux calculation in all species.

Chapter 3 - In vitro enzyme activities

In vitro enzyme activities determined in raw extracts from cultures harvested during exponential growth on glucose.									
Enzymes	Cofactor	Organisms							
		<i>A. tumefaciens</i>	<i>S. meliloti</i>	<i>P. fluorescens</i>	<i>R. sphaeroides</i>	<i>P. versutus</i>	<i>Z. mobilis</i>	<i>E. coli</i>	
6PpDH ^a	NADP ⁺	142 ± 8 ^b	132 ± 4	118 ± 5	45 ± 1	140 ± 15	1515 ± 171	94 ± 3	
	NAD ⁺	60 ± 3	72 ± 4	65 ± 5	21 ± 1	45 ± 4	1324 ± 64	0 ± 0	
	NADP ⁺	116 ± 8	64 ± 6	60 ± 4	15 ± 1	104 ± 4	1157 ± 71	68 ± 2	
6PGDH	NAD ⁺	73 ± 5	41 ± 7	64 ± 4	6 ± 1	24 ± 2	1220 ± 39	0 ± 0	
	NADP ⁺	76 ± 4	42 ± 2	6 ± 1	2 ± 0	10 ± 0	6 ± 0	52 ± 2	
	NAD ⁺	12 ± 2	3 ± 1	5 ± 0	0 ± 0	0 ± 0	5 ± 0	0 ± 1	
G3PDH	NADP ⁺	91 ± 5	28 ± 1	2 ± 0	0 ± 0	8 ± 0	4 ± 0	51 ± 2	
	NAD ⁺	14 ± 2	2 ± 0	3 ± 0	0 ± 0	1 ± 1	9 ± 0	0 ± 0	
	NADP ⁺	0 ± 0	0 ± 0	10 ± 0	2 ± 0	1 ± 1	20 ± 9	5 ± 6	
ICTDH	NAD ⁺	68 ± 4	43 ± 4	48 ± 1	89 ± 5	136 ± 12	1746 ± 53	454 ± 31	
	NADP ⁺	0 ± 0	0 ± 0	7 ± 3	2 ± 0	2 ± 0	0 ± 0	7 ± 1	
	NAD ⁺	59 ± 0	28 ± 1	72 ± 11	83 ± 18	101 ± 0	1032 ± 89	186 ± 19	
MDH	NADP ⁺	438 ± 22	277 ± 11	213 ± 5	75 ± 2	373 ± 14	1 ± 0	469 ± 15	
	NAD ⁺	14 ± 2	5 ± 1	0 ± 3	5 ± 1	2 ± 0	8 ± 3	0 ± 1	
	NADP ⁺	562 ± 28	199 ± 9	177 ± 9	41 ± 1	301 ± 10	0 ± 0	457 ± 16	
MAE ^c	NAD ⁺	8 ± 2	5 ± 0	2 ± 1	1 ± 1	2 ± 1	10 ± 1	1 ± 0	
	NADPH	2 ± 0	1 ± 0	3 ± 1	12 ± 0	5 ± 3	0 ± 3	0 ± 3	
	NADPH	418 ± 42	482 ± 14	16 ± 1	1107 ± 0	1295 ± 42	1 ± 0	359 ± 13	
soluble TH	NADPH	3 ± 2	2 ± 0	1 ± 1	1 ± 4	0 ± 12	1 ± 0	8 ± 4	
	NADH	582 ± 30	357 ± 0	4 ± 3	500 ± 19	995 ± 71	0 ± 3	342 ± 19	
	NADP ⁺	18 ± 1	36 ± 3	239 ± 22	1 ± 0	10 ± 1	5 ± 0	25 ± 1	
mem.-bound TH	NADP ⁺	15 ± 1	43 ± 3	195 ± 9	0 ± 0	2 ± 0	6 ± 0	21 ± 1	
	APAD ⁺	2.0 ± 1.1	3.0 ± 0.0	2.0 ± 0.0	0.7 ± 0.0	4.0 ± 0.0	2.1 ± 0.1	3.8 ± 0.1	
	APAD ⁺	1.5 ± 0.2	1.0 ± 0.0	2.1 ± 0.2	0.2 ± 0.1	4.0 ± 0.0	3.7 ± 1.0	3.4 ± 0.1	
TH	APAD ⁺	13.3 ± 0.9	0.0 ± 0.0	0.2 ± 0.1	25.3 ± 1.1	27.0 ± 1.0	0.0 ± 0.0	30.8 ± 0.9	
	APAD ⁺	11.9 ± 0.6	0.0 ± 0.0	0.3 ± 0.1	±	±	0.0 ± 0.0	23.2 ± 0.7	

^a Enzyme abbreviations: glucose-6P, 6P-glucanase, glycerolaldehyde-3P, isocitrate and malate dehydrogenase (6PpDH, 6PGDH, G3PDH, ICTDH and MDH), malic enzyme (MAE), transhydrogenase (TH).

^b All activities were determined as $\mu\text{mol min}^{-1} \text{g wet protein}^{-1}$. Standard deviations from at least duplicate experiments. Data shaded in grey are from independent growth experiment and extraction.

^c Due to interference with MDH activity, only NADP⁺ dependent malic enzyme was determined.

Appendix

Chapter 4 - Wild-type reference flux solutions for MOMA predicted by MOP using relative weights for ATP and biomass production, fluxes are given in absolute mmol and uptake rates were set to 100 mmol C6 (glucose as reference).

	acetate	gluconate	glucose	glycerole	lactate	succinate	xylose		acetate	gluconate	glucose	glycerole	lactate	succinate	xylose
'glk'	0.00	0.00	0.00	0.00	0.00	0.00	0.00	'ndh'	0.00	0.00	0.00	0.00	0.00	0.00	0.00
'pgi'	-1.80	-2.35	78.50	-2.65	-2.39	-1.99	-4.38	'cyoABCD'	488.59	276.00	254.69	257.20	331.58	317.61	289.84
'pfkA'	0.00	22.12	41.74	0.00	0.00	0.00	35.22	'cydAB'	194.04	64.86	72.63	73.72	94.10	87.14	80.56
'pfkB'	0.00	22.12	41.74	0.00	0.00	0.00	35.22	'narGHI'	0.00	0.00	0.00	0.00	0.00	0.00	0.00
'fbaA'	-3.16	22.12	41.74	-4.65	-4.20	-3.50	35.22	'poxB'	0.00	0.00	0.00	0.00	0.00	0.00	0.00
'fbaB'	-3.16	22.12	41.74	-4.65	-4.20	-3.50	35.22	'sdhABCD'	105.17	18.49	19.03	22.11	31.30	89.41	25.28
'tpiA'	-6.31	44.23	83.49	190.70	-8.40	-7.01	70.43	'sdhABCD'	105.17	18.49	19.03	22.11	45.51	89.41	25.28
'gapA'	-16.32	131.15	168.64	175.94	-21.72	-18.12	176.23	'pfIB'	0.00	31.08	34.13	35.77	43.62	24.53	36.08
'pgk'	-16.32	131.15	168.64	175.94	-21.72	-18.12	176.23	'tdcE'	0.00	31.08	34.13	35.77	43.62	24.53	36.08
'gpmA'	-10.50	62.52	80.85	84.52	-13.97	-11.66	84.79	'fdhF'	0.00	9.10	7.03	8.48	14.33	13.00	10.09
'gpmB'	-10.50	62.52	80.85	84.52	-13.97	-11.66	84.79	'fdoGHI'	0.00	9.10	7.03	8.48	14.33	13.00	10.09
'eno'	-21.00	125.04	161.70	169.04	-27.95	-23.31	169.59	'fdoGHI_r2'	0.00	9.10	7.03	8.48	14.33	13.00	10.09
'pykF'	0.00	50.98	15.92	69.68	0.00	0.00	70.51	'adhE'	5.88	0.00	0.00	0.00	0.00	0.00	0.00
'pykA'	0.00	50.98	15.92	69.68	0.00	0.00	70.51	'mhpf'	5.88	0.00	0.00	0.00	0.00	0.00	0.00
'aceEF'	0.00	40.18	41.16	44.25	57.95	37.53	46.17	'adhE_r2'	3.92	0.00	0.00	0.00	0.00	0.00	0.00
'maeB'	0.00	0.00	0.00	0.00	0.00	58.27	0.00	'adhP'	3.92	0.00	0.00	0.00	0.00	0.00	0.00
'maeA'	15.99	0.00	0.00	0.00	0.00	46.07	0.00	'adhC'	3.92	0.00	0.00	0.00	0.00	0.00	0.00
'pck'	25.19	0.00	0.00	0.00	0.00	27.97	0.00	'pta'	0.00	35.88	41.59	41.98	34.67	35.47	39.29
'fbp'	3.16	0.00	0.00	4.65	4.20	3.50	0.00	'ackA'	0.00	8.97	10.40	10.50	8.67	8.87	9.82
'glpX'	3.16	0.00	0.00	4.65	4.20	3.50	0.00	'ackB'	0.00	8.97	10.40	10.50	8.67	8.87	9.82
'pps'	0.00	0.00	0.00	0.00	33.52	0.00	0.00	'tdcD'	0.00	8.97	10.40	10.50	8.67	8.87	9.82
'zwf'	0.00	0.00	18.84	0.00	0.00	0.00	1.84	'purT'	0.00	8.97	10.40	10.50	8.67	8.87	9.82
'pgl'	0.00	0.00	18.84	0.00	0.00	0.00	1.84	'acs'	300.00	0.00	0.00	0.00	0.00	0.00	0.00
'gnd'	0.00	78.72	17.53	0.00	0.00	0.00	1.84	'dld'	0.00	0.00	0.00	0.00	14.21	0.00	0.00
'rpiA'	2.07	15.82	5.99	3.05	2.75	2.30	23.24	'ldhA'	0.00	0.00	0.00	0.00	185.79	0.00	0.00
'rpiB'	2.07	15.82	5.99	3.05	2.75	2.30	23.24	'gcd'	0.00	0.00	0.00	0.00	0.00	0.00	0.00
'rpe'	-4.13	47.08	5.56	-6.10	-5.50	-4.59	-44.64	'gntV'	0.00	50.00	0.00	0.00	0.00	0.00	0.00
'tktA'	-0.54	12.41	2.12	-0.80	-0.72	-0.60	19.53	'gntK'	0.00	50.00	0.00	0.00	0.00	0.00	0.00
'tktB'	-0.54	12.41	2.12	-0.80	-0.72	-0.60	19.53	'edd'	0.00	21.28	1.31	0.00	0.00	0.00	0.00
'tktA_r2'	-1.52	11.13	0.66	-2.25	-2.03	-1.69	18.14	'eda'	0.00	21.28	1.31	0.00	0.00	0.00	0.00
'tktB_r2'	-1.52	11.13	0.66	-2.25	-2.03	-1.69	18.14	'mgsA'	0.00	0.00	0.00	0.00	0.00	0.00	0.00
'talA'	-0.54	12.41	2.12	-0.80	-0.72	-0.60	19.53	'ptsGHI'	0.00	0.00	-100.00	0.00	0.00	0.00	0.00
'talB'	-0.54	12.41	2.12	-0.80	-0.72	-0.60	19.53	'co2'	354.58	205.20	142.58	144.90	192.96	274.23	166.65
'glTA'	108.83	23.04	24.19	27.24	35.93	18.28	30.22	'o2'	341.31	170.43	163.66	165.46	212.84	202.37	185.20
'prpC'	108.83	23.04	24.19	27.24	35.93	18.28	30.22	'no3'	0.00	0.00	0.00	0.00	0.00	0.00	0.00
'acnA'	108.83	23.04	24.19	27.24	35.93	18.28	30.22	'no2'	0.00	0.00	0.00	0.00	0.00	0.00	0.00
'acnA_r2'	108.83	23.04	24.19	27.24	35.93	18.28	30.22	'ethtransp'	11.75	0.00	0.00	0.00	0.00	0.00	0.00
'acnB'	108.83	23.04	24.19	27.24	35.93	18.28	30.22	'actransp'	-300.00	35.88	41.59	41.98	34.67	35.47	39.29
'acnB_r2'	108.83	23.04	24.19	27.24	35.93	18.28	30.22	'fumtrans'	0.00	0.00	0.00	0.00	0.00	0.00	0.00
'icd'	160.18	42.85	48.38	54.48	50.64	36.56	60.44	'maltransp'	0.00	0.00	0.00	0.00	0.00	0.00	0.00
'sucAB'	153.22	33.75	38.05	44.22	41.38	28.83	50.55	'succtrans'	0.36	0.00	0.00	0.00	0.00	-150.00	0.00
'sucCD'	153.22	33.75	38.05	44.22	41.38	28.83	50.55	'lactransp'	0.00	0.00	0.00	0.00	-200.00	0.00	0.00
'frdABCD'	105.17	18.49	19.03	22.11	31.30	89.41	25.28	'pyrtransp'	0.00	0.00	0.00	0.00	0.00	0.00	0.00
'sdhAB'	0.00	0.00	0.00	0.00	0.00	0.00	0.00	'glctrans'	0.00	-100.00	0.00	0.00	0.00	0.00	0.00
'fumA'	70.11	12.33	12.68	14.74	20.86	59.61	16.85	'fortransp'	0.00	34.86	47.16	46.09	44.26	10.04	41.89
'fumB'	70.11	12.33	12.68	14.74	20.86	59.61	16.85	'glctransp'	0.00	0.00	0.00	0.00	0.00	0.00	0.00
'fumC'	70.11	12.33	12.68	14.74	20.86	59.61	16.85	'glytransp'	0.00	0.00	0.00	-200.00	0.00	0.00	0.00
'mdh'	206.81	40.23	38.05	44.22	83.80	74.49	50.55	'glyconv'	0.00	0.00	0.00	200.00	0.00	0.00	0.00
'mqo'	45.01	0.00	0.00	0.00	0.00	0.00	0.00	'oletransp'	0.00	0.00	0.00	0.00	0.00	0.00	0.00
'aceA'	57.48	3.24	0.00	0.00	21.21	0.00	0.00	'oleconv'	0.00	0.00	0.00	0.00	0.00	0.00	0.00
'aceB'	57.48	3.24	0.00	0.00	21.21	0.00	0.00	'xyltransp'	0.00	0.00	0.00	0.00	0.00	0.00	-120.00
'ppc'	0.00	17.59	23.65	23.50	0.00	0.00	22.62	'xylconv'	0.00	0.00	0.00	0.00	0.00	0.00	120.00
'pntAB'	0.00	0.00	41.94	71.43	63.02	0.00	57.10	'maint'	0.00	0.00	0.00	0.00	0.00	0.00	0.00
'udhA'	74.77	9.94	0.00	0.00	0.00	0.00	0.00	'biomass'	5.44	7.11	8.07	8.02	7.24	6.04	7.72
'atp'	1012.98	612.31	569.78	562.90	711.76	549.60	635.68	fluxes were predicted using the MOP principle: relative weights for ATP and biomass and minimize overall intracellular flux							
'nuo'	427.28	303.88	289.27	286.70	348.88	225.92	319.84								

Chapter 4 - PntAB, UdhA and biomass fluxes for all substrates and mutants predicted by MOMA using wild-type reference flux solutions. Values of -3 indicate infeasible system i.e. that the mutation did not allow for a flux solution with the resulting network. Fluxes are given in absolute mmol.

pntAB MOMA																									
	wt	tpaA	frdA	edd	cyoA	sdhC	pta	pckA	atp	rpe	ppc	sucC	pps	glk	nuoG	zwf	gapC	acs	mgSA	Pgi	UdhA	sfcA	maeB	gnd	pntAB
acetate	0.0	0.0	-3.0	0.0	0.0	0.0	0.0	0.0	-3.0	0.0	0.0	6.7	0.0	0.0	0.0	0.0	0.0	-3.0	0.0	0.0	0.0	0.0	0.0	0.0	0.0
gluconate	0.0	0.0	0.0	0.0	0.0	0.0	0.0	0.0	43.1	0.9	0.0	0.8	0.0	0.0	0.0	0.0	0.0	0.0	0.0	0.0	0.0	0.0	0.0	0.0	0.0
glucose	41.9	11.3	25.9	41.8	4.9	41.9	40.1	41.9	97.2	44.6	37.6	43.5	41.9	41.9	1.0	47.1	10.3	41.9	41.9	0.0	41.9	41.9	41.9	44.3	0.0
glycerol	71.4	6.3	52.2	71.4	32.4	71.4	69.3	71.4	111.9	64.0	65.2	73.1	71.4	71.4	24.5	71.4	15.8	71.4	71.4	20.0	71.4	71.4	71.4	71.4	0.0
lactate	63.0	17.6	36.0	63.0	13.8	63.0	61.5	63.0	99.2	56.2	63.0	64.5	50.3	63.0	3.9	63.0	17.6	63.0	63.0	16.9	63.0	63.0	63.0	63.0	0.0
succinate	0.0	0.0	-3.0	0.0	0.0	0.0	0.0	0.0	150.0	0.0	0.0	0.9	0.0	0.0	0.0	0.0	0.0	0.0	0.0	0.0	0.0	0.0	10.2	0.0	
xylose	57.1	28.8	35.8	57.1	13.3	57.1	55.1	57.1	95.0	2.6	51.2	59.0	57.1	57.1	5.5	57.2	4.7	57.1	57.1	8.8	57.1	57.1	57.1	57.1	0.0

udhA MOMA																									
	wt	tpaA	frdA	edd	cyoA	sdhC	pta	pckA	atp	rpe	ppc	sucC	pps	glk	nuoG	zwf	gapC	acs	mgSA	Pgi	UdhA	sfcA	maeB	gnd	pntAB
acetate	74.8	142.9	-3.0	74.8	130.7	74.8	74.8	84.4	-3.0	83.6	74.8	63.7	74.8	74.8	109.0	74.8	142.9	-3.0	74.8	142.9	0.0	82.7	74.8	74.8	74.8
gluconate	10.0	32.0	37.5	21.2	31.5	10.0	11.8	10.0	76.5	8.7	16.2	8.1	10.0	10.0	28.5	10.0	71.7	10.0	10.0	84.6	0.0	10.0	10.0	29.6	10.0
glucose	0.0	31.3	16.5	0.1	4.7	0.0	1.6	0.0	39.8	0.0	4.8	0.0	0.0	0.0	0.0	0.0	30.1	0.0	0.0	60.4	0.0	0.0	0.0	0.0	
glycerol	0.0	66.5	19.8	0.0	6.5	0.0	1.9	0.0	54.9	7.8	6.8	0.0	0.0	0.0	0.0	0.0	53.7	0.0	0.0	54.8	0.0	0.0	0.0	0.0	
lactate	0.0	49.0	27.8	0.0	7.6	0.0	1.3	0.0	99.2	7.1	0.0	0.0	13.8	0.0	0.0	0.0	49.0	0.0	0.0	49.2	0.0	0.0	0.0	0.0	
succinate	0.0	48.1	-3.0	0.0	5.5	0.0	1.6	10.0	147.4	6.8	0.0	0.0	0.0	0.0	14.0	0.0	48.1	0.0	0.0	48.5	0.0	23.0	0.0	0.0	
xylose	0.0	28.9	22.0	0.0	7.0	0.0	1.7	0.0	73.4	57.0	6.4	0.0	0.0	0.0	0.0	0.0	0.0	51.3	0.0	0.0	51.3	0.0	0.0	0.0	
BM MOMA																									
	wt	tpaA	frdA	edd	cyoA	sdhC	pta	pckA	atp	rpe	ppc	sucC	pps	glk	nuoG	zwf	gapC	acs	mgSA	Pgi	UdhA	sfcA	maeB	gnd	pntAB
acetate	5.4	0.0	-3.0	5.4	0.5	5.4	5.4	5.4	-3.0	5.4	5.4	4.5	5.4	5.4	1.2	5.4	0.0	-3.0	5.4	5.4	0.0	6.7	5.4	5.4	5.4
gluconate	7.1	4.8	4.3	7.4	4.5	7.1	7.2	7.1	1.2	2.9	5.8	6.6	7.1	7.1	4.1	7.1	1.2	7.1	7.1	0.0	7.4	7.1	7.1	0.9	7.1
glucose	8.1	2.4	4.9	8.1	4.5	8.1	8.1	8.1	4.3	7.6	6.0	7.3	8.1	8.1	3.1	6.4	3.0	8.1	8.1	8.9	8.1	8.1	6.8	5.8	5.8
glycerol	8.0	0.0	4.4	8.0	4.2	8.0	8.0	8.0	4.2	8.0	6.1	7.1	8.0	8.0	4.2	8.0	0.0	8.0	8.0	0.0	8.0	8.0	8.0	8.0	3.8
lactate	7.2	0.0	2.0	7.2	2.4	7.2	7.2	7.2	0.0	7.2	7.2	6.4	4.4	7.2	2.5	7.2	0.0	7.2	7.2	0.0	7.2	7.2	7.2	7.2	3.2
succinate	6.0	0.0	-3.0	6.0	5.1	6.0	6.1	5.9	0.2	6.1	6.0	5.4	6.0	6.0	3.4	6.0	0.0	6.0	6.0	0.0	6.0	5.8	3.2	6.0	6.0
xylose	7.7	3.6	3.5	7.7	3.2	7.7	7.7	7.7	1.8	7.6	5.7	6.7	7.7	7.7	3.3	7.5	0.0	7.7	7.7	0.0	7.7	7.7	7.7	7.6	4.3

Chapter 4 - Integrated GFP expression data from triplicate experiments

Integrated GFP expression values																											
pntAB		wt	tp1A	frdA	edd	cyoA	sdhC	pta	pckA	atp	rpe	ppc	sucC	pps	glk	nucG	zwf	gapC	acs	mgSA	pgi	udhA	sfcA	moeB	gnd	pntAB	
acetat stddev gluconat stddev glucose stddev glycerol stddev lactate stddev succinat stddev xylose stddev	0.18	0.12	0.13	0.16	0.18	0.00	0.05	0.10	0.00	0.00	0.11	0.12	0.00	0.00	0.16	0.16	0.10	0.00	0.13	0.17	0.29	0.08	0.00	0.16	0.18	0.16	
	0.02	0.02	0.01	0.02	0.03	0.00	0.01	0.00	0.00	0.00	0.01	0.01	0.01	0.00	0.00	0.01	0.02	0.00	0.02	0.00	0.06	0.02	0.00	0.01	0.01	0.02	
	0.11	0.09	0.08	0.20	0.12	0.28	0.09	0.10	0.13	0.00	0.00	0.29	0.00	0.00	0.12	0.14	0.18	0.00	0.10	0.16	0.13	0.10	0.21	0.11	0.12	0.10	
	0.01	0.01	0.01	0.00	0.01	0.00	0.01	0.00	0.01	0.00	0.00	0.00	0.00	0.02	0.01	0.02	0.00	0.01	0.03	0.02	0.01	0.04	0.02	0.02	0.01	0.11	
	0.20	0.22	0.15	0.12	0.19	0.28	0.09	0.19	0.13	0.20	0.00	0.37	0.21	0.23	0.21	0.23	0.26	0.00	0.14	0.18	0.19	0.25	0.39	0.20	0.21	0.20	
	0.05	0.02	0.03	0.00	0.00	0.02	0.01	0.01	0.01	0.02	0.00	0.06	0.03	0.01	0.03	0.01	0.03	0.00	0.01	0.01	0.03	0.02	0.00	0.03	0.02	0.00	
	0.29	0.13	0.24	0.28	0.25	0.25	0.23	0.26	0.13	0.05	0.00	0.33	0.28	0.33	0.28	0.23	0.22	0.00	0.24	0.29	0.36	0.15	0.30	0.25	0.27	0.26	
	0.03	0.01	0.04	0.04	0.02	0.01	0.03	0.04	0.02	0.01	0.00	0.01	0.00	0.01	0.01	0.01	0.01	0.00	0.01	0.04	0.05	0.01	0.02	0.02	0.00	0.00	
	0.16	0.12	0.16	0.21	0.18	0.26	0.10	0.20	0.00	0.06	0.06	0.22	0.15	0.16	0.20	0.16	0.17	0.00	0.14	0.20	0.23	0.11	0.22	0.14	0.17	0.14	
	0.03	0.00	0.00	0.01	0.01	0.01	0.01	0.00	0.01	0.01	0.01	0.01	0.01	0.03	0.01	0.01	0.03	0.00	0.00	0.01	0.03	0.02	0.03	0.01	0.01	0.02	
	0.17	0.09	0.11	0.15	0.15	0.00	0.14	0.16	0.00	0.09	0.18	0.23	0.16	0.16	0.16	0.16	0.17	0.00	0.12	0.16	0.23	0.11	0.21	0.15	0.17	0.16	0.16
	0.02	0.01	0.02	0.02	0.02	0.00	0.02	0.02	0.00	0.03	0.02	0.00	0.02	0.02	0.02	0.02	0.02	0.00	0.02	0.03	0.07	0.00	0.01	0.02	0.00	0.01	0.01
	0.16	0.14	0.11	0.14	0.15	0.27	0.11	0.15	0.17	0.00	0.07	0.27	0.13	0.18	0.18	0.18	0.00	0.00	0.13	0.23	0.28	0.15	0.17	0.12	0.15	0.12	0.13
	0.03	0.00	0.01	0.01	0.01	0.02	0.01	0.01	0.01	0.00	0.01	0.00	0.01	0.02	0.01	0.01	0.03	0.03	0.01	0.04	0.04	0.01	0.01	0.01	0.01	0.00	0.01
Integrated GFP expression values																											
udhA		wt	tp1A	frdA	edd	cyoA	sdhC	pta	pckA	atp	rpe	ppc	sucC	pps	glk	nucG	zwf	gapC	acs	mgSA	pgi	udhA	sfcA	moeB	gnd	pntAB	
acetat stddev gluconat stddev glucose stddev glycerol stddev lactate stddev succinat stddev xylose stddev	0.32	0.26	0.34	0.35	0.13	0.00	0.06	0.20	0.00	0.00	0.32	0.29	0.00	0.00	0.41	0.34	0.18	0.32	0.31	0.40	0.61	0.21	0.00	0.35	0.47	0.34	0.37
	0.00	0.04	0.02	0.02	0.01	0.00	0.02	0.00	0.00	0.00	0.02	0.02	0.00	0.00	0.24	0.21	0.26	0.21	0.20	0.29	0.20	0.18	0.74	0.24	0.25	0.22	0.20
	0.23	0.16	0.19	0.32	0.34	0.33	0.25	0.25	0.29	0.00	0.00	0.00	0.30	0.24	0.24	0.21	0.26	0.21	0.20	0.29	0.20	0.18	0.74	0.24	0.25	0.22	0.20
	0.03	0.02	0.01	0.03	0.01	0.00	0.01	0.00	0.00	0.00	0.00	0.00	0.00	0.03	0.02	0.01	0.00	0.01	0.01	0.01	0.02	0.01	0.12	0.02	0.03	0.01	0.01
	0.20	0.32	0.17	0.15	0.26	0.21	0.18	0.26	0.21	0.33	0.00	0.29	0.25	0.23	0.25	0.23	0.30	0.19	0.20	0.27	0.18	0.29	0.41	0.24	0.23	0.18	0.22
	0.01	0.01	0.02	0.01	0.02	0.03	0.02	0.01	0.01	0.04	0.00	0.04	0.00	0.04	0.03	0.02	0.03	0.00	0.02	0.02	0.01	0.01	0.05	0.03	0.02	0.01	0.03
	0.31	0.15	0.21	0.21	0.21	0.26	0.28	0.23	0.19	0.13	0.00	0.31	0.30	0.30	0.30	0.23	0.24	0.28	0.28	0.36	0.28	0.15	0.41	0.22	0.32	0.23	0.24
	0.06	0.04	0.04	0.00	0.01	0.02	0.03	0.01	0.01	0.05	0.00	0.03	0.01	0.01	0.01	0.01	0.01	0.02	0.01	0.03	0.02	0.02	0.03	0.03	0.03	0.01	0.01
	0.34	0.20	0.28	0.32	0.29	0.60	0.31	0.32	0.00	0.18	0.09	0.43	0.35	0.28	0.31	0.34	0.34	0.30	0.48	0.38	0.22	0.57	0.28	0.44	0.30	0.28	0.28
	0.03	0.01	0.01	0.02	0.03	0.04	0.00	0.01	0.07	0.03	0.01	0.03	0.01	0.03	0.03	0.04	0.05	0.03	0.01	0.06	0.00	0.04	0.07	0.02	0.00	0.03	0.03
	0.31	0.18	0.30	0.28	0.03	0.00	0.29	0.28	0.00	0.20	0.35	0.39	0.36	0.28	0.32	0.28	0.32	0.34	0.33	0.28	0.33	0.19	0.57	0.28	0.37	0.33	0.33
	0.06	0.01	0.02	0.01	0.02	0.00	0.02	0.01	0.00	0.02	0.01	0.00	0.11	0.07	0.02	0.04	0.03	0.06	0.02	0.04	0.02	0.01	0.08	0.01	0.04	0.01	0.03
	0.28	0.20	0.27	0.25	0.32	0.32	0.29	0.29	0.29	0.47	0.00	0.16	0.29	0.16	0.29	0.27	0.25	0.34	0.23	0.25	0.37	0.21	0.38	0.26	0.28	0.23	0.24
	0.05	0.02	0.01	0.02	0.03	0.02	0.00	0.02	0.00	0.02	0.01	0.01	0.01	0.04	0.03	0.06	0.10	0.01	0.01	0.07	0.04	0.01	0.02	0.00	0.01	0.01	0.01
values are from triplicate experiments except few case for which they are duplicates, zero values indicated absent growth																											

all values are from triplicate experiments except few case for which they are duplicates, zero values indicated absent growth

Chapter 4 - Calculation of correlation distance for clustering the integrated promoter activity data

Correlation distance: one minus the sample correlation between points (treated as sequence of values).

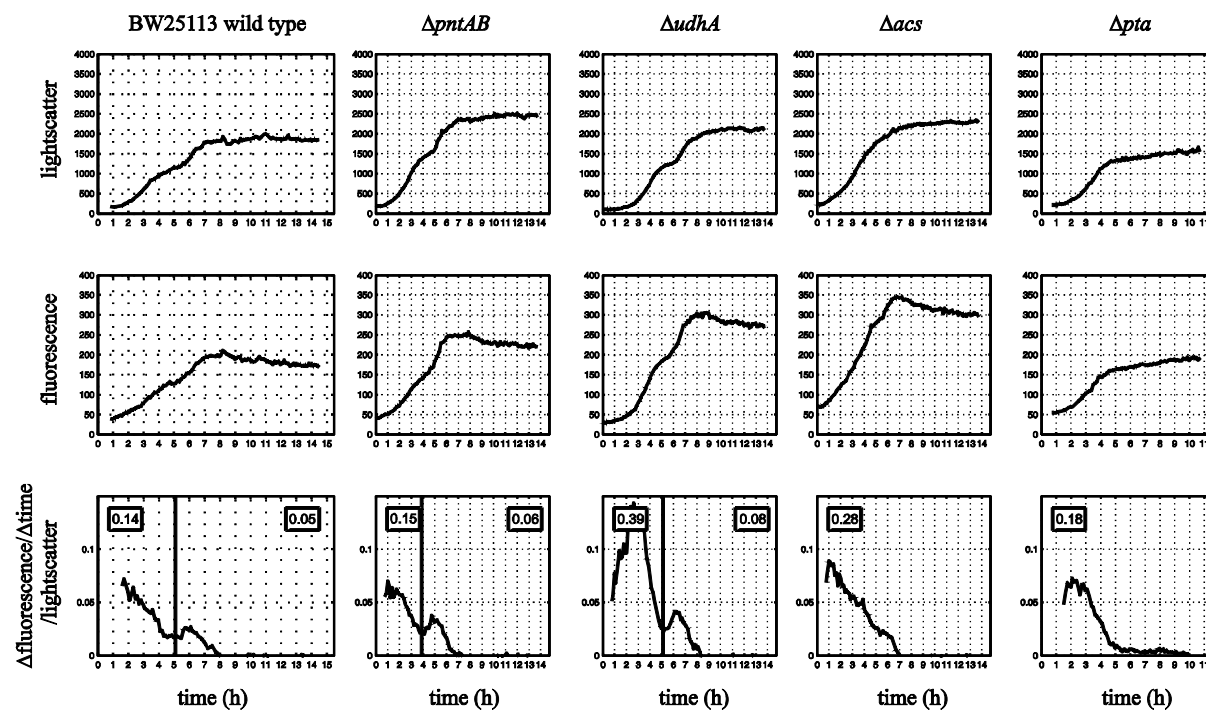
Metric definition:

$$d_{rs} = 1 - \frac{(x_r - \bar{x}_r)(x_s - \bar{x}_s)^T}{\left[\frac{1}{n} \sum_j (x_{rj} - \bar{x}_r)^2 \right]^{\frac{1}{2}} \left[\frac{1}{n} \sum_j (x_{sj} - \bar{x}_s)^2 \right]^{\frac{1}{2}}}$$

where

$$\bar{x}_r = \frac{1}{n} \sum_j x_{rj} \quad \text{and} \quad \bar{x}_s = \frac{1}{n} \sum_j x_{sj}$$

r and s are the index of observations and j is the index of the variable within an observation.

Chapter 4 - Complementary plot to Figure 7 for expression of *udhA*

Time courses of light scatter (biomass, top row), fluorescence (middle row) and promoter activity from the *udhA* reporter plasmid ($\Delta \text{fluorescence} / \Delta \text{time} / \text{light scatter}$, bottom row) for *E. coli* BW25113 wild-type and PntAB, UdhA, Acs and Pta mutants during growth on glucose minimal medium. Integrated promoter activity is indicated in the insets, which reflects the total amount of GFP formed per cell (area below the curve left and right of the vertical line). The vertical line splits the time course in two phases observed in the top row (biomass).

Chapter 5 - Additional information on kinetics of glucose-6P- and 6P-gluconate dehydrogenase

Complete velocity equation for a ordered Bi-Bi system (189):

$$v = \frac{V_f V_r \left([A][B] - \frac{[P][Q]}{K_{eq}} \right)}{V_r K_{iA} K_{m_B} + V_r K_{m_B} [A] + V_r K_{m_A} [B] + \frac{V_f K_{m_Q} [P]}{K_{eq}} + \frac{V_f K_{m_P} [Q]}{K_{eq}} + V_r [A][B] + \frac{V_f K_{m_Q} [A][P]}{K_{eq} K_{iA}} + \frac{V_f [P][Q]}{K_{eq}} + \frac{V_r K_{m_B} [B][Q]}{K_{iQ}} + \frac{V_r [A][B][P]}{K_{iP}} + \frac{V_f [B][P][Q]}{K_{iB} K_{eq}}$$

A, B, P and Q are the substrates and product concentrations; V_f and V_r are forward and reverse maximal reaction rates; K_M , K_i and K_{eq} are the Michaelis-Menten, dissociation and equilibrium constants respectively. Dividing out V_r leads to equation 1.

Chapter 5- Additional rate laws for prediction

$$\begin{aligned}
 (I) \quad V_{G6PDH} &= \frac{V_{max} [NADP^+][G6P]}{K_{1,NADP^*} K_{m,G6P} \left(1 + \frac{[NADPH]}{K_{ic,NADPH,G6P}} \right) + K_{m,G6P} [NADP^+] \left(1 + \frac{[NADPH]}{K_{ic,NADPH,NADP^*}} \right) + K_{m,NADP^*} [G6P] \left(1 + \frac{[NADPH]}{K_{ic,NADPH,NADP^*}} \right) + [NADP^+][G6P]} \\
 (II) \quad V_{G6PDH} &= \frac{V_{max} [NADP^+][G6P]}{K_{1,NADP^*} K_{m,G6P} \left(1 + \frac{[NADPH]}{K_{ic,NADPH,G6P}} + \frac{[6PG]}{K_{ic,6PG,G6P}} \right) + K_{m,G6P} [NADP^+] \left(1 + \frac{[NADPH]}{K_{ic,NADPH,NADP^*}} \right) + K_{m,NADP^*} [G6P] \left(1 + \frac{[NADPH]}{K_{ic,NADPH,NADP^*}} \right) + [NADP^+][G6P] \left(1 + \frac{[6PG]}{K_{ic,6PG,NADP^*}} \right)} \\
 (III) \quad V_{G6PDH} &= \frac{V_{max} [NADP^+][6PG]}{K_{1,NADP^*} K_{m,6PG} \left(1 + \frac{[NADPH]}{K_{ic,NADPH,6PG}} \right) + K_{m,6PG} [NADP^+] \left(1 + \frac{[NADPH]}{K_{ic,NADPH,6PG}} \right) + K_{m,NADP^*} [6PG] \left(1 + \frac{[NADPH]}{K_{ic,NADPH,NADP^*}} \right) + [NADP^+][6PG] \left(1 + \frac{[NADPH]}{K_{ic,NADPH,6PG}} \right)} \\
 (IV) \quad V_{G6PDH} &= \frac{V_{max} [NADP^+][6PG]}{K_{1,NADP^*} K_{m,6PG} \left(1 + \frac{[R5P]}{K_{ic,R5P,6PG}} \right) + K_{m,6PG} [NADP^+] \left(1 + \frac{[R5P]}{K_{ic,R5P,6PG}} \right) + K_{m,NADP^*} [6PG] \left(1 + \frac{[R5P]}{K_{ic,R5P,NADP^*}} \right) + [NADP^+][6PG] \left(1 + \frac{[R5P]}{K_{ic,R5P,NADP^*}} \right)} \\
 (V) \quad V_{G6PDH} &= \frac{V_{max} [NADP^+][6PG]}{K_{1,NADP^*} K_{m,6PG} \left(1 + \frac{[R5P]}{K_{ic,R5P,6PG}} + \frac{[NADPH]}{K_{ic,NADPH,6PG}} \right) + K_{m,6PG} [NADP^+] \left(1 + \frac{[R5P]}{K_{ic,R5P,NADP^*}} \right) + K_{m,NADP^*} [6PG] \left(1 + \frac{[NADPH]}{K_{ic,NADPH,NADP^*}} \right) + [NADP^+][6PG] \left(1 + \frac{[R5P]}{K_{ic,R5P,NADP^*}} + \frac{[NADPH]}{K_{ic,NADPH,6PG}} \right)}
 \end{aligned}$$

Chapter 5 - Energy costs to generate NADPH by PP pathway or transhydrogenase

An energy-balance for both PntAB and PP pathway was calculated to compare the costs for NADPH regeneration in terms of ATP. Typically, 37 and 42 % of the NADPH are provided by the PP pathway and PntAB reaction respectively in *E. coli* grown on glucose at 37°C. During catabolism of one molecule of glucose, maximally 20.8 ATP can be generated assuming a published P/O ratio of 1.4 (Fig. I)(142). Considering the PP pathway as the alternative route to EMP pathway and lumping it into a single reaction, we can summarize it as shown in Figure I: per molecule of glucose two of NADPH are generated, one of CO₂ and two of NADP⁺ are consumed. In addition, the reaction catalyzed by the transketolase yields directly a triose-3P molecule, which circumvents the consumption of ATP in the EMP pathway step from fructose-6P towards triose-3P. Considering a typical *E. coli* flux distribution, about 17% of the PP pathway flux defined by the reaction catalyzed by the 6P-gluconate dehydrogenase is channeled through this transketolase, which therefore saves 0.17 ATP (Fig. I)(67). The reaction catalyzed by PntAB can be summarized as follows: one molecule of NADPH is regenerated from NADP⁺ at expense of one molecule of NADH, which is oxidized to NAD⁺ and of one proton translocated over the membrane (21). The ATP costs per molecule of NADPH generate by the two mechanisms were almost equal with 1.64 and 1.73 ATP per NADPH for the PP pathway and the PntAB reaction respectively (Fig. I).

Chapter 5 - Figure I

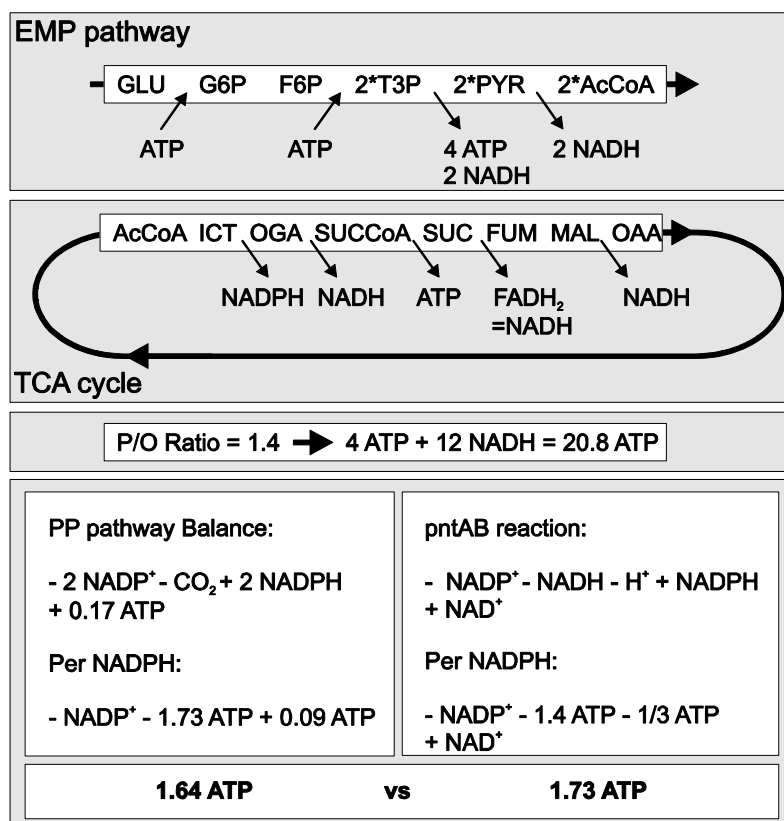


Figure I - ATP generation in *E. coli* and ATP costs comparison of PP pathway versus membrane-bound transhydrogenase for NADPH regeneration. One NADPH generated through the PP pathway causes the release of half a molecule of CO₂, which corresponds to 1/12 of a molecule of glucose. One molecule of NADPH therefore corresponds to 20.8 ATP/12 = 1.73 ATP. In the ATPase reaction, 3 H⁺ are required to generate one molecule of ATP.

Chapter 5 - Flux balance analysis for wild-type and PntAB mutant

Preference of either use of PP pathway or PntAB reaction for NADPH regeneration was investigated by FBA assuming different objective functions and constraints from experimental data (62, 186). A basic network of *E. coli* central carbon metabolism was used, which consisted of 33 reactions and 28 metabolites (60). The *E. coli* network previously published was modified as follows: the transhydrogenases were incorporated as two distinct directions including the proton transfer in the case of PntAB reaction; respiration yields $P/O \cdot 6 \cdot H^+$ instead of directly ATP; ATPase reaction generating ATP from 3 H^+ (65). The biomass requirements were adjusted to the experimentally observed growth using a published biomass composition model (60).

Biomass or biomass per flux unit maximization led to absent catabolic PP pathway, no or few ATP production and transhydrogenase activity from NADH towards NADPH (Table I). The PntAB reaction provided about 79 or 64% of the total NADPH required for biomass production and the PP pathway was only of minor importance. When optimizing for ATP at a fixed experimentally determined yield of 0.4, both PPP pathway and PntAB reaction were not relevant for NADPH production. However, PPP pathway and PntAB reaction contributed 40 and 50% of NADPH respectively when optimizing ATP per flux unit, which correlates roughly with the experimentally found values of 37 and 42% (179). Generally, the PntAB reaction was always used if available and more important than PP pathway except when normalizing on intracellular flux (per fluxunit or overall intracellular flux). Minimizing intracellular flux provoked flux through glucose-6P dehydrogenase and subsequently ED pathway but not through PP pathway, which would involve more enzyme activity than ED pathway. Thus, the PntAB reaction regenerates the NADPH necessary for biomass from the NADH formed elsewhere in catabolism. The biomass precursor in the PP pathway are produced by a small backward flux into the PP pathway from fructose-6P and triose-3P. Catabolic PP pathway was used only if the PntAB reaction was shut off. This finding indicates that the uncoupled PntAB reaction, which also converts NADH into NAD^+ is advantageous for the cell, at least in in silico calculations.

Chapter 5 - Table I

Table I - Contribution of PP pathway and PntAB reaction to NADPH production

	biomass	biomass per flux unit	min. overall flux	ATP	ATP per flux unit
biomass yield / %	69 ^a - 67	56 - 61	0.4 - fixed	0.4 - fixed	0.4 - fixed
ATP balance ^b / %	0 - 29	20 - 53	204 - 211	1316 - 1315	397 - 485
PPP contribution ^c / %	0 - 92	28 - 92	88 - 92	0 - 6	40 - 92
PntAB contribution ^d / %	79 - 0	64 - 0	4 - (-8)	5 - 0	50 - 0

^a Wild-type (left) versus PntAB mutant (right)^b Summed ATP production minus requirements for biomass^c Percentage fraction of NADPH produced by glucose-6P- and 6P-gluconate dehydrogenase^d Percentage fraction of NADPH produced by PntAB reaction

However, the experimental finding of significant catabolic glucose degradation through the PP pathway (typically 22%) with its concomitant NADPH regeneration pointed towards other reasons to use the PP pathway besides just providing NADPH and biomass precursors. Network-embedded thermodynamic analysis indicates that glucose-6P dehydrogenase may be a target of regulation under batch growth conditions (personal communication) while 6P-gluconolactonase was shown to have a positive effect upon overexpression during fedbatch conditions and also was identified as target of regulation under chemostat conditions (117, 221). For 6P-gluconate dehydrogenase no clear conclusion was possible (117). To clarify if kinetic regulation is present here or if just limitation by enzyme activity takes place, we purified and kinetically characterized the two dehydrogenases of the oxidative PP pathway, namely glucose-6P- and 6P-gluconate dehydrogenase.

Chapter 5 - Net flux solutions from FBA analysis for wild-type, fluxes are given in absolute mmol.

		wildtype				
1	glk	GLC + ATP -> G6P	0	0	0	0
2	glctransp	GLC <-> GLCxt + Hxt	0	0	0	0
3	ptsGHI	G6P + PYR <-> GLCxt + PEP	-100	-100	-100	-100
4	pgi	G6P <-> F6P	95.9191	52.733	-1.3457	97.624
5	zwf	G6P <-> D6PGL + NADPH	0	43.9346	98.9697	0
6	pgl	D6PGL -> 6PGC	0	43.9346	98.9697	0
7	gnd	6PGC -> NADPH + CO2 + RL5P	0	0	0	0
8	rpi	RL5P <-> R5P	9.3985	7.6746	5.472	5.472
9	rpe	RL5P <-> X5P	-9.3985	-7.6746	-5.472	-5.472
10	tkt_r1	R5P + X5P <-> GA3P + S7P	-2.4733	-2.0196	-1.44	-1.44
11	tkt_r2	X5P + E4P <-> F6P + GA3P	-6.9252	-5.655	-4.032	-4.032
12	tal	GA3P + S7P <-> E4P + F6P	-2.4733	-2.0196	-1.44	-1.44
13	edd	6PGC -> 2KD6PG	0	43.9346	98.9697	0
14	eda	2KD6PG -> GA3P + PYR	0	43.9346	98.9697	0
15	pfk	F6P + ATP -> FDP	85.655	44.3515	51.3414	91.648
16	fba	FDP <-> DHAP + GA3P	85.655	44.3515	-7.3217	91.648
17	fbp	FDP -> F6P	0	0	58.6632	0
18	tpiA	DHAP <-> GA3P	85.655	44.3515	-7.3217	91.648
19	gapA	GA3P <-> NADH + 13DPG	162.9008	125.7708	79.4303	178.4
20	pgk	13DPG <-> 3PG + ATP	162.9008	125.7708	79.4303	178.4
21	gpm	3PG <-> 2PG	152.2657	117.0864	73.2383	172.208
22	eno	2PG <-> PEP	152.2657	117.0864	73.2383	172.208
23	pyk	PEP -> PYR + ATP	6.51	0	16.1755	45.568
24	pps	PYR + 2 ATP -> PEP	0	20.2769	93.8291	0
25	pck	OA + ATP -> PEP + CO2	0	0	32.3283	0
26	ppc	PEP + CO2 -> OA	36.2335	29.5877	77.6762	21.096
27	maeB	MAL -> PYR + NADPH + CO2	0	0	0	0
28	sfcA	MAL -> PYR + NADH + CO2	0	0	24.2519	0
29	ace	PYR + COA -> ACCOA + CO2 + NADH	70.1528	93.9691	124.4	124.4
30	glt	ACCOA + OA -> COA + CIT	40.3498	12.9257	9.216	107.048
31	acnA	CIT <-> CAC	40.3498	12.9257	9.216	107.048
32	acnB	CAC <-> ICIT	40.3498	12.9257	9.216	107.048
33	icd	ICIT <-> CO2 + NADPH + AKG	40.3498	12.9257	9.216	107.048
34	sucAB	AKG + COA -> CO2 + NADH + SUCCOA	24.5208	0	0	97.832
35	sucCD	SUCCOA <-> ATP + COA + SUCC	24.5208	0	0	97.832
36	sdhAB	SUCC <-> FUM + NADH	24.5208	0	0	97.832
37	fum	FUM <-> MAL	24.5208	0	0	97.832
38	mdh	MAL <-> NADH + OA	24.5208	0	-24.2519	97.832
39	aceA	ICIT <-> GLX + SUCC	0	0	0	0
40	aceB	GLX + ACCOA -> MAL + COA	0	0	0	0
41	pta	ACCOA -> ACTP + COA	0	56.7068	97.832	0
42	ack	ACTP <-> ATP + AC	0	56.7068	97.832	0
43	actransp	AC <-> ACxt	0	56.7068	97.832	0
44	pntAB	NADH + Hxt -> NADPH	153.8027	101.6812	75.8446	5.992
45	udhA	NADPH -> NADH	0	0	70.9903	0
46	atp	4 Hxt -> ATP	388.8526	308.3746	477.3349	1375.286
47	resp	O2 + 2 NADH -> 18 Hxt	94.9563	74.1766	110.288	305.952
48	co2	CO2 -> CO2xt	98.7899	77.3071	112.52	308.184
49	o2	O2xt -> O2	94.9563	74.1766	110.288	305.952
50	maint	ATP ->	0	0	110.0046	0
51	biomass	0.46 E4P + 0.12 NADH + 0.86 3PG + 0.77 PEP + 2.94	12.3664	10.0982	7.2	7.2
			12.3664	10.0982	0	1315.998
						397.4387
yield			0.4*18	0.4*18	0.4*18	0.4*18
obj			BM	BM	BM	ATP
ratio			none	none	none	none
ptsGH			YES	YES	YES	YES
mode			LP	NLP	QP	LP
NADPH reqs			194	159	113	113
% pntAB contribution			79	64	4	5
net TH NADPH			154	102	5	6
ATP prod			497	426	493	1605
ATP req			497	406	289	289
net ATP			0	20	204	1316
% ppp contribution			0	28	88	0
yield			69	56	40	40

Appendix

Chapter 5 - Net flux solutions from FBA analysis for PntAB mutant, fluxes are given in absolute mmol.

		pntAB				
1	glk	GLC + ATP -> G6P	0	0	0	0
2	glctransp	GLC <=> GLCxt + Hxt	0	0	0	0
3	ptsGHI	G6P + PYR <=> GLCxt + PEP	-100	-100	-100	-100
4	pgi	G6P <=> F6P	3.8282	-8.862	-6.728	94.0288
5	zwf	G6P <=> D6PGL + NADPH	92.1638	105.2248	104.352	3.5952
6	pgl	D6PGL -> 6PGC	92.1638	105.2248	104.352	3.5952
7	gnd	6PGC -> NADPH + CO2 + RL5P	82.9722	53.7076	0	3.5952
8	rpi	RL5P <=> R5P	36.8879	26.279	5.472	6.6704
9	rpe	RL5P <=> X5P	46.0843	27.4286	-5.472	-3.0752
10	tkt_r1	R5P + X5P <=> GA3P + S7P	25.2283	15.6982	-1.44	-0.2416
11	tkt_r2	X5P + E4P <=> F6P + GA3P	20.856	11.7304	-4.032	-2.8336
12	tal	GA3P + S7P <=> E4P + F6P	25.2283	15.6982	-1.44	-0.2416
13	edd	6PGC -> 2KD6PG	9.1916	51.5172	104.352	0
14	eda	2KD6PG -> GA3P + PYR	9.1916	51.5172	104.352	0
15	pfk	F6P + ATP -> FDP	49.0624	17.7951	49.7356	90.4496
16	fba	FDP <=> DHAP + GA3P	49.0624	17.7951	-12.704	90.4496
17	fbp	FDP -> F6P	0	0	62.4396	0
18	tpiA	DHAP <=> GA3P	49.0624	17.7951	-12.704	90.4496
19	gapA	GA3P <=> NADH + 13DPG	126.7149	97.5152	74.048	177.2016
20	pgk	13DPG <=> 3PG + ATP	126.7149	97.5152	74.048	177.2016
21	gpm	3PG <=> 2PG	116.2699	88.0366	67.856	171.0096
22	eno	2PG <=> PEP	116.2699	88.0366	67.856	171.0096
23	pyk	PEP -> PYR + ATP	0	0	13.1845	44.3696
24	pps	PYR + 2 ATP -> PEP	28.6679	52.7436	98.9907	0
25	pck	OA + ATP -> PEP + CO2	0	0	32.0285	0
26	ppc	PEP + CO2 -> OA	35.5859	32.2935	80.1467	21.096
27	maeB	MAL -> PYR + NADPH + CO2	0	0	8.8314	0
28	sfcA	MAL -> PYR + NADH + CO2	0	0	18.1908	0
29	ace	PYR + COA -> ACCOA + CO2 + NADH	44.8164	66.37	124.4	123.2016
30	glt	ACCOA + OA -> COA + CIT	15.5461	14.1077	9.216	105.8496
31	acnA	CIT <=> CAC	15.5461	14.1077	9.216	105.8496
32	acnB	CAC <=> ICIT	15.5461	14.1077	9.216	105.8496
33	icd	ICIT <=> CO2 + NADPH + AKG	15.5461	14.1077	9.216	105.8496
34	sucAB	AKG + COA -> CO2 + NADH + SUCCOA	0	0	0	96.6336
35	sucCD	SUCCOA <=> ATP + COA + SUCC	0	0	0	96.6336
36	sdhAB	SUCC <=> FUM + NADH	0	0	0	96.6336
37	fum	FUM <=> MAL	0	0	0	96.6336
38	mdh	MAL <=> NADH + OA	0	0	-27.0222	96.6336
39	aceA	ICIT <=> GLX + SUCC	0	0	0	0
40	aceB	GLX + ACCOA -> MAL + COA	0	0	0	0
41	pta	ACCOA -> ACTP + COA	0	25.7	97.832	0
42	ack	ACTP <=> ATP + AC	0	25.7	97.832	0
43	actransp	AC <=> ACxt	0	25.7	97.832	0
44	pntAB	NADH + Hxt -> NADPH	0	0	0	0
45	udhA	NADPH -> NADH	0	0	9.3594	0
46	atp	4 Hxt -> ATP	467.9265	443.138	496.296	1376.784
47	resp	O2 + 2 NADH -> 18 Hxt	103.9837	98.4751	110.288	305.952
48	co2	CO2 -> CO2xt	107.7487	101.8918	112.52	308.184
49	o2	O2xt -> O2	103.9837	98.4751	110.288	305.952
50	maint	ATP ->	0	0	112.1751	0
51	biomass	70.2 Glt + 10.7 NADH + 0.33 COA + 0.07 Cit + 0.30 NADH + 0.36 E4P + 0.12 GA3P + 0.86 3PG + 0.77 PEP + 2.94	12.1454	11.0217	7.2	7.2
			12.1454	11.0217	0	1315.0992
yield			0.4*18	0.4*18	0.4*18	0.4*18
obj			BM	BM	BM	ATP
ratio			none	none	none	none
ptsGH			YES	YES	YES	YES
mode			LP	NLP	QP	NLP
NADPH reqs			191	173	113	113
% pntAB contribution			0	0	-8	0
net TH NADPH			0	0	-9	0
ATP prod			517	496	501	1605
ATP req			488	443	289	289
net ATP			29	53	211	1315
% ppp contribution			92	92	92	6
yield			67	61	40	40

Chapter 5 - Sampling, quenching procedures specific for cycling assay and recoveries of NAD(H) and NADP(H)

Different quenching methods and the quantification of cofactors by the cycling assay were tested but finally not used for various reasons (see Materials and Methods in **Chapter 5** and Appendix for details). Mainly because not only the concentrations of cofactors NADPH, NADP⁺, NADH and NAD⁺ were needed but also the metabolites of the PP pathway, glucose-6P, 6P-gluconolactone, 6P-gluconate and the pentose pool. Hence, quantification of cofactors and metabolites was possible within one procedure only by LC-MS/MS.

Sampling and extraction for enzymatic cycling assays

Whole cell broth extraction was used for the cycling assay, i.e. 1 ml cell broth was added to 1 ml 0.02 M HCL and to 1 ml 0.02 M NaOH at 90°C in 2 ml Eppendorf tubes in a heating block. The cells were quenched and extracted at the same time. Since NAD⁺ and NADP⁺ are stable at high temperatures at low pH and NADH and NADPH are stable at high pH, even evaporating the samples in the heat block for about 2 hours was possible to concentrate the samples (120). With the chosen concentrations of HCL and NaOH, neutralization prior to the cycling assay was not necessary because of the cycling assay buffer. As a control, samples were also quenched and extracted with hot buffer at neutral pH (100 mM Tris-HCL, pH 7.2) to detect the summed concentration of the oxidized or reduced forms. Alternatively, quenching by ethanol and 2-propanol were tested as quenching solutions to quantify recoveries compared to non quenched cells.

Cycling assay for quantification of NADP⁺, NADPH, NAD⁺ and NADH

The well established cycling assay was tested and adapted for reliable quantification of NADH, NADPH, NAD⁺ and NADP⁺ (121, 208, 210, 219). The assay contained: 1 ml cycling assay buffer (0.1 M TrisHCl pH 7.5, 10 mM MgCl₂, and 0.1 mM nicotineamide), 100 µl of phenazine ethosulfate (PES, 25 mM in H₂O), 50 µl thiazolyl blue tetrazolium bromide (MES, 10 mM in H₂O) and 2 or 10 units of glucose-6P- or alcohol dehydrogenase respectively. The sample was added and the well mixed assay was incubated for 3 min at 30°C. 10 µl 1 M

glucose-6P or 40 μ l 100% ethanol were added, well mixed and after 30 sec of centrifugation at 15,000 rpm, formation of formazan (reduced MES) was recorded in the supernatant at 570 nm in 1 ml cuvettes in a Unicam UV4 UV/VIS spectrometer. The slope was linearly dependent on the catalyzing amount of NADH/NAD⁺ or NADPH/NADP⁺ present in the sample in the range of 8-160 pmol of cofactor in the final assay mixture.

Results

The well known basic and acidic extraction methods were adapted by mixing whole cell broth with either 0.02 M NaOH or 0.02 M HCL. The impact of basic or acidic treatment was tested only with the reduced cofactors NADH and NADPH since accurate standard solutions were required, which was only possible by measuring absorbance at 340 nm shortly before testing the harsh pH conditions (however oxidized cofactors may be quantified at 260 nm with an extinction coefficient $\epsilon = 17.8 \text{ mM}^{-1} \text{ cm}^{-1}$). While NADH and NADPH standard solution had recoveries of about 85 and 80% in 0.02 M NaOH, they were not completely destroyed in 0.02 M HCL with recoveries of about 5 and 25%. Much worse, by incubating the standards with glucose minimal medium at acidic and basic conditions, the recoveries dropped to zero for all forms which confirms the degradation of cofactors in presence of high salt conditions. To avoid degradation by minimal medium salts, quenching by cold ethanol or 2-propanol was tested and concentrations of oxidized and reduced forms of cofactors were compared to ones of non quenched cells. Compared to non-quenched cells, recoveries of cofactors was in the range of 50 and 25% for ethanol and 2-propanol respectively for NAD(H). Recovery of NADP(H) was about 33% for both ethanol and 2-propanol.

Outlook and Conclusion - Purification of UdhA, inhibitor screen and initial kinetic characterization

UdhA from *E. coli* MG1655 was cloned into the IPTG-inducible overexpression vector pTrc99 α and overexpression was done with *E. coli* JM101 strain in 2L LB medium containing 0.5 mM IPTG and 50 mg/L ampicillin at 37°C and 110 rpm. Cells were harvested at a maximally achievable optical density of 1.6, concentrated 40 times and disrupted by French Press. Pure, membrane-free cell extract was obtained by ultra-centrifugation at 132000 x g and 4°C for 4 hours and was loaded onto a size exclusion column (Fractogel EMD BioSec with particle size of 20-40 μ m) at a flow rate of 0.5 ml/min at 4°C. Totally 42 ml was eluted in 2 ml fractions and 2 out of 8 fractions containing UdhA pooled for the kinetic characterization (Fig. I).

Both the inhibitory screen and the kinetic characterization were conducted similar to the procedure used for glucose-6P- and 6P-gluconate dehydrogenase in **Chapter 5** (Table I and Fig. II, III).

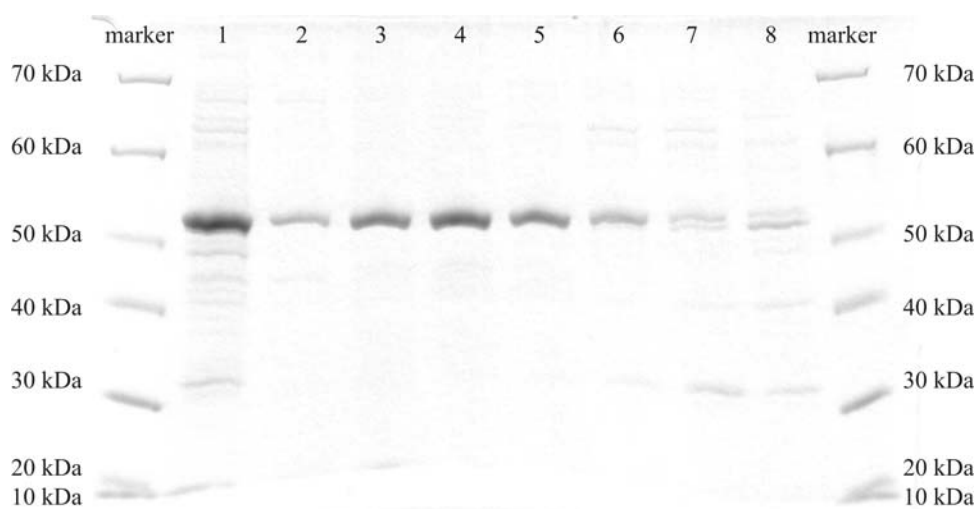


Figure I - Coomassie Blue stained SDS-PAGE of crude cell extracts containing overexpressed UdhA. Pure, membrane-free cell extract (lane 1) was loaded onto a size exclusion column and eluted at a flow-rate of 0.5 ml/min (fractions with highest protein concentrations, lanes 2-8). Fractions 4 and 5 were pooled and used for kinetic characterization and inhibitor screen.

Outlook and Conclusion - Figure II and III

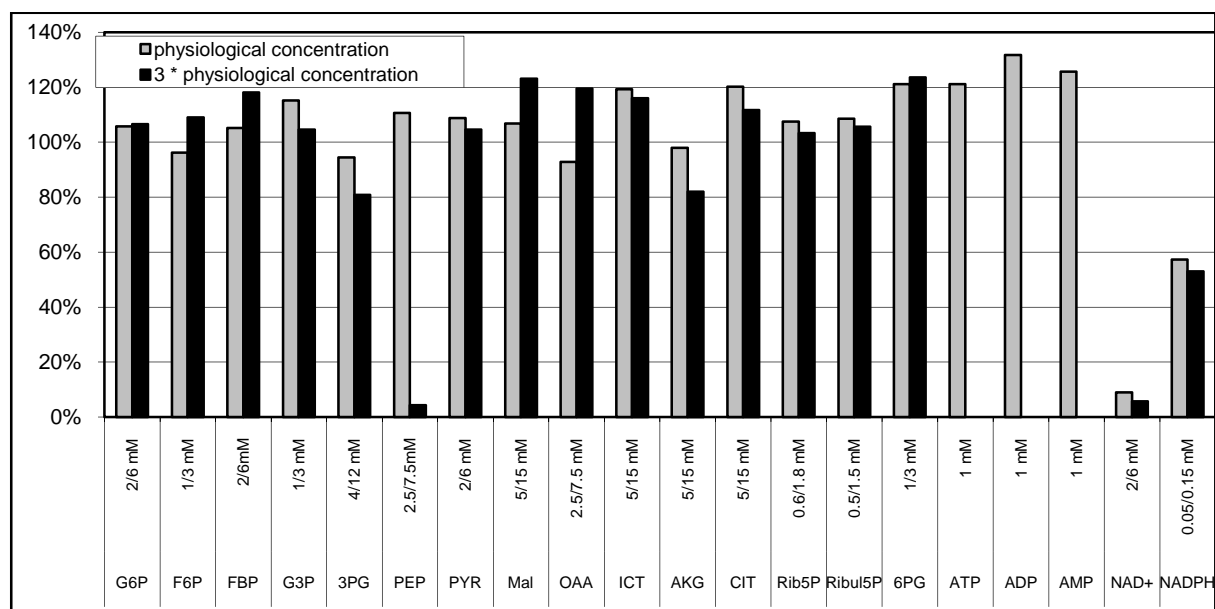


Figure II - Relative in vitro reaction rates for the forward reaction ($\text{NAD}^+ + \text{APADPH} \rightarrow \text{NADH} + \text{APADP}^+$) in the presence of potential inhibitors normalized to the velocities of the purified enzyme without inhibitors.

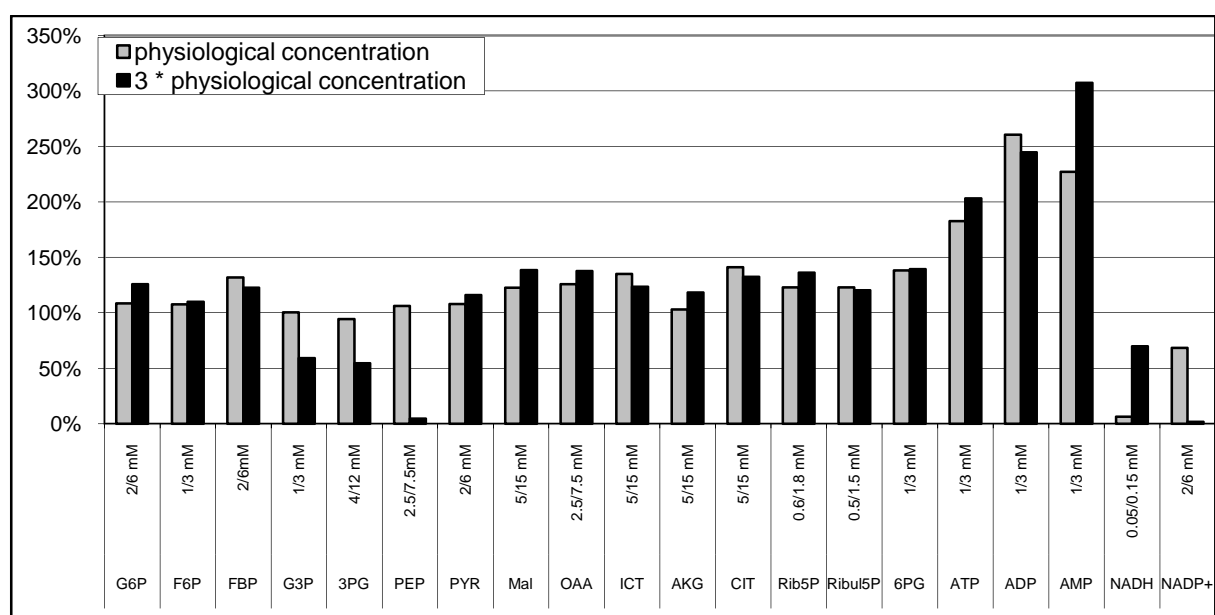


Figure III - Relative in vitro reaction rates for the backward reaction ($\text{APAD}^+ + \text{NADPH} \rightarrow \text{APADH} + \text{NADP}^+$) in the presence of potential inhibitors normalized to the velocities of the purified enzyme without inhibitors.

Outlook and Conclusion - Table I

Table I - Kinetic parameters of purified *E. coli* UdhA [μM]

	NADPH	NADH	APADP ⁺	APAD ⁺
K_M	61	122	356	76
K_i	40		95	

Contact Information

Name	Tobias Fuhrer
Address	Habsburgstr. 41 8037 Zürich Switzerland
Telephone	office +41-44-6332131 mobile +41-76-5165431
E-mail	fuhrer@imsb.biol.ethz.ch
Date of Birth	12/01/1979 in Uster, Switzerland
Nationality	Swiss

University Education

11/2003 – 03/2008	Ph.D. thesis at the Institute of Molecular Systems Biology, ETH, Zurich: “Microbial NADPH balancing mechanisms in seven diverse species and its regulation in <i>Escherichia coli</i> ”, Prof. Dr. U. Sauer.
10/1999 – 10/2003	Dipl. Natw. Biology, ETH, Zurich. Diploma thesis: “Experimental identification of metabolic networks in 10 bacterial species”, Prof. Dr. U. Sauer.

Special Courses

- | | |
|-------------------------|---|
| 19/11/2006 – 24/11/2006 | “Introductory Modeling Course”, Max-Planck-Institute for Molecular Genetics, Berlin. |
| 05/09/2005 – 16/09/2005 | “Basic Management Skills”, ETH Zurich and Management College Zurich. |
| 12/03/2005 – 18/03/2005 | “1 st FEBS Advanced Lecture Course in Systems Biology: From Molecules & Modelling to Cells”, The Federation of European Biochemical Societies, Gosau, Austria. |
| 22/05/2004 – 29/05/2004 | “Ph.D. Course in Metabolic Engineering and Functional Genomics”, Center for Microbial Biotechnology, Technical University of Denmark, Lyngby. |
| 11/03/2002 – 22/03/2002 | “Proteomics”, Prof. Dr. R. Aebersold, University Zurich and ETH Zurich. |

School Education

- | | |
|-------------------|---|
| 08/1994 – 08/1998 | Graduated with “Eidgenössische Matura Typ C” from Kantonsschule Wattwil, Switzerland. Main subjects: biology, chemistry, physics and mathematics. |
| 08/1986 – 08/1994 | Primary and Secondary School in Jona, Switzerland. |

Work Experience

- | | |
|-------------------|---|
| 02/2002 – 07/2003 | Technical assistant, Institute of Materials Chemistry and Corrosion, ETH, Zurich, Switzerland.
Task: High resolution current-voltage analyses of alloys. |
| 02/1999 – 06/1999 | Compulsory military service, Moudon, Switzerland.
Task: Hospital logistics. |
| 09/1998 – 02/1999 | Securities Backoffice UBS AG, Zurich, Switzerland.
Task: Admission of securities to official quotation. |

Awards

- | | |
|--------------|--|
| July 6, 2004 | “Prix Jeunes Chercheurs 2004” (3000 CHF) of the Swiss Academy of Sciences SAS for a Diploma thesis in the field of experimental biology. |
|--------------|--|

Extras

- | | |
|-----------|--|
| Languages | German (native language), English (fluent), Spanish (fluent) and French (basic). |
|-----------|--|

Computer Skills

Operating Systems Microsoft Windows, Linux, MacOS

Office Applications Microsoft Office, CorelDraw, HTML

Scientific Software SigmaPlot, MatLab, Darwin, Copasi, CellDesigner

Scientific Methods

Molecular Genetics and Assays, Physiology, Cell Metabolism and Tracer Experiments, Gas Chromatography / Mass Spectrometry, High Pressure Liquid Chromatography, Enzymatic Assays, Protein purification and Kinetics

July 15, 2008 Zurich

Publications

Journal Articles

Fuhrer, T.; Christen S. and Sauer, U., Pentose phosphate pathway flux in *Escherichia coli* is limited by the levels of glucose-6P- and 6P-gluconate dehydrogenase. in preparation.

Fuhrer, T.; Heinemann M. and Sauer, U., Transhydrogenase expression in *Escherichia coli* is substrate dependent. in preparation.

Fuhrer, T. and Sauer, U., Different biochemical mechanisms ensure network-wide balancing of reducing equivalents in microbial metabolism. submitted.

Fuhrer, T.; Chen, L.; Sauer, U. and Vitkup D., Computational prediction and experimental verification of the gene encoding the NAD⁺/NADP⁺-dependent succinate semialdehyde dehydrogenase in *Escherichia coli*. 2007. Journal of Bacteriology, Vol. 189, No. 22, p. 8073-8078.

Revelles, O.; Espinosa-Urgel, M.; **Fuhrer, T.**; Sauer, U. and Ramos, J.L., Multiple and interconnected pathways for L-lysine catabolism in *Pseudomonas putida* KT2440. 2005 Journal of Bacteriology, Vol. 187, No. 21, p. 7500-7510.

Del Castillo, T.; Ramos, J.L.; Rodríguez-Herva, J.J.; **Fuhrer, T.**; Sauer, U. and Duque, E., Convergent peripheral pathways catalyze initial glucose catabolism in *Pseudomonas putida*: Genomic and flux analysis. 2007. Journal of Bacteriology, Vol. 189, No. 14, p. 5142-5152.

Fuhrer, T.; Fischer, E. and Sauer, U., Experimental identification and quantification of glucose metabolism in seven bacterial species. 2005. Journal of Bacteriology, Vol. 187, No. 5, p. 1581-1590.

Book Chapters

Perrenoud, A.; **Fuhrer, T.** and Sauer, U., Determination of metabolic flux ratios from ^{13}C -experiments and GC-MS data: protocol and principles. 2006 Materials and Methods in Molecular Biology, Vol. 358, p. 177-198.

Master Thesis

Fuhrer, T., Experimental identification of metabolic networks in 10 bacterial species. Diploma Thesis. July 2003, ETH Zurich, Zurich, Switzerland.

Posters

Fuhrer, T.; E. Fischer and U. Sauer, Metabolic network analysis in six microbial species. March 2005. 1st FEBS Advanced Lecture Course in Systems Biology: From Molecules & Modeling to Cells. Gosau, Austria.

Fuhrer, T. and U. Sauer, Microbial NADPH metabolism. October 2006. Metabolic Engineering VI: From recDNA towards Engineering Biological Systems. Noordwijkerhout, The Netherlands.